NASA Technical Memorandum 81922

High Reynolds Number Tests of a Boeing BAC I Airfoil in the Langley 0.3-Meter Transonic Cryogenic Tunnel

William G. Johnson, Jr., Acquilla S. Hill,
Edward J. Ray, Roger A. Rozendaal,
and Thomas W. Butler

APRIL 1982

NASA

NASA Technical Memorandum 81922

High Reynolds Number Tests of a Boeing BAC I Airfoil in the Langley 0.3-Meter Transonic Cryogenic Tunnel

William G. Johnson, Jr., Acquilla S. Hill, and Edward J. Ray
Langley Research Center
Hampton, Virginia

Roger A. Rozendaal and Thomas W. Butler
Boeing Commercial Airplane Company
Seattle, Washington

National Aeronautics and Space Administration

Scientific and Technical Information Branch

1982

Use of trade names or names of manufacturers in this report does not constitute an official endorsement of such products or manufacturers, either expressed or implied, by the National Aeronautics and Space Administration.

SUMMARY

In a cooperative effort with the U.S. manufacturers of large transport aircraft, NASA has recently undertaken an extensive program to provide a systematic study of well-known conventional and advanced-technology airfoil concepts over a wide range of Reynolds numbers. This airfoil program, referred to as the Advanced Technology Airfoil Tests (ATAT) program, is being conducted in the two-dimensional test section of the Langley 0.3-Meter Transonic Cryogenic Tunnel (TCT).

The results presented in this report are from the first NASA/U.S. industry airfoil investigation conducted in the ATAT program. The industry participant for this investigation was the Boeing Commercial Airplane Company (Boeing). Test temperature was varied from ambient to about 100 K at pressures ranging from about 1.2 to 6.0 atm. Mach number was varied from about 0.40 to 0.80. These variables provided a Reynolds number (based on airfoil chord) range from about 4.4×10^6 to 50.0×10^6. This investigation was specifically designed to (1) test a Boeing advanced airfoil from low to flight-equivalent Reynolds numbers; (2) provide Boeing with experience in cryogenic wind-tunnel model design and testing techniques; and (3) demonstrate the suitability of the 0.3-m TCT as an airfoil test facility.

All the objectives of the cooperative test were met. Data are included which demonstrate the effects of fixed transition, Mach number, and Reynolds number on the aerodynamic characteristics of the airfoil. Also included are remarks on the model design, the model structural integrity, and the overall test experience.

INTRODUCTION

The growing interest in energy-efficient transport aircraft for the subsonic-transonic flight regime has stimulated the development of advanced-technology airfoils. Theoretical and experimental studies have shown that significant performance gains and increased fuel efficiency can be realized by the application of such airfoil concepts (ref. 1). The National Aeronautics and Space Administration (NASA) has recently undertaken an extensive program to provide a systematic study of both conventional and advanced-technology airfoil concepts over a wide range of Reynolds numbers. This airfoil program, described in reference 2, is referred to as the Advanced Technology Airfoil Tests (ATAT) program and is being conducted in the Langley 0.3-Meter Transonic Cryogenic Tunnel (TCT). Reference 3 describes the operating envelope of this transonic, cryogenic pressure tunnel.

A significant portion of the advanced-airfoil phase of the ATAT program will be carried out in cooperation with U.S. industry. Three of the major U.S. manufacturers of large commercial transport aircraft (Boeing, Douglas, and Lockheed) will participate individually in this phase of the program by providing technical personnel, airfoil design concepts, and airfoil models. The overall objectives of the ATAT program are: (1) to provide the industry participants with the opportunity to test and compare their advanced airfoils with the latest NASA designs at high Reynolds numbers in the same facility; (2) to provide industry with experience in cryogenic wind-tunnel model design, construction, and testing techniques; (3) to expand the high Reynolds number airfoil data base; and (4) to provide each participant with the opportunity to evaluate their own current levels of airfoil technology. Consistent

with these overall objectives, the industry participants have been encouraged to explore innovative airfoil designs which may, for instance, be subject to strong Reynolds number effects and, therefore, may not represent an attempt to achieve an optimum level of performance. Consequently, caution should be exercised in drawing conclusions regarding overall levels of technology from direct comparisons of the results obtained on the various airfoils.

The test results presented in this report are from the first NASA/U.S. industry airfoil study conducted in the ATAT program. The industry participant for this study was the Boeing Commercial Airplane Company (Boeing). The tests were conducted in the Langley 0.3-m TCT with a two-dimensional, 20- by 60-cm test section installed. Test temperature was varied from ambient to cryogenic temperatures (about 100 K) at pressures ranging from about 1.2 to 6 atm. Mach number was varied from about 0.40 to 0.80. These variables provided a Reynolds number (based on airfoil chord) range from about 4.4×10^6 to 50.0×10^6. The aerodynamic results are presented as integrated forces and moments. Detailed pressure distributions and airfoil coordinates are considered proprietary and are not included in this report. In keeping with the ATAT program objectives to provide the U.S. industry with cryogenic testing experience, the airfoil model was designed and fabricated by Boeing. Details regarding model design, fabrication techniques, and operational experience are included herein.

SYMBOLS

The measurements of this investigation are presented in the International System of Units (SI). The measurements and calculations were made in the U.S. Customary Units. Factors relating these two systems of units can be found in reference 4.

AOA	angle of attack
b	airfoil model span, cm
c	airfoil model chord, cm
c_d	section drag-force coefficient from wake measurements
c_m	section pitching-moment coefficient about quarter-chord point
c_n	section normal-force coefficient from airfoil pressures
c_{n_α}	slope of normal-force coefficient versus angle-of-attack curve
C_p	pressure coefficient
d	section drag from wake measurements
M	free-stream Mach number
n	section normal force from airfoil pressures
p_t	tunnel stagnation pressure, atm (1 atm = 101.3 kPa)
R	Reynolds number based on airfoil chord
T_t	tunnel stagnation temperature, K

x chordwise distance from leading edge of airfoil, cm

y spanwise distance along model from centerline of tunnel and model, cm

α uncorrected angle of attack, deg

Subscripts:

dd conditions at drag divergence, $\partial c_d/\partial M = 0.1$

max maximum

min minimum

te trailing edge

WIND TUNNEL AND MODEL

Wind Tunnel

The tests of the present investigation were made in the 20- by 60-cm two-dimensional test-section insert of the 0.3-m TCT. A photograph of the tunnel is shown in figure 1(a). A schematic drawing showing some physical characteristics of the tunnel is shown in figure 1(b). A photograph and sketch of the 20- by 60-cm two-dimensional test section are shown in figure 2. In the photograph, figure 2(a), the plenum lid and test-section ceiling have been removed to show model installation. This tunnel is a continuous-flow, fan-driven, transonic tunnel which uses nitrogen gas as the test medium. It is capable of operating at temperatures varying from about 80 K to about 327 K and stagnation pressures ranging from slightly greater than 1 atm to 6 atm. Test-section Mach number can be varied from about 0.2 to 0.85. The ability to operate at cryogenic temperatures and 6-atm pressure provides an extremely high Reynolds number capability at relatively low model loadings. A summary of Reynolds number and Mach number capabilities (ref. 3) is shown in figure 3.

The two-dimensional test section contains computer-driven angle-of-attack and momentum-rake systems. The angle-of-attack system is capable of varying the angle of attack over a range of about 40°. The momentum rake, located just downstream of the airfoil (see fig. 2(a)), provides up to five total-pressure measurements across the span of the tunnel. These pressures are converted to drag levels and provide a mechanism for determining the extent of two-dimensionality in the flow. The momentum-rake system is designed to traverse automatically through the wake, determine the boundaries of the wake, and then step through the wake at a selected rate and number of steps. Both the angle-of-attack and momentum-rake systems have a manual override capability. Additional design features and characteristics regarding the cryogenic-tunnel concept, in general, and the 0.3-m TCT, in particular, are presented in references 5 and 6.

Model

The airfoil model used in this test is a 10-percent-thick advanced-technology airfoil with a chord of 15.24 cm. The model was designed and fabricated by Boeing in accordance with NASA aerodynamic and structural requirements for the ATAT program models. The aerodynamic specifications require airfoil contour accuracies of

±0.00254 cm, surface finishes of 0.254 μm or better, and a sufficient coverage of pressure orifices with diameters of about 0.0254 cm. The structural specifications included tolerance requirements for the model chord and span dimensions, a selection of material suitable for use at cryogenic temperatures, safety factors of at least 3 at all operating conditions, Charpy impact strengths of at least 20.34 J at 77 K, and compatibility with existing 0.3-m TCT sidewall turntables. A photograph of the Boeing model installed in the 0.3-m TCT test section is shown in figure 4. (In this view, the plenum and test-section ceiling have been removed and the model module is in the "raised" position above the test section.) The photograph shows the Boeing-selected transition tripping devices located at the 10-percent-chord line. The trips were aluminum discs, 0.159 cm in diameter, 0.00254 cm thick, and spaced on 0.38-cm centers. The discs were glued along the 10-percent-chord line, on both the upper and lower surfaces, with Locktite Corp. Depend two-part adhesive. The glue bond added an additional thickness of approximately 0.00254 cm to the disk and resulted in an overall trip-device height of approximately 0.00508 cm. The model was equipped with 54 static-pressure orifices, each having a diameter of 0.0254 cm. Figure 5 is a schematic drawing which indicates the general location of the orifices and the general shape of the airfoil section. Table 1 lists the x/c and $y/(b/2)$ locations for each orifice.

Model fabrication.- The model was fabricated at the Boeing Aeronautical Laboratory model shop using A-286 stainless steel as the basic model material. The contouring was done in stages to allow for material stabilization and to reduce the possibility of model distortion. A "cover plate" type of construction was used. This type of construction requires trenches to be cut into the upper and lower surfaces of the model block, which had been machined to a slightly oversize contour. Holes were then drilled in the bottom of these trenches to within approximately 0.127 cm of the opposite surface. Stainless-steel tubing, with a 0.0813-cm outside diameter, was then soldered into these holes with Eutectic EutecRod 157 solder. The pressure tubes were routed along the trench and out a slot to the side of the model. Figure 6 is a photograph of the model during construction. The trailing-edge pressure orifice was connected using a final section of tubing with a 0.0254-cm outside diameter in order to remain within the cambered contour at the model trailing edge. The cover plates were then electron-beam welded over the trenches, and the model surfaces were machined to the final contour. The static-pressure orifices were then cut into the model surfaces to meet the soldered tubes using an electron discharge machine. This orifice fabrication technique was made possible by using a computer-aided design system which improved the accuracy of the drawing and provided precise determination of the tangents to any point on the airfoil surface. This then allowed the use of the leading edge of the model as a machining reference. Surface finishing was done by hand using fine-grit sand paper.

Model stress analysis.- The Boeing stress analysis used a severe loading distribution anticipated at high angle of attack and a free-stream dynamic pressure of 196.31 kPa. Calculating stresses in various critical parts of the model with these loads and A-286 material properties using classical methods gave safety factors of 8 or greater. A finite-element analysis of the model under load indicated a positive deflection of 0.0142 cm at the centerline section of the model. The decambering effect of trailing-edge movement under load was calculated to be only a 0.00097-cm deflection with respect to the local airfoil chord; therefore, aeroelastic studies during the wind-tunnel test were considered unnecessary.

Model accuracy and integrity.- Final contour and pressure-port locations were checked with a Brown & Sharpe Validator 200 probe. The actual airfoil contour (near the centerline) checked to within 0.00305 cm and -0.00102 cm of the specified airfoil

contour. These measurements were made at 10 chordwise locations on the upper and lower surfaces. The leading edge of the airfoil was checked with a template and the trailing-edge thickness was examined with a micrometer. The surface finish was measured by a surface-roughness measuring device as 0.102 μm.

Prior to installation in the tunnel, the model was cycled twice to cryogenic temperatures and back to ambient temperatures at a rate similar to actual operating conditions in the 0.3-m TCT. Visual and dye penetrant checks were made before and after the thermal cycling, and no flaws were found on the model.

TEST APPARATUS AND PROCEDURES

Test Instrumentation and Apparatus

A detailed discussion of the instrumentation and procedures selected for the calibration and control of the 0.3-m TCT can be found in reference 7. However, since the airfoil data are derived from (1) the pressure distributions around the airfoil, (2) the definition of the wake defect, and (3) the corresponding angle of attack, the details of the relevant instrumentation are discussed herein.

Airfoil pressures.- The 0.3-m TCT is equipped to obtain static-pressure measurements on the airfoil surface by using a series of pressure-scanning valves, each capable of 47 individual pressure samples. Because of the large changes in dynamic pressure of the tunnel over its operational range (a factor of about 75), conventional strain-gage pressure transducers are not used. Instead, individual commercially available high-precision capacitive potentiometer-type pressure transducers are connected to each of the scanning valves. The pressure transducers are located adjacent to the test section in order to reduce response time. For increased accuracy, the transducers are mounted on thermostatically controlled heater bases to maintain a constant temperature and on "shock" mounts to reduce possible vibration effects. The electrical outputs from the transducers are connected to individual signal conditioners located in the tunnel control room. The signal conditioners have autoranging capability and have seven ranges available. As a result of the autoranging capability, the analog electrical output to the data-acquisition system is kept at a high level, even though the pressure transducer may be operating at the low end of its range. The maximum range of these transducers is about 6.8 atm, with an accuracy of ±0.25 percent of the reading from -25 percent to 100 percent of full scale.

Wake pressures.- A vertically traversing probe is located on the sidewall of the two-dimensional test section downstream of the turntable (fig. 2). The mechanism has a traversing range of 25.4 cm. The probe support can be located with the probe measurement plane at either tunnel station, 21.0 cm or 26.0 cm. For this test, the measurements were made at the 26.0-cm station, which placed the measurement plane about 1.1 chord lengths downstream of the airfoil trailing edge. The probe is driven by an electric stepper motor and is designed to operate at speeds from about 0.25 cm/sec to about 15 cm/sec. The stroke and speed can be controlled from the operators panel in the control room to suit the research requirements. The vertical position of the probe is automatically recorded using the output from a digital shaft encoder geared to the probe drive mechanism. The wake-survey probe is synchronized with the scanning valves so that the probe is moved to a different vertical location each time the scanning valves are advanced to a new port. There are five wake total-pressure probes at different spanwise locations $y/(b/2)$. These locations are 0.125, 0.0, -0.125, -0.375, and -0.5. Tunnel sidewall static-pressure taps positioned in

the plane of the probes are used to determine the momentum loss and, therefore, airfoil drag coefficient, based on the method outlined in reference 8. Individual transducers of the type described previously are used on each tube on the probe assembly and for each of the wall taps.

Angle of attack.- The angle-of-attack mechanism has a traversing range of ±20°, which can be offset from 0° in either direction at model installation. The mechanism is driven by an electric stepper motor, which is connected through a yoke to the perimeter of both model mounting turntables. This arrangement drives both ends of the model through the angle-of-attack range to eliminate possible model twisting. The angular position of the turntable and, therefore, the angle of attack of the model are recorded using the output from a digital shaft encoder geared to the turntable.

Test Program

Figure 7 shows the test program (R versus M) used in this investigation. The selection of test conditions was made by Boeing in an effort to overlap some of their existing experimental and theoretical work. The extent of the effort to establish transition effects (fixed and free), R effects, and M effects can be seen in this figure.

Test Procedures

Delay times.- After model installation and instrumentation checkout and calibration, it is necessary to establish the delay times required for the sampling of the airfoil pressures. Both experience and theoretical analysis have shown that the delay times are strongly dependent on the tubing diameters downstream of the model orifice, the pressure change from one orifice to another, and the magnitude of the pressure to be measured. As a result of these studies, the general recommendation was made to keep the inside diameter of the tubing within the model to greater than 0.076 cm. This would result in normal delay times on the order of 1 to 2 seconds per orifice. However, this model had tubing with inside diameters of about 0.051 cm, which was expected to cause significant increases in delay times. Following normal procedures to determine delay times, predicted or preliminary pressure distributions for highly loaded model conditions were used to establish levels of individual orifice pressures and changes in level from adjoining orifices. These "known" pressures were applied to the airfoil statically and with tunnel flow, and the response of the pressure measuring system (orifice, tubing, and transducer) was determined by recording, on a strip chart, the time and pressure transient for the pressure to reach a settled pressure. For this test, 98 percent of the known level was selected as the settled pressure, and the resulting time was identified as the appropriate delay time. This procedure defined some delay times up to or in excess of 9.95 seconds/port, which was the maximum capability of the controller. The remaining ports were also above normal in delay times, but could be grouped at 3 seconds/port. A capability of the pressure-scanning-valve controller to vary delay times for groups of orifices provides near-minimum time consumed with near-maximum accuracy for each orifice. The groupings and delay times for the model orifices for this test are as follows:

Orifices	≈x/c	Delay time, sec
1	0	9.9
2 to 19	0.01 to 0.54	3.0
20 to 23	0.58 to 0.70	9.9
24 to 27	0.75 to 0.88	3.0
28	0.92	9.9
29	1.0	3.0

The other spanwise orifices had similar delay times based on their x/c location. The resulting total time for the average data point to be taken approached 6 minutes.

Use of wake rake.- To provide maximum definition of the airfoil wake, the stroke of the rake and number of steps within the stroke were generally changed for each angle of attack and Mach number. The range of values for these variables was determined from initial experimental runs. An example of this variation is shown in figure 8 for $M \approx 0.76$.

DATA REDUCTION, QUALITY, AND CORRECTIONS

Data Reduction

In the data-reduction process, the thermodynamic properties of the nitrogen gas are calculated using the Beattie-Bridgeman equation of state. This equation of state has been shown to give essentially the same thermodynamic properties and flow-calculation results as the more complicated Jacobsen equation of state (ref. 9) in the temperature-pressure regime of the 0.3-m TCT. Detailed discussions of real-gas effects when testing in cryogenic nitrogen are contained in references 10 and 11. The test Mach number reflects the average of the longitudinal Mach number distributions, which were measured as a function of Reynolds number in the calibration of the "empty" test section.

As previously mentioned, the pressures on the surface of the airfoil were measured using pressure-scanning valves. The raw data were obtained by sampling 5 scans per port for the first portion of the test. This was later changed to 3 scans per port in order to reduce the time required to record a data point. The data were reduced according to a process described in an unpublished in-house data reduction program. Normal-force coefficients and pitching-moment coefficients were then calculated from pressure integration around the airfoil.

The wake pressures were measured by individual transducers and were reduced according to the in-house program. The drag force was obtained as an integration of total-pressure decrement across the airfoil wake corrected for a "threshold" decrement, which accounted for a nonzero pressure decrement outside the wake. This threshold decrement, in the form of incremental drag coefficient, was derived by looking at several wake profiles early in the test. The compromise value for the entire test was 0.0002. For some data points, small portions of the airfoil wake were missed in the rake traverse. In a few other cases, the data system erroneously recorded zero values for certain portions of the wake profile. In each of these cases, the wake profile was extrapolated or interpolated manually as needed to complete the profile. The resulting addition to the drag coefficient was generally less than one count (0.0001).

The results from the data-reduction process are presented in table 2. Specific notation is made of those points which were adjusted by the extrapolation or interpolation process. As previously noted, the detailed pressure distributions are considered proprietary information and are not included in this report.

Data Quality

Mach number fluctuations.- In all wind-tunnel testing, and especially in transonic testing, the stability of the tunnel flow conditions, such as Mach number, has a direct bearing on the quality of the final aerodynamic data. In table 2, values of Mach number and Reynolds number are shown as average values for the specific points. Because the delay times for some of the groupings of pressure orifices were very high, the variation in average values of Mach number and Reynolds number does not represent an inability to set the precise tunnel test conditions in the short term, but rather indicates a long-term drift in the test conditions during the extended time required for the acquisition of a single data point during these tests. In addition to the drift in test conditions due to the data-acquisition time, two other factors have been identified as causes of the undesired variations in Mach and Reynolds numbers. First, the manual control of the pressure and temperature control systems resulted in some nonuniformity in the level of the Mach number. Second, the electrical drive system of the 0.3-m TCT has some inherent speed-control problems that feed directly into the tunnel flow through the fan drive. In all three areas, corrective measures have been identified.

Repeatability of data.- Several examples illustrating the degree of repeatability for the normal-force, pitching-moment, and drag-force results are shown in figures 9, 10, and 11. The repeatability shown in these figures is considered to be generally good, although there is some scatter in the data at the higher angles of attack.

Evaluation of hysteresis effects.- An airfoil may exhibit substantially different aerodynamic characteristics at a given condition, such as angle of attack, when it is "approached" from different directions. A very brief forced attempt to develop hysteresis was made during this investigation, and the results determined during this evaluation are reflected in table 2 and figure 12. The hysteresis data points for this test were obtained by increasing the airfoil angle of attack until substantial separation occurred, and then decreasing the angle of attack to the desired condition before taking data. The hysteresis points shown in figure 12 (square symbols) indicate an absence of detectable hysteresis effect.

Correction to Results

Because of the absence of detailed pressure distributions and the general uncertainty of the corrections for this test set-up, no attempt has been made to correct the data for wall-interference effects due either to the top or bottom slotted walls or to sidewall boundary-layer growth. However, the dashed line in figure 9 shows a sample calculation of the change in the slope of the normal-force curve c_{n_α} based on the method described in reference 12.

PRESENTATION OF RESULTS

The results are presented in table 2, and an outline of the plotted data presented herein follows:

DISCUSSION

Assessment of Tunnel Sidewall Effects

The 0.3-m TCT momentum-loss (drag) survey rake, described in the section "Test Apparatus and Procedures" and shown in figure 2(a), is equipped with several spanwise total-pressure probes which enable an assessment of the airfoil drag levels across the tunnel. These drag levels also give an indication of the two-dimensionality of the flow over the airfoil. A review of these data, as shown in figure 13 and 14, indicates that at high Reynolds numbers there is exceptional uniformity in the spanwise drag characteristics at normal-force coefficients below about 0.8. However, for normal-force coefficients above approximately 0.8 (high angles of attack), separation effects begin to occur and the uniformity deteriorates. For example, the

c_n = 0.937 case shown in figure 14(a) suggests a significant drag-reduction trend near the tunnel wall. This appears to be the typical behavior when wall separation occurs as a result of interaction between the wall boundary layer and the airfoil shock. An exception to the low-angle-of-attack drag uniformity is the low Reynolds number, free-transition case (fig. 14(a)). At this condition, as is discussed subsequently, the flow over the model is believed to be partially laminar. It is also believed that in the low Reynolds number, free-transition case, the pressure orifices on the airfoil and other factors are changing the chordwise transition location at the various spanwise stations. By plotting the free-transition, low Reynolds number data from the same run used for figure 14(a) at normal-force coefficients which are the same as those of the fixed-transition, low Reynolds number run, a direct comparison between the effect of free transition (fig. 15(a)) and fixed transition (fig. 15(b)) on spanwise drag can be made. The data show that fixing the transition at the low Reynolds number condition results in a very uniform spanwise drag distribution.

Effects of Transition on Aerodynamic Characteristics

Figures 16 to 25 show how the basic aerodynamic characteristics (normal force, pitching moment, and drag force) are affected by the presence of the transition devices. The transition strip evaluation was conducted over a Mach number range from 0.70 to 0.80 and a Reynolds number range from 4.4×10^6 to 30.0×10^6. Figures 16 to 18 illustrate that, at the low Reynolds number condition (4.4×10^6) in the range where the flow over the airfoil would be partially laminar, the addition of the transition devices results in small changes to the normal-force characteristics and substantial changes to the pitching-moment and drag-force characteristics. The differences due to the transition strips largely disappear when Reynolds number is increased to 7.7×10^6 (figs. 19 to 21). For the 7.7×10^6 condition, the summary presentations shown in figures 43 and 46 illustrate closer agreement than at 4.4×10^6 in the normal-force, pitching-moment, and drag-force characteristics of the airfoil with and without the transition devices. These results and other unpublished studies suggest that the turbulent transition is very near the leading edge of the airfoil at Reynolds numbers of about 8 to 10×10^6 in the 0.3-m TCT. Data at the higher Reynolds numbers of 14 and 30×10^6 (figs. 22 to 25) do not indicate any significant changes in the normal-force or pitching-moment characteristics as a result of the addition of the artificial transition devices. There is, however, an indication that the selected "tripping" devices cause some artificial transition drag because of their penetration of the airfoil boundary layer at Reynolds numbers of 14×10^6 and higher. (See fig. 46(b), e.g.)

Effects of Mach Number and Reynolds Number on Basic Aerodynamic Characteristics

Figures 26 to 34 show the effects of Mach number (for each test Reynolds number) on the basic aerodynamic characteristics of the airfoil. The trends shown in these results are generally similar, illustrating the expected increases in normal-force slopes and nose-down pitching moments with increasing Mach number. As the Mach number is increased, stall occurs at progressively lower angles of attack. Also, for Mach numbers in the range of 0.70 to 0.76, both the normal-force and pitching-moment curves exhibit abrupt changes in slopes in the mid angle-of-attack range. These changes appear (based on the unpublished airfoil pressure results) to correspond with the rapid rearward movement of shocks on the airfoil. At the highest Mach numbers,

the substantial changes in drag levels and normal-force and pitching-moment slopes in the low-to-moderate geometric angle-of-attack range indicate the expected drag rise effects.

In figures 35 to 40, the basic data presented earlier have been arranged and compared in a different format to clearly illustrate the effects of Reynolds number (at a given Mach number) on the basic force and moment characteristics of the airfoil. In general, these results exhibit the expected increases in normal-force slope with increasing Reynolds number. The nose-down pitching moments (at low-to-moderate normal forces) typically increase as the Reynolds number is increased. The longitudinal stability parameter dc_m/dc_n appears to be relatively insensitive to Reynolds number changes at Mach numbers below about 0.76. The drag results, with the exception of the free-transition data for $R = 4.4 \times 10^6$, display the expected reductions in drag levels with increasing Reynolds number. The overall stability, performance, and efficiency characteristics of the airfoil are discussed further in subsequent sections.

Effect of Mach Number and Reynolds Number on Trailing-Edge Pressure Coefficient

Figures 41 and 42 illustrate the effects of Mach number on the variation of pressure coefficients with Reynolds number and normal-force coefficients determined from the orifice located at the trailing edge of the model (see fig. 5). Trailing-edge pressure results were obtained only for the free-transition portion of the study and were monitored during the test to provide an indication of the onset of substantial flow separation. A significant decrease in trailing-edge pressure was taken to be an indication of trailing-edge separation. For instance, the results shown in figure 41 suggest progressive reductions in the normal-force coefficient at which separation occurs with increasing Mach number. Likewise, as discussed previously, the force and moment curves indicated separation at similar normal-force coefficients (e.g., examine the results for $R = 14.0 \times 10^6$ shown in figs. 28 and 41(c)). Figure 42 illustrates (at a constant normal-force coefficient) the increasing trailing-edge pressure recovery with increasing Reynolds number. This increased recovery is associated with the decreasing trailing-edge velocities, drag reductions, and changing boundary-layer conditions expected at the higher Reynolds numbers.

Stability, Performance, and Efficiency Characteristics

Figure 43 is a summary of the effect of Mach number on the variation of normal-force and pitching-moment coefficients with Reynolds number. The variations in pitching-moment coefficient c_m with Reynolds number (at a normal-force coefficient of 0.6) display the characteristic increase in nose-down pitching-moment and normal-force coefficient with increasing Reynolds number. For the free-transition case, there is a significantly higher nose-down pitching-moment and normal-force coefficient at the lowest test Reynolds number. This is attributable to what appears to be significant laminar flow over the airfoil and the resulting thinner boundary layer, increased camber, and increased lift. The addition of the transition devices results in a low Reynolds number pitching-moment and normal-force behavior consistent with trends observed when the airfoil is tested at conditions conducive to a turbulent boundary layer over most of the model. Figure 44 is a summary of the variation of normal-force slope c_{n_α} with Mach number for Reynolds numbers of 14.0,

30.0, and 45.0 × 10^6. These results illustrate the characteristic increase in c_{n_α} with increasing Mach number. There is a rapid increase in the normal-force slopes as the Mach number approaches 0.76 to 0.77, which is followed by less severe slope increases for the higher Mach numbers. In fact, the curve for $R = 30.0 \times 10^6$ begins to show a trend of decreasing slope. In addition, these results show a definitive trend of increasing normal-force slopes with increasing Reynolds number at a given Mach number. Figure 45 indicates the relatively flat variation of the stability parameter dc_m/dc_n with Mach number for test conditions below about M = 0.72. At the highest test Mach numbers, the results indicated significant rearward movements of the shock and center of pressure (more negative values dc_m/dc_n) with increasing Mach number. The effects of increasing Reynolds number on the stability parameter were not as pronounced as the Mach number effects, and the results did not appear to provide a consistent trend.

The effect of Mach number on the variation of airfoil drag characteristics with Reynolds number is summarized in figure 46 for several normal-force coefficients. With the exception of the free-transition low Reynolds number results, the general trends illustrate the expected decreases in drag coefficient with increasing Reynolds number. At the highest Mach number (fig. 46(e)), the results show the characteristic drag rise, particularly at the higher normal-force coefficients.

The "bump" in the curve of drag coefficient versus Mach number, which occurs between low Mach numbers and the abrupt Mach divergence drag rise, has been the subject of many discussions on supercritical airfoil technology. As an example, reference 13 addresses this drag-rise phenomenon in discussions related to a low Reynolds number study of an early, 10-percent-thick, NASA supercritical airfoil. This drag rise, referred to by many researchers as "drag creep," has been shown to be a complicated phenomenon which can occur as a result of several different causes, and is highly dependent upon boundary-layer conditions and the associated fluid shape of the airfoil. It is, therefore, of primary interest in high Reynolds number airfoil testing. Figure 47 is a summary of the effect of Reynolds number on the variation of drag with Mach number. The drag-creep characteristic becomes more pronounced as the normal-force coefficients increase. In addition, figures 47(b) and 47(c) show that the drag-creep characteristic diminishes with increasing Reynolds number.

The results shown in figure 47 also illustrate that as the normal force is increased, the drag divergence occurs at lower Mach numbers. This behavior is further illustrated in figure 48, which summarizes this relationship between the drag-divergence Mach numbers M_{dd} and normal-force coefficients. The area to the left of the curve represents the test conditions which can be achieved with this airfoil before encountering the transonic drag rise. (It should be noted again that these data have not been adjusted for tunnel-wall-interference effects.)

The changes in airfoil performance with Mach number and Reynolds number are shown in figure 49. In general, these results indicate an increase in the performance factor with increasing Mach number up to the conditions where the transonic drag rise results in significant reductions in performance. The "dip" in performance reduction that is most prominent for the low Reynolds number case at a Mach number of about 0.74 is directly related to the low Reynolds number drag-creep characteristic discussed previously.

Model Assessment

One of the primary objectives of the ATAT program is to provide the U.S. industry participants with the opportunity to gain cryogenic testing experience and, in particular, cryogenic model design and fabrication experience. Recent experience gained by NASA in airfoil testing in the 0.3-m TCT has indicated that the physical stability of models tested at cryogenic temperature is a function of the material, the configuration design, and the overall processing procedures used during model fabrication. Model accuracies are a major consideration for the high Reynolds number boundary-layer conditions provided by cryogenic pressure wind tunnels. Therefore, in this relatively new area of research, a thorough assessment of the accuracy of the model contours and a quantitative definition of the model surface finish, both before and after the tests, are considered to be essential parts of the overall research effort.

No structural problems were encountered with the load-carrying parts of the model. Post-test examinations of the model did not indicate any obvious distortions or structural failures in the cover plates or associated weld joints. In addition, the post-test examination did not reveal any change in the spanwise or chordwise shape or dimensions of the model. It did appear, however, that there was some deterioration of the surface finish near the leading edge of the center portion of the model. The 0.3-m TCT is considered to be an inherently "clean" tunnel with its closed-circuit, liquid-nitrogen injection and continuous exhaust features. The exact cause of the surface-finish deterioration is not known, but it is believed to be associated with the fact that the tunnel had been partially dismantled for major maintenance just prior to this test. It is suspected that, during the maintenance period, small particles of dust, grit, etc. were inadvertently introduced into relatively inaccessible portions of the tunnel circuit and served as "sandblasting" agents during the early portions of the test program. This conjecture is supported by visual observations made during the tests, which indicated that most of the finish deterioration did, in fact, occur during the initial (fixed transition) portion of the study. Detailed examinations of other models tested after the Boeing airfoil have not revealed surface-finish deterioration during testing. In addition, some minor problems were experienced with the soldered joints in the static pressure tubes during the model installation and initial runs. The joints external to the model, unlike the more critical internal joints (see section entitled "Model"), were originally bonded with a relatively low-melting-temperature solder. Several of these joints failed during the initial thermal cycling of the tunnel and the model. It was necessary to resolder these joints with a higher-melting-temperature, cryogenically compatible solder of the type used internal to the model and mentioned in the section entitled "Model." Several static lines still leaked slightly, but there was only one line that was considered to be unusable. In general, the design and fabrication techniques used for this model were found suitable for models to be tested in a cryogenic environment.

SUMMARY OF RESULTS

A wind-tunnel investigation, which represents the first NASA/U.S. industry two-dimensional airfoil study to be completed in the Advanced Technology Airfoil Tests (ATAT) program, has been conducted in the Langley 0.3-Meter Transonic Cryogenic Tunnel (TCT). This investigation was designed to (1) test a Boeing advanced-technology airfoil from low to flight-equivalent Reynolds numbers; (2) provide Boeing with experience in cryogenic wind-tunnel model design and testing techniques; and (3) demonstrate the suitability of the 0.3-m TCT as an airfoil test facility.

All the objectives of this cooperative test were met. Limited analysis of the data from this investigation indicates the following results:

1. A limited amount of data indicated that the repeatability of these data is good with no apparent hysteresis effects.

2. The spanwise measurements of the flow behind the airfoil model appear to be uniform for unseparated flow conditions and indicate minimum tunnel sidewall effects. For high-angle-of-attack post-separation conditions, the flow becomes less uniform and less two-dimensional.

3. The boundary-layer transition devices satisfactorily tripped the flow at low Reynolds numbers with no substantial effect at higher Reynolds numbers.

4. These data show the expected changes in the airfoil characteristics with increasing Mach number, such as increased normal-force slope, increased drag force, and increased nose-down pitching moment.

5. Increasing Reynolds number resulted in increased normal force, increased nose-down pitching moment, and generally decreased drag force. Likewise, increasing Reynolds number resulted in a diminished drag creep at a given normal-force coefficient.

6. The design and fabrication techniques used for this model were found suitable for models to be tested in a cryogenic environment. The model was structurally sound, dimensionally proper, and finished to an adequate tolerance.

7. The 0.3-m TCT demonstrated its suitability for studying this airfoil through a broad range of Mach and Reynolds numbers.

Langley Research Center
National Aeronautics and Space Administration
Hampton, VA 23665
February 19, 1982

REFERENCES

1. Whitcomb, Richard T.: Review of NASA Supercritical Airfoils. ICAS Paper No. 74-10, Aug. 1974.

2. Ladson, Charles L.; and Ray, Edward J.: Status of Advanced Airfoil Tests in the Langley 0.3-Meter Transonic Cryogenic Tunnel. Advanced Aerodynamics - Selected NASA Research, NASA CP-2208, 1981, pp. 37-53.

3. Ray, Edward J.; Ladson, Charles L.; Adcock, Jerry B.; Lawing, Pierce L.; and Hall, Robert M.: Review of Design and Operational Characteristics of the 0.3-Meter Transonic Cryogenic Tunnel. NASA TM-80123, 1979.

4. Standard for Metric Practice. E 380-79, American Soc. Testing & Mater., c.1980.

5. Kilgore, Robert A.; Adcock, Jerry B.; and Ray, Edward J.: The Cryogenic Transonic Wind Tunnel for High Reynolds Number Research. Windtunnel Design and Testing Techniques, AGARD-CP-174, 1976, pp. 1-1 - 1-20.

6. Kilgore, Robert A.: Design Features and Operational Characteristics of the Langley 0.3-Meter Transonic Cryogenic Tunnel. NASA TN D-8304, 1976.

7. Ladson, Charles L.; and Kilgore, Robert A.: Instrumentation for Calibration and Control of a Continuous-Flow Cryogenic Tunnel. NASA TM-81825, 1980.

8. Baals, Donald D.; and Mourhess, Mary J.: Numerical Evaluation of the Wake-Survey Equations for Subsonic Flow Including the Effect of Energy Addition. NACA WR L-5, 1945. (Formerly NACA ARR L5H27.)

9. Hall, Robert M.; and Adcock, Jerry B.: Simulation of Ideal-Gas Flow by Nitrogen and Other Selected Gases at Cryogenic Temperatures. NASA TP-1901, 1981.

10. Adcock, Jerry B.: Real-Gas Effects Associated With One-Dimensional Transonic Flow of Cryogenic Nitrogen. NASA TN D-8274, 1976.

11. Adcock, Jerry B.; and Johnson, Charles B.: A Theoretical Analysis of Simulated Transonic Boundary Layers in Cryogenic-Nitrogen Wind Tunnels. NASA TP-1631, 1980.

12. Barnwell, Richard W.: Design and Performance Evaluation of Slotted Walls for Two-Dimensional Wind Tunnels. NASA TM-78648, 1978.

13. Harris, Charles D.: Transonic Aerodynamic Characteristics of the 10-Percent-Thick NASA Supercritical Airfoil 31. NASA TM X-3203, 1975.

TABLE 1.- PRESSURE TAP COORDINATES

Orifice	x/c	y/(b/2)
Upper surface		
1	0.000	0.176
2	.008	-.263
3	.010	-.138
4	.020	-.160
5	.030	-.188
6	.040	-.213
7	.061	-.238
8	.080	-.113
9	.100	↓
10	.150	
11	.200	
12	.250	
13	.299	
14	.340	
15	.379	
16	.420	
17	.460	
18	.500	
19	.540	
20	.580	
21	.620	
22	.660	
23	.700	
24	.749	-.263
25	.799	-.240
26	.835	-.213
27	.879	-.188
28	.921	-.163
29	1.000	-.138
Lower surface		
1	0.005	0.159
2	.010	.147
3	.020	.130
4	.050	.116
5	.081	.098
6	.120	.075
7	.180	↓
8	.240	
9	.300	
10	.359	
11	.419	
12	.479	
13	.539	
14	.599	
15	.651	
16	.720	
17	.774	.157
18	.839	.115
19	.900	.068
20	.949	.028
[1]Additional spanwise orifices		
1	0.050	-0.338
2	.395	↓
3	.501	
4	.605	
5	.700	

TABLE 2.- BAC I TEST RESULTS

[There are no runs 1, 2, 42, and 54]

(a) Fixed transition

Point	M	R	α	c_n	c_m	c_d
			Run 3			
1	0.795	4.317×10^6	-2.05	-0.041	-0.089	0.01077
2	.802	4.466	-.98	.124	-.097	.00933
3	.799	4.460	.02	.268	-.101	[a].00918
			Run 4			
4	0.796	4.438×10^6	1.03	0.411	-0.103	[a]0.00943
5	.802	4.474	1.05	.415	-.103	[a].00982
6	.801	4.450	2.03	.560	-.107	.01178
7	.798	4.432	3.02	.692	-.113	[a].01646
8	.807	4.484	3.51	.718	-.119	[a].02763
10	.808	4.528	2.50	.634	-.117	[a].01853
[b]11	.802	4.453	2.52	.632	-.114	[a].01522
			Run 5			
1	0.758	4.456×10^6	-1.99	-0.010	-0.088	0.00855
2	.758	4.458	-1.00	.126	-.092	.00821
3	.758	4.459	.00	.261	-.095	.00823
4	.757	4.453	1.00	.394	-.095	.00842
5	.762	4.476	2.01	.530	-.096	.00886
6	.759	4.440	3.02	.673	-.092	[a].01075
7	.760	4.431	3.50	.759	-.095	[a].01306
8	.758	4.435	4.01	.833	-.098	[a].01766
10	.760	4.442	5.01	.930	-.104	[a].03518
11	.761	4.447	6.02	.977	-.109	[a].06703
			Run 6			
1	0.696	4.459×10^6	-2.05	-0.015	-0.084	0.00841
2	.696	4.462	.04	.245	-.089	.00805
3	.698	4.484	1.04	.367	-.090	.00814
4	.698	4.481	2.05	.493	-.090	.00842
5	.697	4.481	3.05	.616	-.088	.00876
6	.697	4.461	3.52	.675	-.085	.00942
7	.697	4.452	4.03	.751	-.083	.01089
8	.698	4.449	4.51	.817	-.082	.01369
9	.697	4.458	5.01	.896	-.079	.01817
10	.698	4.450	6.02	1.038	-.078	[a].03243
11	.695	4.442	7.03	1.117	-.075	.04912
12	.698	4.461	8.01	1.153	-.080	.07070

[a]Value of c_d corrected for lost wake information.

[b]This point is a repeat of a previous one in this run. The angle of attack was approached from below.

[c]This is a hysteresis point. The angle of attack was approached from above.

TABLE 2.- Continued

(a) Continued

Point	M	R	α	c_n	c_m	c_d
			Run 7			
1	0.800	7.834×10^6	-2.03	-0.029	-0.093	[a]0.01038
2	.797	7.796	-.98	.126	-.099	.00844
3	.798	7.794	.03	.277	-.105	[a].00862
4	.802	7.802	1.03	.426	-.110	[a].00984
5	.796	7.745	2.03	.575	-.111	.01105
6	.801	7.757	2.52	.640	-.119	[a].01522
7	.800	7.757	3.02	.694	-.118	[a].01926
8	.806	7.772	3.50	.728	-.124	[a].02770
			Run 8			
2	0.762	7.837×10^6	-2.01	-0.008	-0.092	0.00811
3	.758	7.764	-.99	.132	-.094	.00771
4	.758	7.775	.01	.267	-.097	.00763
5	.756	7.694	1.00	.401	-.098	.00785
6	.757	7.706	2.00	.538	-.098	.00830
7	.758	7.759	3.01	.697	-.097	[a].01001
8	.756	7.725	3.50	.768	-.096	.01242
10	.755	7.728	4.50	.902	-.105	[a].02266
11	.762	7.836	5.00	.938	-.109	.03300
12	.765	7.732	6.02	.964	-.115	[a].06682
[c]14	.754	7.632	4.00	.841	-.103	
			Run 9			
[b]1	0.699	7.777×10^6	-2.02	-0.005	-0.085	
[b]2	.702	7.843	-2.06	-.007	-.086	0.00766
3	.699	7.775	.04	.251	-.090	.00757
4	.697	7.785	1.02	.373	-.091	.00767
5	.697	7.708	2.03	.499	-.092	.00781
6	.698	7.786	3.05	.627	-.090	.00839
7	.697	7.771	3.51	.683	-.089	.00904
8	.698	7.763	4.03	.754	-.086	.01076
9	.702	7.787	4.52	.837	-.083	.01399
10	.698	7.701	5.03	.900	-.080	.01830
11	.700	7.729	6.01	1.036	-.078	
[b]12	.701	7.776	6.02	1.042	-.080	
[b]13	.701	7.720	6.04	1.042	-.079	.03336
14	.699	7.782	7.02	1.110	-.075	[a].05600
[b]15	.700	7.779	7.04	1.109	-.076	.05146
16	.696	7.706	8.00	1.135	-.080	[a].07941

See footnotes on page 18.

TABLE 2.- Continued

(a) Continued

Point	M	R	α	c_n	c_m	c_d
			Run 10			
1	0.760	7.923×10^6	0.00	0.268	-0.097	0.00791
2	.761	7.872	1.00	.406	-.099	.00818
3	.758	7.742	3.00	.684	-.095	[a].00996
4	.757	7.684	3.51	.772	-.098	[a].01276
5	.760	7.727	4.00	.847	-.104	[a].01758
7	.760	7.822	4.51	.900	-.105	.02413
[b]8	.756	7.800	4.00	.846	-.102	.01733
[b]9	.758	7.807	3.49	.770	-.098	.01269
[b]10	.757	7.840	3.01	.700	-.097	[a].00999
			Run 11			
1	0.800	1.403×10^7	-2.14	-0.031	-0.098	0.00948
2	.798	1.398	-.99	.135	-.102	.00786
3	.797	1.390	.01	.283	-.106	.00785
4	.804	1.392	1.00	.437	-.114	.00936
5	.798	1.372	2.00	.587	-.116	.01060
6	.806	1.385	2.50	.643	-.124	.01704
7	.806	1.385	3.02	.690	-.124	.02206
8	.796	1.373	3.51	.773	-.127	.02278
9	.802	1.379	4.02	.782	-.127	
			Run 12			
1	0.755	1.397×10^7	-2.02	-0.011	-0.094	0.00733
2	.757	1.404	.00	.278	-.099	.00717
3	.758	1.403	1.00	.414	-.100	.00747
4	.760	1.405	2.01	.551	-.101	.00784
5	.757	1.389	3.01	.695	-.098	.00948
6	.762	1.397	3.54	.787	-.102	[a].01300
7	.761	1.407	4.02	.845	-.104	[a].01705
8	.755	1.393	4.53	.905	-.105	[a].02266
9	.766	1.410	5.01	.952	-.116	.03364
10	.760	1.391	6.03	.980	-.110	[a].06281
11	.759	1.400	7.04	.973	-.108	

See footnotes on page 18.

TABLE 2.- Continued

(a) Concluded

Point	M	R	α	c_n	c_m	c_d
Run 13						
2	0.703	1.419×10^7	-2.01	-0.008	-0.089	0.00707
3	.692	1.378	.05	.251	-.093	.00703
4	.702	1.423	1.07	.383	-.094	.00721
5	.698	1.407	2.05	.506	-.094	.00740
6	.706	1.417	3.07	.638	-.093	.00790
7	.699	1.408	3.51	.694	-.090	.00855
8	.699	1.399	4.04	.766	-.088	.01017
9	.702	1.398	4.50	.844	-.086	.01349
10	.700	1.405	5.02	.907	-.082	.01816
11	.699	1.405	6.03	1.040	-.079	.03238
12	.702	1.412	7.05	1.126	-.079	.05261
13	.701	1.430	8.04	1.086	-.090	.08067
Run 14						
1	0.755	3.010×10^7	-2.02	-0.009	-0.098	0.00655
2	.759	3.017	-2.02	-.008	-.099	.00668
3	.760	3.022	.03	.290	-.104	.00646
4	.756	3.010	1.03	.428	-.104	.00658
5	.757	2.998	2.04	.566	-.104	.00704
6	.760	3.007	3.04	.730	-.104	.00902
7	.757	3.007	3.53	.798	-.104	.01175
8	.756	3.001	4.04	.870	-.109	.01711
9	.763	3.026	4.57	.938	-.122	.02511
10	.760	3.010	5.03	.973	-.119	.03307
Run 15						
11	0.754	3.000×10^7	6.04	1.016	-0.118	0.06643
Run 16						
1	0.764	2.992×10^7	3.93	0.890	-0.117	[a]0.01661
2	.759	2.980	6.03	1.006	-.126	.07106
Run 17						
1	0.749	2.893×10^7	4.04	0.865	-0.107	0.01648
2	.759	2.954	4.04	.894	-.118	[a].01680
3	.762	2.963	6.04	.970	-.121	.07232

See footnotes on page 18.

TABLE 2.- Continued

(b) Free transition

Point	M	R	α	c_n	c_m	c_d
			Run 18			
1	0.802	4.480×10^6	-2.05	-0.020	-0.098	0.00835
2	.803	4.479	-.99	.148	-.109	.00631
3	.802	4.478	.03	.295	-.113	[a].00689
4	.800	4.468	1.02	.435	-.115	[a].00826
5	.802	4.459	2.05	.614	-.129	.01056
6	.799	4.442	2.09	.600	-.118	[a].00926
7	.799	4.441	2.53	.670	-.124	.01136
8	.803	4.454	3.02	.719	-.128	.01702
9	.800	4.435	3.52	.781	-.135	[a].02100
10	.803	4.440	4.02	.813	-.138	[a].02967
			Run 19			
1	0.779	4.415×10^6	-2.00	0.006	-0.099	0.00738
2	.783	4.454	-.99	.153	-.105	.00636
3	.781	4.444	.01	.294	-.107	.00600
4	.781	4.443	.99	.427	-.108	.00652
[a]5	.780	4.432	2.01	.572	-.106	[a].00718
[a]6	.779	4.415	3.03	.731	-.110	[a].00957
[a]7	.785	4.439	3.52	.796	-.119	[a].01466
[a]8	.777	4.410	4.01	.845	-.117	[a].01835
[a]9	.779	4.412	4.50	.889	-.120	[a].02511
[a]10	.778	4.397	5.01	.930	-.123	[a].03376
[a]11	.779	4.406	6.01	1.014	-.139	[a].05607
			Run 20			
1	0.759	4.423×10^6	-2.01	0.009	-0.097	0.00722
2	.758	4.417	.00	.285	-.103	.00618
3	.758	4.433	1.00	.413	-.103	.00692
4	.760	4.426	2.00	.541	-.100	[a].00741
5	.759	4.433	2.01	.540	-.101	.00722
6	.761	4.466	3.01	.698	-.099	[a].00954
7	.762	4.431	3.50	.780	-.102	[a].01048
8	.764	4.441	4.00	.852	-.107	[a].01568
9	.757	4.411	4.51	.900	-.106	[a].02250
[b]10	.765	4.440	4.52	.900	-.110	[a].02288
11	.762	4.421	5.02	.937	-.108	[a].03095
12	.755	4.400	6.02	1.018	-.107	.04978
13	.760	4.417	7.02	1.085	-.117	.07357

See footnotes on page 18.

TABLE 2.- Continued

(b) Continued

Point	M	R	α	c_n	c_m	c_d
			Run 21			
1	0.739	4.472×10^6	-2.03	0.007	-0.095	0.00721
2	.736	4.478	.00	.276	-.100	.00658
3	.737	4.483	1.00	.402	-.100	.00654
4	.739	4.470	2.00	.527	-.099	.00698
5	.741	4.445	3.00	.666	-.095	.00843
6	.738	4.431	3.49	.738	-.094	.01044
7	.739	4.444	4.03	.828	-.094	[a].01470
8	.737	4.424	4.49	.898	-.096	.02001
9	.737	4.419	5.00	.952	-.095	.02735
10	.746	4.459	6.03	1.001	-.099	[a].04579
[b]11	.738	4.460	6.03	1.038	-.098	.04398
12	.738	4.432	7.01	1.098	-.100	.06162
			Run 22			
13	0.745	4.419×10^6	8.02	1.156	-0.109	0.08576
			Run 23			
1	0.701	4.525×10^6	-2.01	0.021	-0.092	0.00714
2	.699	4.470	.00	.266	-.095	.00672
3	.697	4.461	1.01	.384	-.095	.00650
4	.700	4.505	2.00	.507	-.096	.00689
5	.698	4.492	3.00	.629	-.090	.00778
6	.700	4.474	3.50	.683	-.089	.00861
7	.699	4.464	4.00	.748	-.087	.00967
8	.700	4.474	4.50	.832	-.084	.01240
9	.699	4.458	5.00	.899	-.082	.01698
10	.698	4.452	6.03	1.049	-.081	.03115
11	.700	4.462	7.00	1.128	-.081	.04887
12	.701	4.485	7.99	1.170	-.082	.06418
13	.700	4.478	9.05	1.178	-.087	.07533

See footnotes on page 18.

TABLE 2.- Continued

(b) Continued

Point	M	R	α	c_n	c_m	c_d
			Run 24			
1	0.603	4.516×10^6	-2.12	-0.012	-0.079	0.00786
3	.601	4.491	-.02	.229	-.084	.00609
4	.601	4.490	1.02	.345	-.085	.00635
5	.602	4.491	2.04	.456	-.085	.00679
6	.601	4.480	3.05	.563	-.084	.00746
7	.605	4.490	3.52	.617	-.084	.00780
8	.601	4.474	4.03	.673	-.083	.00809
9	.601	4.468	4.51	.726	-.081	.00858
10	.602	4.464	5.02	.766	-.078	.00960
11	.603	4.460	6.01	.880	-.070	.01445
12	.601	4.445	7.02	1.005	-.060	.02351
13	.601	4.443	8.01	1.061	-.051	.03601
14	.601	4.452	9.04	1.052	-.055	.05453
			Run 25			
1	0.404	4.498×10^6	-2.00	0.016	-0.070	0.00750
2	.400	4.524	-.01	.213	-.073	.00691
3	.401	4.535	1.01	.317	-.075	.00681
4	.403	4.549	2.00	.412	-.077	.00693
5	.402	4.541	3.00	.502	-.075	.00730
6	.400	4.528	3.49	.551	-.075	.00763
7	.402	4.545	4.00	.600	-.076	.00775
8	.402	4.551	4.50	.643	-.075	.00810
9	.401	4.522	4.99	.692	-.075	.00827
10	.403	4.552	6.01	.789	-.075	.00896
11	.400	4.527	7.00	.879	-.075	.00994
12	.400	4.526	8.00	.952	-.071	.01307
13	.402	4.541	8.99	.989	-.060	.02488
14	.401	4.540	10.01	1.006	-.051	.03833
			Run 26			
1	0.799	7.843×10^6	-2.09	-0.035	-0.091	0.00933
2	.802	7.817	-1.00	.128	-.099	.00858
3	.798	7.823	.00	.274	-.103	.00842
4	.800	7.820	1.00	.416	-.106	.00893
5	.801	7.786	2.01	.563	-.108	.01125
[b]6	.798	7.662	2.52	.658	-.125	.01497
7	.802	7.761	2.53	.643	-.115	.01404
8	.801	7.718	3.01	.702	-.117	.01719
9	.804	7.748	3.49	.737	-.123	[a].02322
[b]10	.800	7.757	3.50	.757	-.123	.02158
11	.798	7.721	4.01	.805	-.124	.02824

See footnotes on page 18.

TABLE 2.- Continued

(b) Continued

Point	M	R	α	c_n	c_m	c_d
			Run 27			
1	0.779	7.824×10^6	-2.05	-0.019	-0.092	
2	.779	7.822	-2.05	-.021	-.092	0.00824
3	.781	7.838	-1.01	.129	-.096	.00812
4	.779	7.819	-.00	.268	-.098	.00802
5	.782	7.833	1.00	.407	-.101	.00836
6	.781	7.783	2.00	.554	-.101	.00870
7	.779	7.742	3.00	.703	-.103	.01076
8	.780	7.747	3.00	.704	-.103	.01110
9	.783	7.750	3.49	.769	-.109	[a].01527
10	.781	7.741	4.00	.825	-.112	.02038
11	.783	7.736	4.49	.867	-.116	.02839
12	.780	7.724	5.00	.882	-.109	.03988
			Run 28			
1	0.759	7.835×10^6	-2.02	-0.009	-0.091	0.00792
2	.756	7.846	-.01	.263	-.095	.00775
3	.760	7.841	.99	.397	-.097	.00806
4	.760	7.833	2.00	.533	-.097	.00835
5	.760	7.823	3.00	.678	-.094	.01022
6	.760	7.798	3.49	.760	-.096	.01261
7	.763	7.794	4.00	.824	-.099	.01696
8	.758	7.758	4.49	.877	-.098	.02431
9	.763	7.730	5.00	.914	-.103	.03392
10	.756	7.691	6.02	.991	-.103	.05504
[c]11	.754	7.635	5.00	.919	-.099	.03253
[c]12	.759	7.684	4.51	.879	-.100	.02394
[c]13	.759	7.740	4.00	.825	-.099	.01689
[c]14	.763	7.764	3.51	.757	-.095	[a].01227
[c]15	.763	7.726	2.00	.680	-.095	
[c]16	.752	7.314	.99	.395	-.098	.00795

See footnotes on page 18.

TABLE 2.- Continued

(b) Continued

Point	M	R	α	c_n	c_m	c_d
			Run 29			
1	0.740	7.790×10^6	-2.05	-0.010	-0.089	0.00778
2	.737	7.783	.00	.261	-.093	.00760
3	.738	7.798	1.00	.389	-.095	.00781
4	.733	7.799	1.99	.512	-.093	.00805
5	.743	7.779	3.01	.654	-.092	.00964
6	.740	7.731	3.50	.730	-.090	.01159
8	.743	7.797	4.00	.826	-.093	.01677
9	.740	7.780	4.50	.891	-.091	.02186
10	.742	7.789	5.00	.939	-.092	.02992
11	.744	7.791	6.01	1.005	-.094	.04705
12	.741	7.733	7.01	.995	-.102	.08168
			Run 30			
1	0.756	7.813×10^6	0.00	0.264	-0.096	0.00777
2	.758	7.837	2.01	.534	-.097	.00836
3	.756	7.642	3.50	.761	-.097	[a].01271
4	.758	7.725	3.99	.823	-.097	.01690
5	.756	7.751	4.50	.888	-.101	.02424
[b]6	.762	7.781	2.01	.534	-.097	.00837
[b]7	.762	7.792	3.49	.764	-.097	.01264
[b]8	.761	7.790	4.00	.833	-.100	.01706
[b]9	.762	7.795	4.49	.892	-.105	.02365
			Run 31			
1	0.700	7.827×10^6	-2.01	-0.014	-0.085	0.00756
2	.700	7.836	.06	.243	-.089	.00759
3	.700	7.827	1.04	.365	-.090	.00780
4	.702	7.843	2.04	.488	-.090	.00795
5	.700	7.786	3.08	.619	-.089	.00842
6	.699	7.775	3.55	.681	-.086	.00896
7	.697	7.745	4.04	.730	-.084	.01025
8	.699	7.771	4.53	.814	-.082	.01294
9	.707	7.746	5.02	.909	-.081	.01892
10	.700	7.757	6.04	1.017	-.075	.03158
11	.700	7.721	7.03	1.102	-.076	.05126
12	.701	7.719	8.01	1.085	-.093	.08795

See footnotes on page 18.

TABLE 2.- Continued

(b) Continued

Point	M	R	α	c_n	c_m	c_d
			Run 32			
1	0.604	7.754×10^6	-2.01	0.006	-0.080	0.00733
2	.603	7.771	-.00	.238	-.082	.00730
3	.602	7.787	.99	.348	-.083	.00744
4	.603	7.798	1.99	.458	.084	.00762
5	.601	7.752	3.00	.569	-.084	.00791
6	.603	7.791	3.50	.623	-.083	.00817
7	.601	7.779	4.00	.680	-.083	.00837
8	.599	7.732	4.51	.732	-.081	.00861
9	.600	7.729	5.00	.783	-.078	.00960
10	.603	7.787	6.01	.893	-.071	.01507
11	.600	7.726	7.01	.985	-.063	.02502
[b]12	.603	7.796	7.04	.988	-.064	.02532
13	.607	7.817	8.00	1.068	-.054	.04054
14	.602	7.780	9.01	1.030	-.056	.05489
			Run 33			
1	0.804	1.399×10^7	-2.01	-0.017	-0.098	[a]0.00907
2	.801	1.396	-.98	.136	-.102	.00772
3	.797	1.390	.02	.282	-.106	.00776
4	.799	1.393	1.00	.428	-.110	.00826
5	.804	1.395	2.00	.581	-.117	[a].01230
6	.804	1.391	2.50	.650	-.121	.01444
7	.806	1.391	3.01	.708	-.125	.01990
8	.801	1.385	3.51	.770	-.128	.02341
9	.805	1.376	4.09	.750	-.122	[a].03298
			Run 34			
1	0.779	1.416×10^7	-2.01	-0.032	-0.095	0.00750
2	.773	1.405	-1.00	.128	-.098	.00724
3	.778	1.416	.02	.270	-.102	.00726
4	.778	1.408	1.03	.411	-.103	.00750
5	.775	1.397	2.04	.551	-.102	.00800
6	.777	1.387	3.05	.705	-.103	.01010
7	.776	1.388	3.52	.768	-.105	.01408
8	.778	1.389	4.08	.837	-.115	[a].02055
9	.786	1.460	4.52	.906	-.130	.03211
10	.779	1.417	5.02	.906	-.118	.03808
11	.769	1.381	6.05	.919	-.110	.07040

See footnotes on page 18.

TABLE 2.- Continued

(b) Continued

Point	M	R	α	c_n	c_m	c_d
Run 35 (repeat of run 33)						
1	0.803	1.405×10^7	-0.99	0.134	-0.103	0.00787
2	.800	1.403	.01	.281	-.107	.00778
3	.804	1.384	2.02	.587	-.121	[a].01217
[b]4	.803	1.397	2.04	.591	-.119	.01179
5	.801	1.392	2.50	.654	-.120	.01386
[b]6	.802	1.393	2.52	.653	-.120	.01457
7	.797	1.399	1.00	.425	-.109	.00818
Run 36						
1	0.760	1.416×10^7	-2.01	-0.011	-0.094	0.00735
2	.757	1.403	.01	.263	-.098	.00719
3	.761	1.407	1.01	.404	-.101	.00744
4	.761	1.404	2.00	.538	-.100	.00774
5	.768	1.407	3.04	.699	-.098	[a].00959
6	.759	1.398	3.51	.764	-.097	.01216
7	.762	1.401	4.03	.843	-.105	[a].01673
8	.764	1.402	4.53	.884	-.105	.02303
9	.761	1.404	5.02	.934	-.104	.03157
10	.762	1.403	6.03	.957	-.113	.05901
Run 37						
1	0.742	1.408×10^7	-2.02	-0.011	-0.092	0.00718
2	.739	1.405	-.01	.262	-.096	.00707
3	.743	1.407	1.00	.395	-.097	.00724
4	.740	1.402	2.02	.524	-.097	.00749
5	.741	1.401	3.01	.663	-.093	.00892
6	.740	1.398	3.51	.737	-.092	.01120
7	.742	1.388	4.03	.826	-.094	.01602
8	.738	1.411	4.49	.872	-.090	.02121
9	.744	1.403	5.01	.933	-.095	.02999
10	.740	1.394	6.03	1.025	-.095	.04569
11	.743	1.399	7.02	.999	-.102	.07602

See footnotes on page 18.

TABLE 2.- Continued

(b) Continued

Point	M	R	α	c_n	c_m	c_d
			Run 38			
1	0.702	1.413×10^7	-2.00	-0.003	-0.089	0.00699
2	.703	1.417	-.00	.245	-.092	.00701
3	.703	1.417	1.02	.380	-.094	.00709
4	.703	1.415	2.03	.501	-.093	.00730
5	.701	1.419	3.01	.632	-.091	.00786
6	.697	1.402	3.50	.690	-.088	.00841
7	.710	1.406	4.03	.770	-.087	.01086
8	.709	1.428	4.50	.842	-.086	.01426
9	.704	1.406	5.00	.904	-.080	
[b]10	.706	1.405	5.01	.917	-.082	.01916
11	.701	1.399	6.02	1.041	-.079	.03260
12	.704	1.410	7.04	1.112	-.078	.05286
			Run 39			
1	0.606	1.429×10^7	-2.03	0.002	-0.082	
[b]2	.601	1.406	-2.03	.004	-.082	0.00682
3	.603	1.401	-.01	.240	-.085	.00670
4	.601	1.402	1.00	.353	-.085	.00683
5	.604	1.419	2.01	.469	-.087	.00697
6	.602	1.411	2.99	.580	-.086	.00735
7	.603	1.409	3.49	.641	-.087	.00754
8	.602	1.410	4.00	.699	-.087	.00775
10	.602	1.421	4.49	.751	-.084	.00810
11	.606	1.414	5.00	.803	-.081	.00949
12	.604	1.409	6.00	.921	-.073	.01506
13	.601	1.389	7.00	.995	-.064	.02490
14	.606	1.425	8.00	1.039	-.054	.04507
			Run 40			
1	0.800	3.009×10^7	-2.08	-0.020	-0.102	0.00813
2	.800	2.982	-.98	.143	-.107	.00681
3	.804	3.045	.05	.306	-.116	[a].00728
4	.801	3.027	1.02	.447	-.117	.00792
5	.801	2.992	2.04	.593	-.122	[a].01130
6	.801	2.992	2.54	.669	-.127	.01481
8	.801	2.997	3.01	.718	-.131	.01972
9	.805	3.010	3.53	.756	-.131	.02780

See footnotes on page 18.

TABLE 2.- Continued

(b) Continued

Point	M	R	α	c_n	c_m	c_d
			Run 41			
1	0.780	2.983×10^7	-2.03	-0.014	-0.100	0.00680
2	.780	2.987	-.98	.147	-.104	.00651
3	.785	3.003	.03	.294	-.108	.00669
4	.781	2.979	1.03	.435	-.109	.00671
5	.781	2.999	2.04	.595	-.111	.00722
6	.783	3.010	3.03	.743	-.118	.01255
7	.783	2.988	3.53	.791	-.120	[a].01626
8	.781	3.004	4.03	.859	-.125	.02220
9	.783	3.003	4.53	.892	-.130	.03191
10	.780	2.990	5.04	.898	-.126	.04301
			Run 43			
1	0.763	3.039×10^7	-2.01	-0.002	-0.098	0.00653
2	.760	3.024	.01	.283	-.103	.00640
3	.758	3.013	1.01	.420	-.104	.00651
4	.761	3.003	2.04	.562	-.104	.00700
5	.762	2.987	3.03	.727	-.103	[a].00876
6	.763	2.997	3.53	.816	-.111	[a].01213
7	.759	2.974	4.02	.864	-.110	[a].01560
8	.762	2.996	4.53	.916	-.113	.02384
9	.765	2.976	5.01	.961	-.120	.03312
10	.760	2.994	6.04	.998	-.120	[a].06696
[c]11	.760	2.986	4.96	.968	-.117	.03070
[c]12	.760	2.980	4.47	.915	-.112	[a].02269
[b]13	.759	3.030	.01	.281	-.103	
[b]14	.760	3.010	.01	.283	-.103	.00637
[b]15	.762	3.030	1.02	.425	-.106	.00661
[b]16	.762	3.029	2.04	.564	-.105	.00694
[b]17	.759	3.000	3.02	.728	-.104	.00881
			Run 44			
1	0.743	2.999×10^7	-2.13	-0.014	-0.096	0.00645
2	.739	2.999	.02	.279	-.100	.00632
3	.738	3.000	1.03	.414	-.101	.00633
4	.743	3.000	2.04	.550	-.102	.00677
5	.741	3.004	3.03	.696	-.098	.00854
6	.741	3.000	3.52	.780	-.098	.01196
7	.743	2.983	4.04	.857	-.098	.01605
8	.740	2.984	4.53	.924	-.100	.02234
9	.742	2.960	5.03	.991	-.105	.03238
10	.741	2.973	6.03	1.046	-.104	.04957

See footnotes on page 18.

TABLE 2.- Continued

(b) Continued

Point	M	R	α	c_n	c_m	c_d
			Run 45			
1	0.702	3.021×10^7	-2.00	0.009	-0.092	0.00629
2	.702	3.008	.03	.270	-.096	.00625
3	.702	3.019	1.03	.399	-.096	.00635
4	.701	3.004	2.04	.526	-.097	.00657
5	.704	3.039	3.03	.660	-.094	.00706
6	.702	2.997	3.53	.706	-.093	.00801
7	.701	3.005	4.01	.787	-.089	.00963
8	.704	3.035	4.51	.869	-.087	[a].01388
9	.704	2.995	5.01	.944	-.085	.01947
10	.704	2.989	6.02	1.087	-.085	.03501
11	.703	3.006	7.03	1.150	-.085	.05298
12	.707	3.009	8.05	1.092	-.098	[a].08398
			Run 46			
1	0.404	3.025×10^7	-2.00	0.011	-0.075	0.00609
2	.400	3.000	.06	.229	-.078	.00596
3	.399	2.989	1.06	.332	-.078	.00619
4	.401	2.986	2.04	.435	-.079	.00641
5	.401	2.994	3.00	.531	-.080	.00671
6	.401	3.008	3.52	.586	-.080	.00676
7	.399	2.981	4.01	.636	-.081	.00714
8	.402	3.009	4.51	.688	-.081	.00728
9	.401	2.996	5.02	.740	-.081	.00746
10	.399	2.958	6.00	.836	-.080	.00809
11	.400	2.969	7.02	.939	-.080	.00910
12	.399	2.961	8.02	1.004	-.073	.01401
13	.401	2.983	9.00	1.038	-.057	.04130
			Run 47			
1	0.599	2.981×10^7	-2.02	0.012	-0.084	0.00625
2	.600	3.000	-.01	.255	-.088	.00602
3	.601	3.011	1.00	.372	-.088	.00618
4	.600	3.013	2.01	.487	-.089	.00639
5	.601	3.019	3.00	.602	-.089	.00684
6	.600	3.016	3.51	.660	-.089	.00707
7	.602	3.027	3.98	.715	-.088	.00726
8	.601	3.000	4.50	.771	-.086	.00805
9	.599	3.014	5.00	.818	-.083	.00891
10	.601	3.003	6.02	.950	-.073	[a].01496
11	.603	3.015	7.01	1.024	-.066	[a].02512
12	.598	3.008	8.02	1.045	-.055	[a].04282

See footnotes on page 18.

TABLE 2.- Continued

(b) Continued

Point	M	R	α	c_n	c_m	c_d
Run 48						
1	0.802	5.010×10^7	-1.99	0.002	-0.106	0.00760
2	.800	4.991	-.97	.158	-.112	.00626
3	.801	5.021	.00	.314	-.117	.00651
4	.802	5.009	1.00	.468	-.123	[a].00785
Run 49						
[b]2	0.806	4.537×10^7	-2.12	-0.023	-0.104	[a]0.00897
3	.806	4.532	-1.99	.000	-.106	.00825
4	.804	4.519	-.99	.157	-.112	.00668
5	.803	4.518	.02	.312	-.117	[a].00659
6	.803	4.531	1.02	.468	-.123	[a].00837
Run 50						
1	0.701	4.491×10^7	-2.06	0.004	-0.093	0.00589
2	.701	4.499	.02	.274	-.097	.00583
3	.702	4.511	1.02	.405	-.098	.00595
4	.702	4.508	2.04	.536	-.098	.00608
5	.704	4.520	3.00	.669	-.096	.00657
6	.701	4.498	3.49	.714	-.094	.00734
7	.700	4.485	4.00	.799	-.091	.00932
8	.701	4.479	4.52	.874	-.088	[a].01279
9	.699	4.488	5.01	.953	-.085	[a].01849
10	.707	4.523	6.01	1.112	-.092	
Run 51						
1	0.803	4.467×10^7	2.03	0.611	-0.132	[a]0.01321
2	.799	4.478	2.54	.702	-.137	.01590
Run 52						
1	0.760	4.501×10^7	-2.02	-0.000	-0.100	0.00613
2	.762	4.489	.02	.294	-.106	.00590
3	.762	4.513	1.02	.437	-.107	.00615
4	.761	4.495	2.02	.577	-.107	.00639
5	.761	4.492	3.02	.735	-.103	.00810
6	.756	4.491	3.53	.825	-.110	.01127
7	.770	4.524	4.02	.905	-.129	[a].02043

See footnotes on page 18.

TABLE 2.- Concluded

(b) Concluded

Point	M	R	α	c_n	c_m	c_d
Run 53						
1	0.784	4.483×10^7	-1.98	-0.002	-0.102	0.00642
2	.781	4.457	-.98	.156	-.107	.00626
3	.780	4.455	-.02	.300	-.110	.00614
4	.784	4.464	1.03	.454	-.113	.00652
5	.779	4.438	2.04	.603	-.111	.00683
6	.785	4.479	3.01	.779	-.131	[a].01468
[b]7	.784	4.463	3.01	.770	-.127	[a].01536
[b]8	.783	4.462	2.03	.612	-.116	.00754
9	.780	4.453	2.49	.686	-.114	.00929
Run 55						
1	0.737	4.484×10^7	0.01	0.287	-0.102	0.00589
2	.739	4.501	1.00	.423	-.103	.00606
3	.741	4.493	2.00	.559	-.103	.00618
4	.742	4.494	3.00	.720	-.101	.00803
5	.740	4.479	4.00	.868	-.101	.01579

See footnotes on page 18.

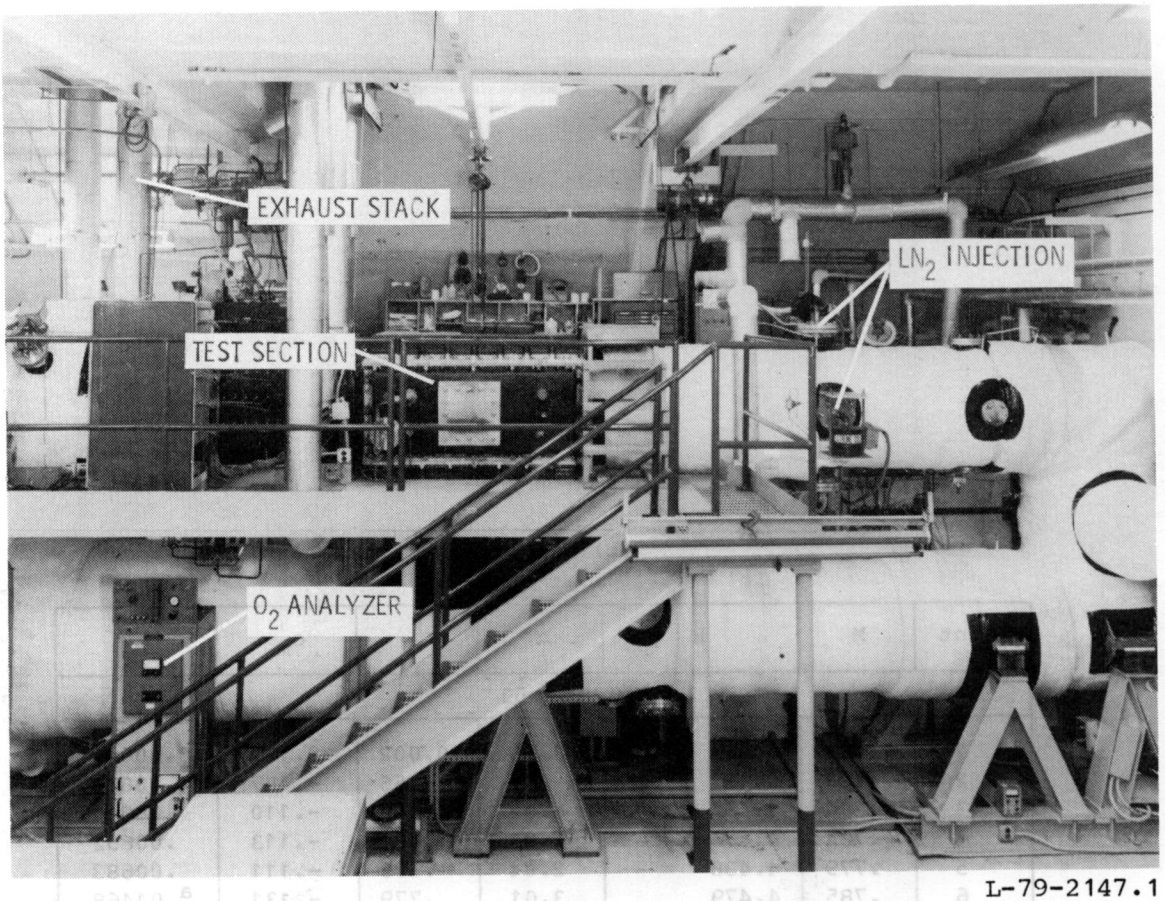

(a) Photograph.

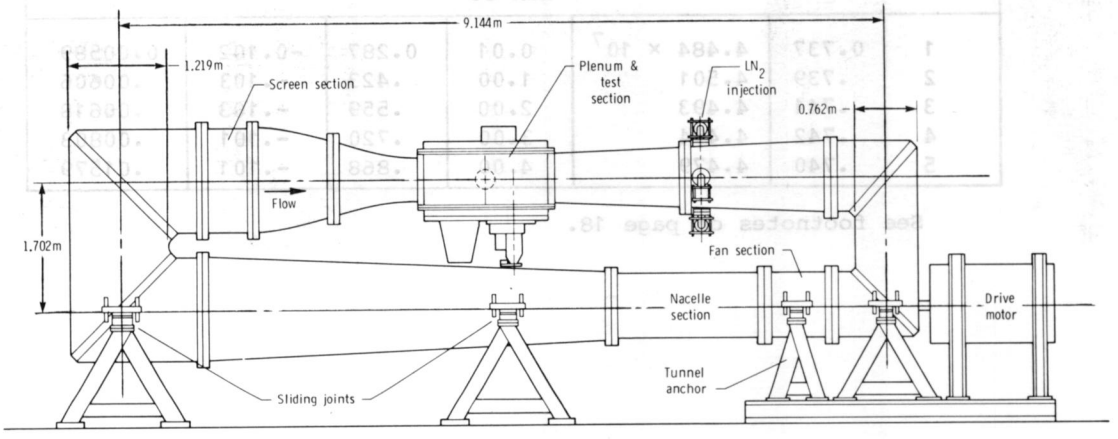

(b) Schematic drawing.

Figure 1.- Elevation view of Langley 0.3-Meter Transonic Cryogenic Tunnel with two-dimensional test section installed.

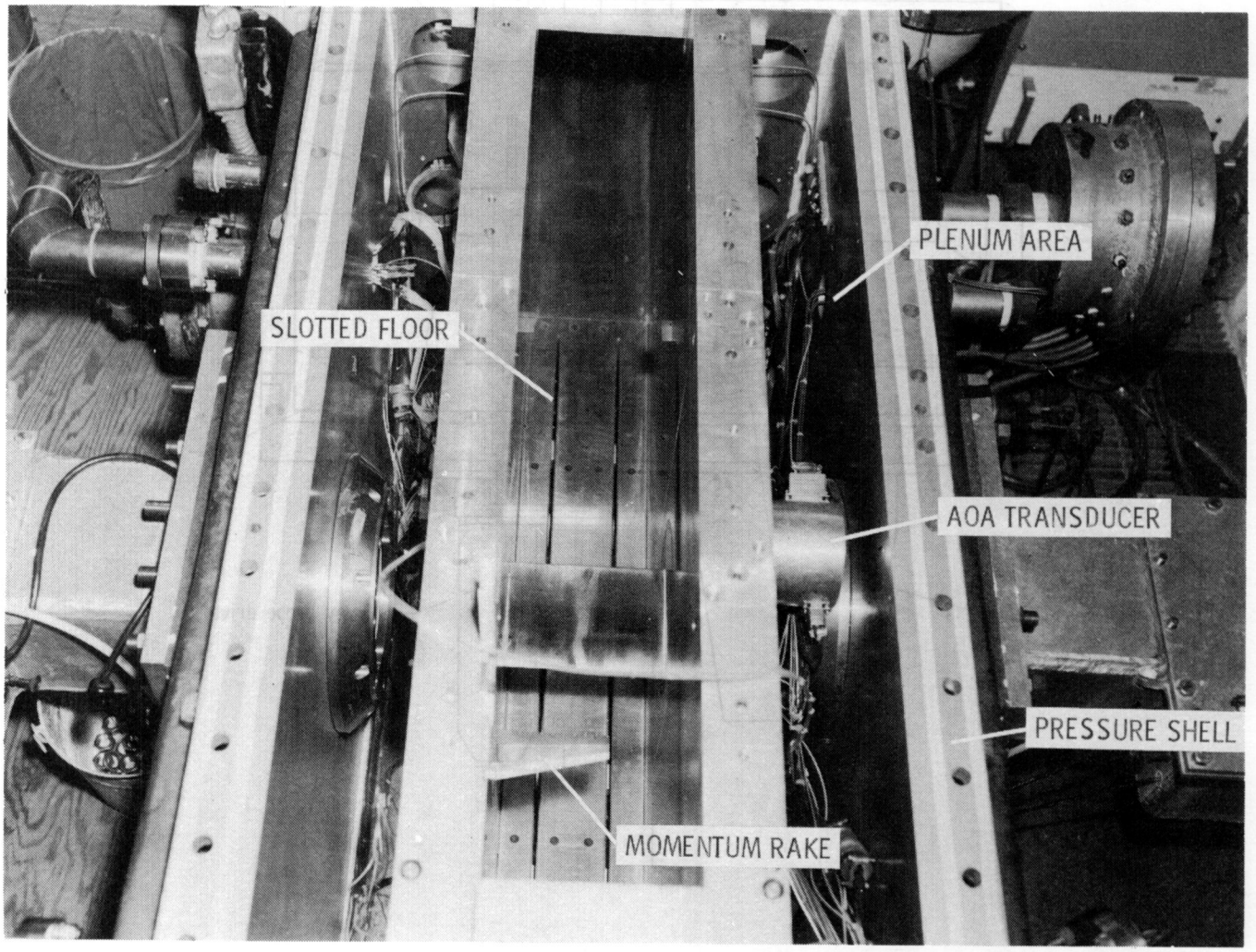

L-79-8913.1

(a) Top-view photograph.

Figure 2.- Two-dimensional test section.

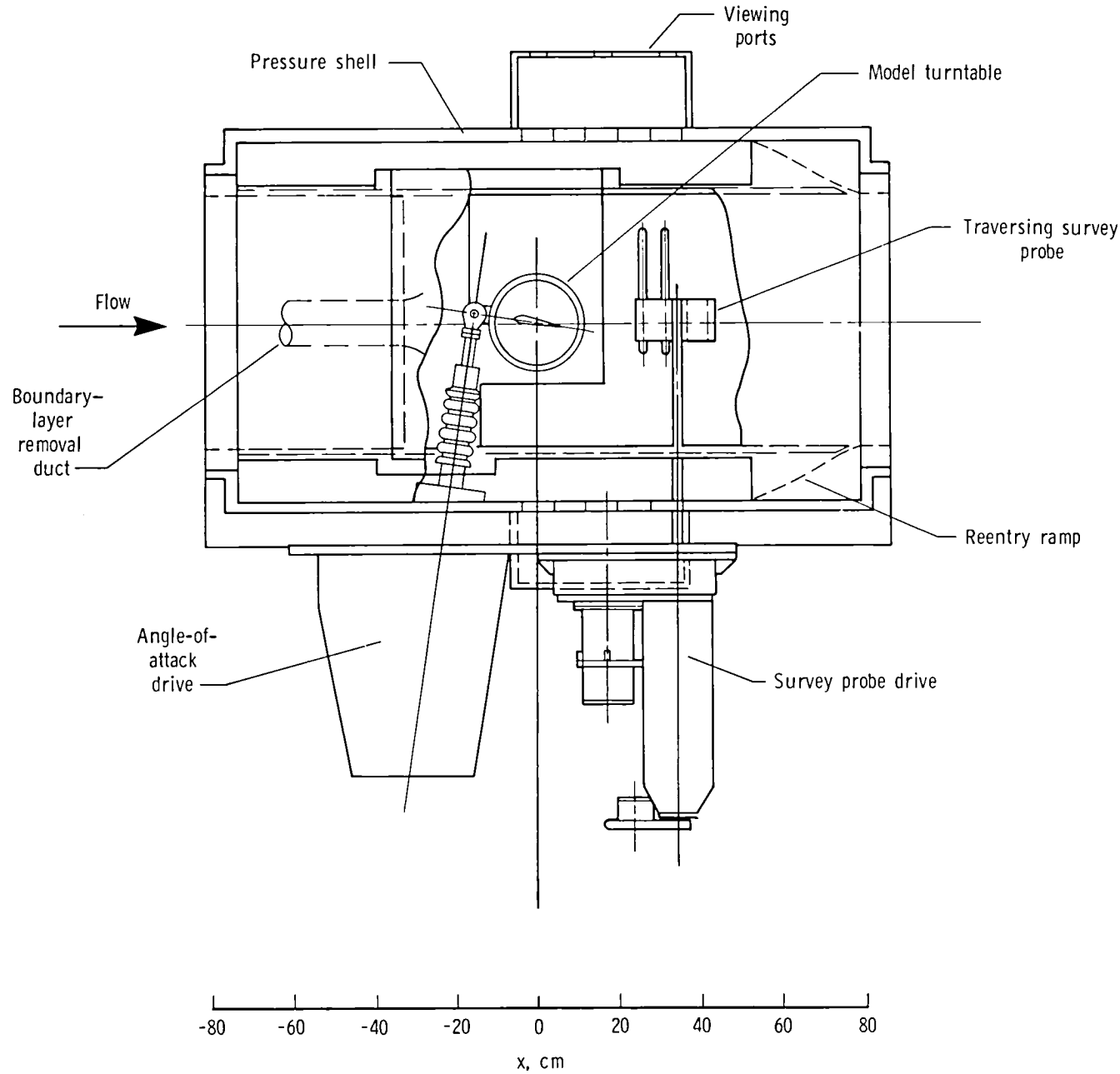

(b) Schematic drawing showing major components.

Figure 2.- Concluded.

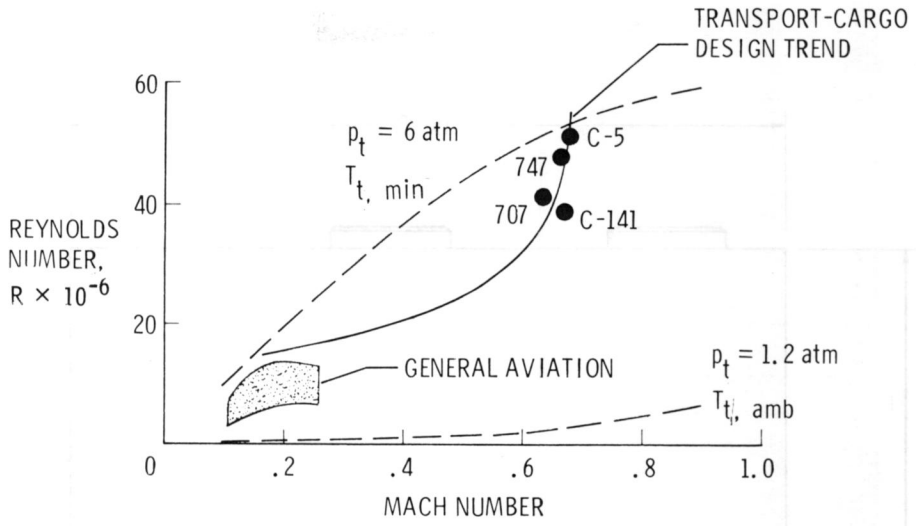

Figure 3.- Reynolds number capability of two-dimensional test section of Langley 0.3-Meter Transonic Cryogenic Tunnel.

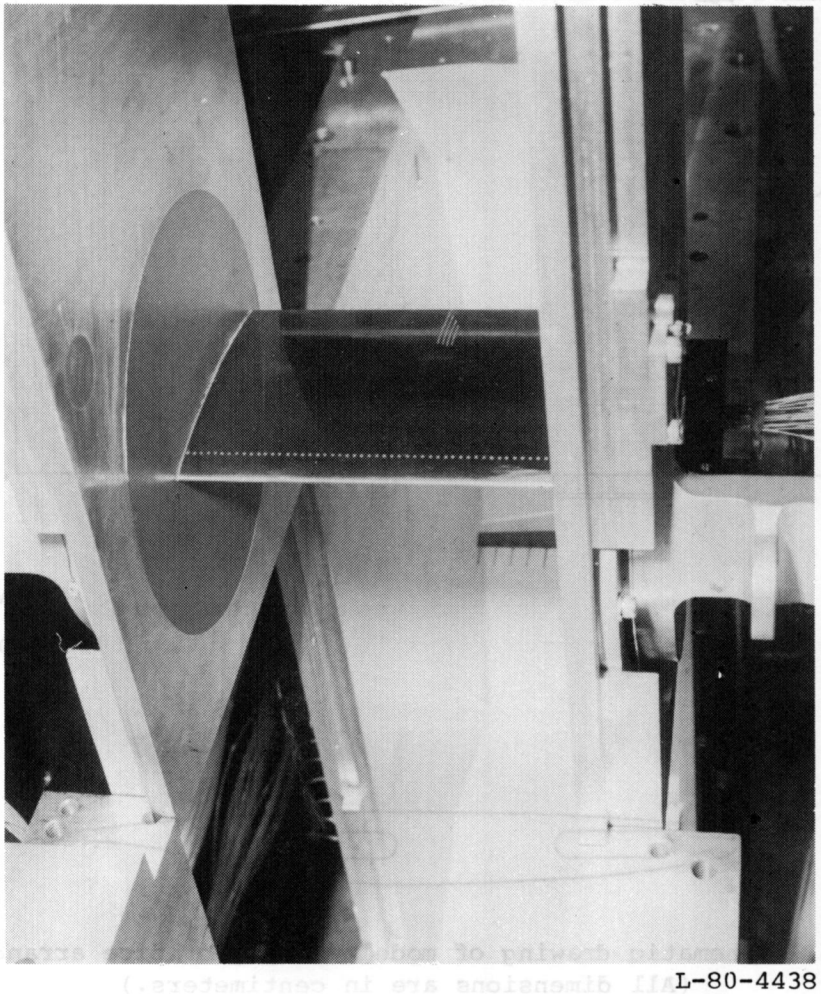

L-80-4438

Figure 4.- Installation of airfoil model in tunnel test section.

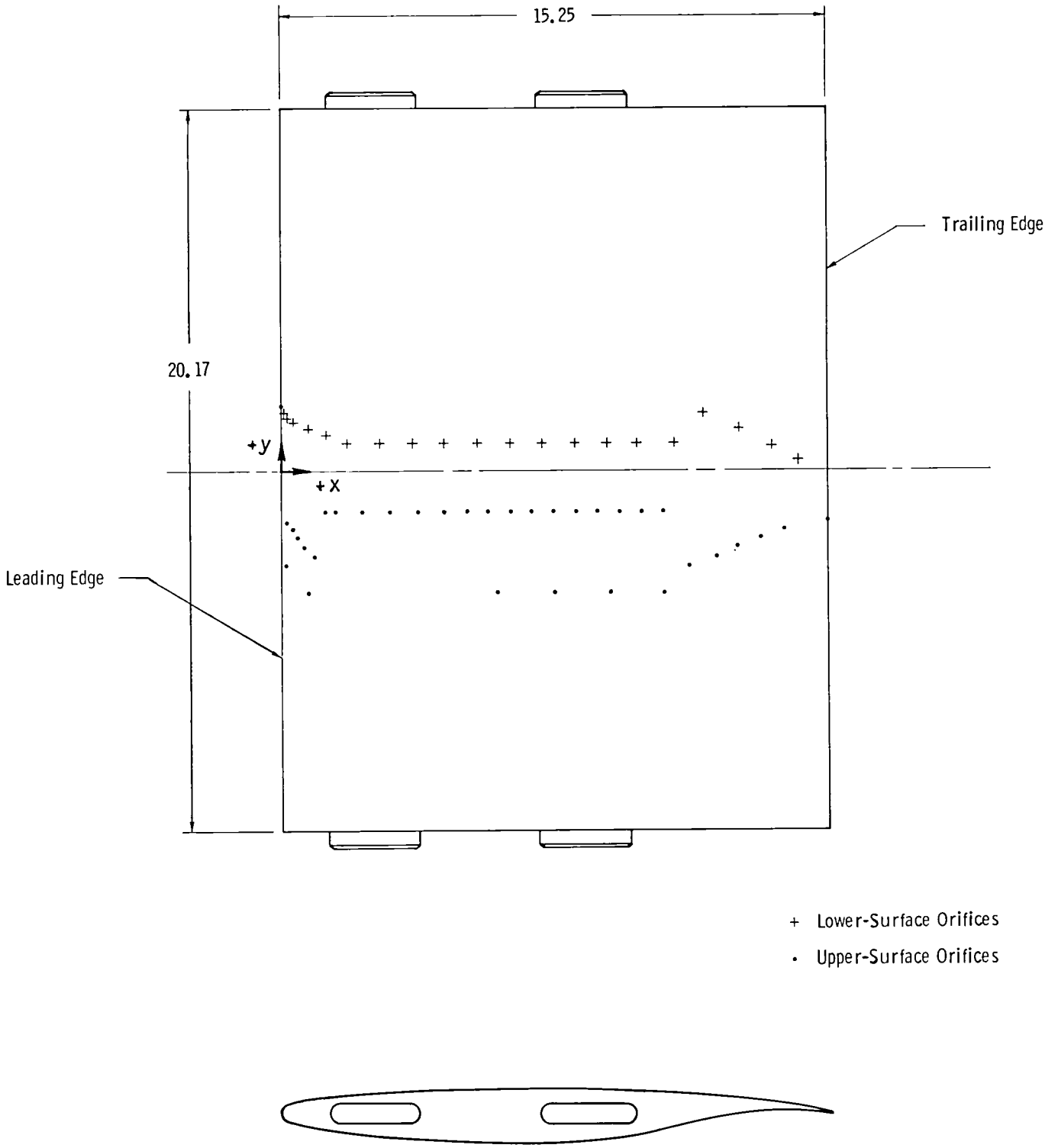

Figure 5.- Schematic drawing of model showing orifice arrangement.
(All dimensions are in centimeters.)

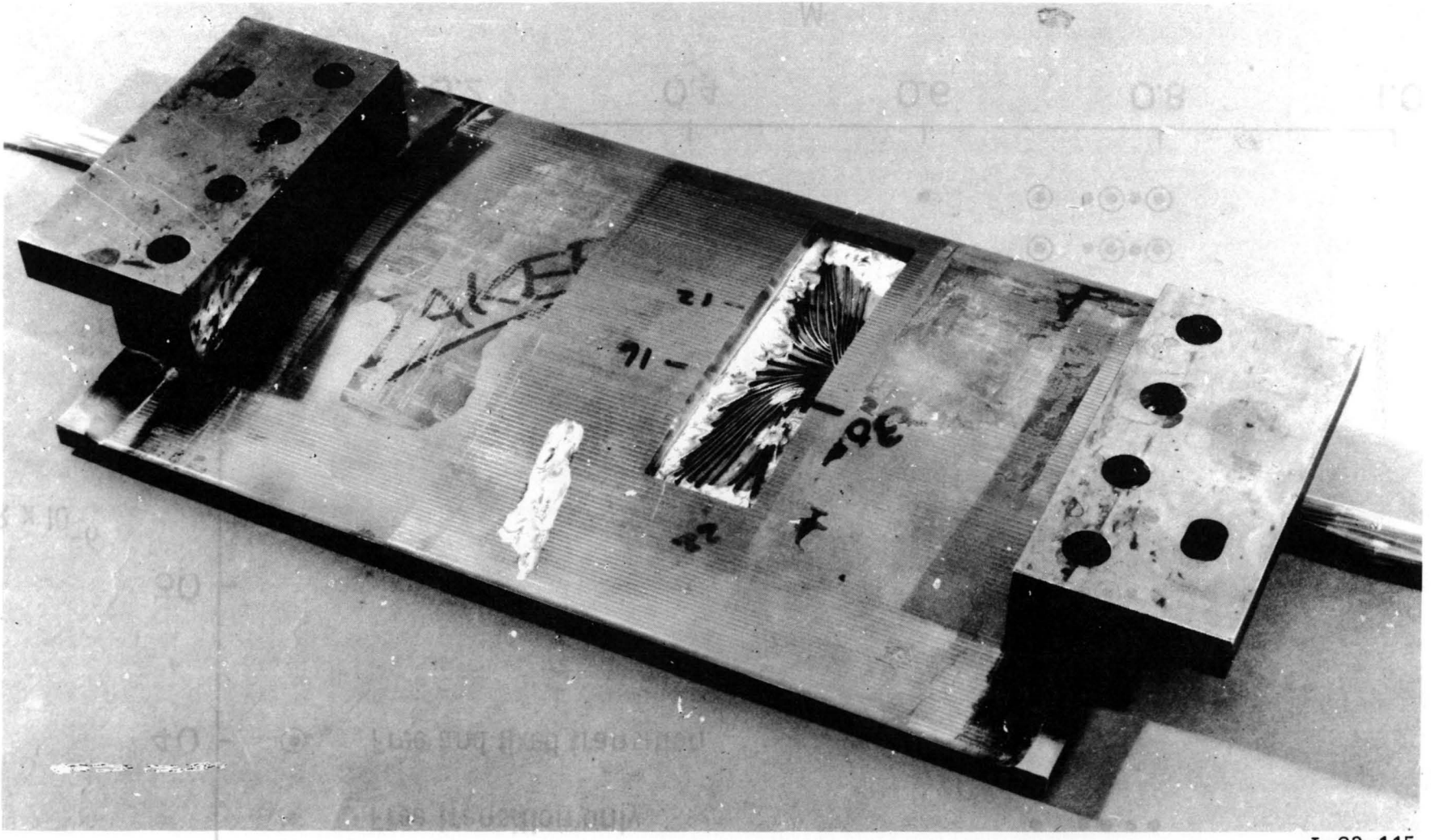

L-82-115

Figure 6.- Model under construction.

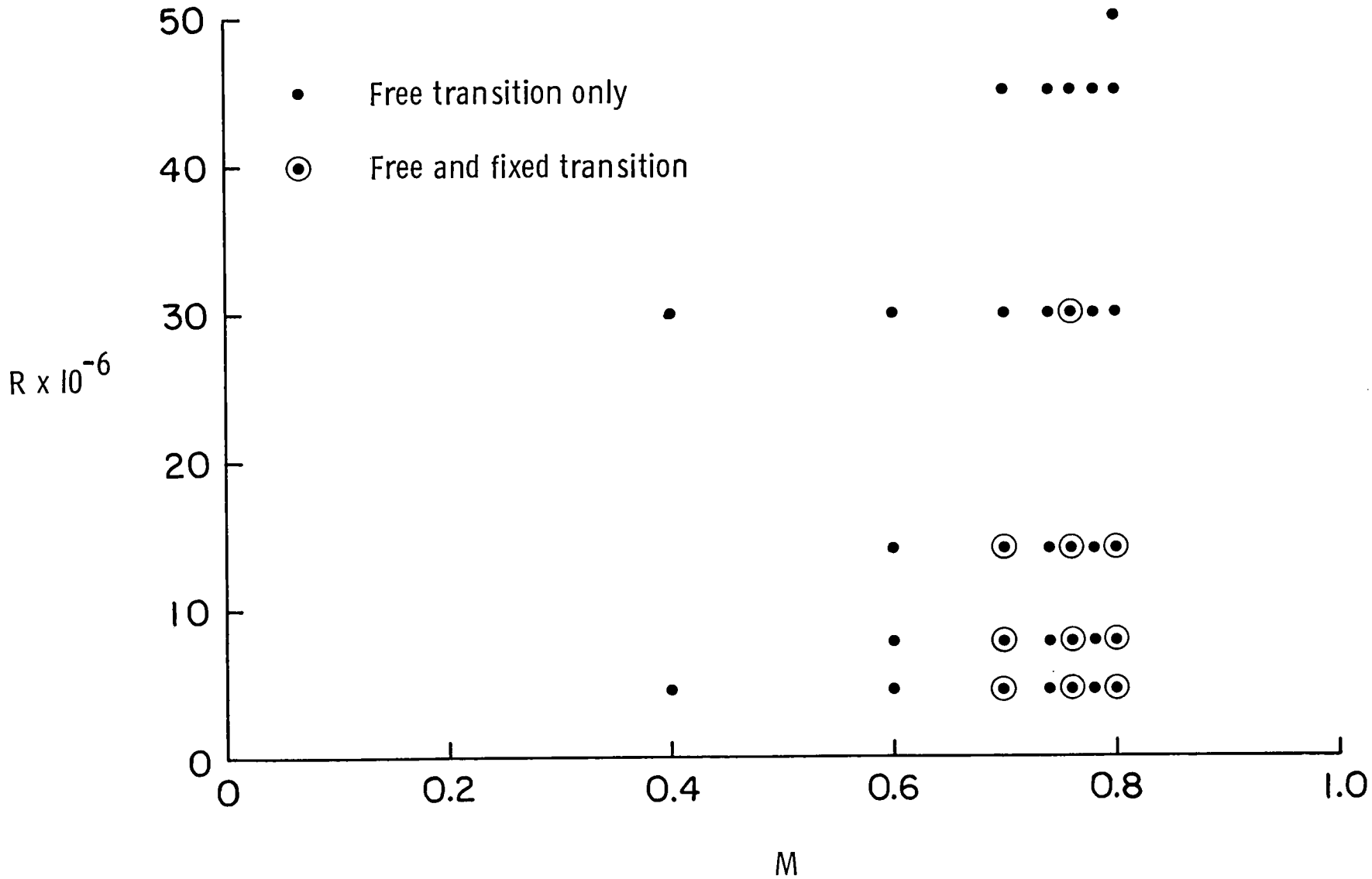

Figure 7.- Range of Reynolds number and Mach number used in test program.

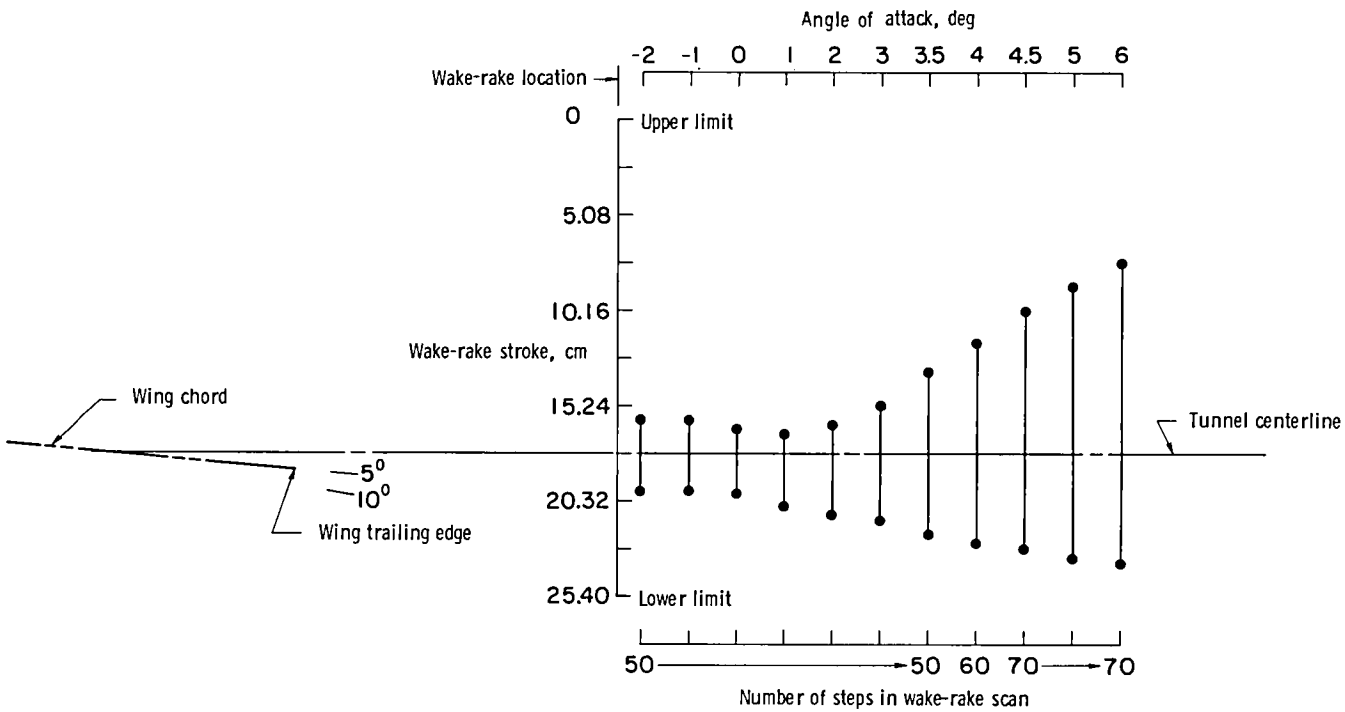

Figure 8.- Variation of stroke length and number of steps used to define wake at $M \approx 0.76$.

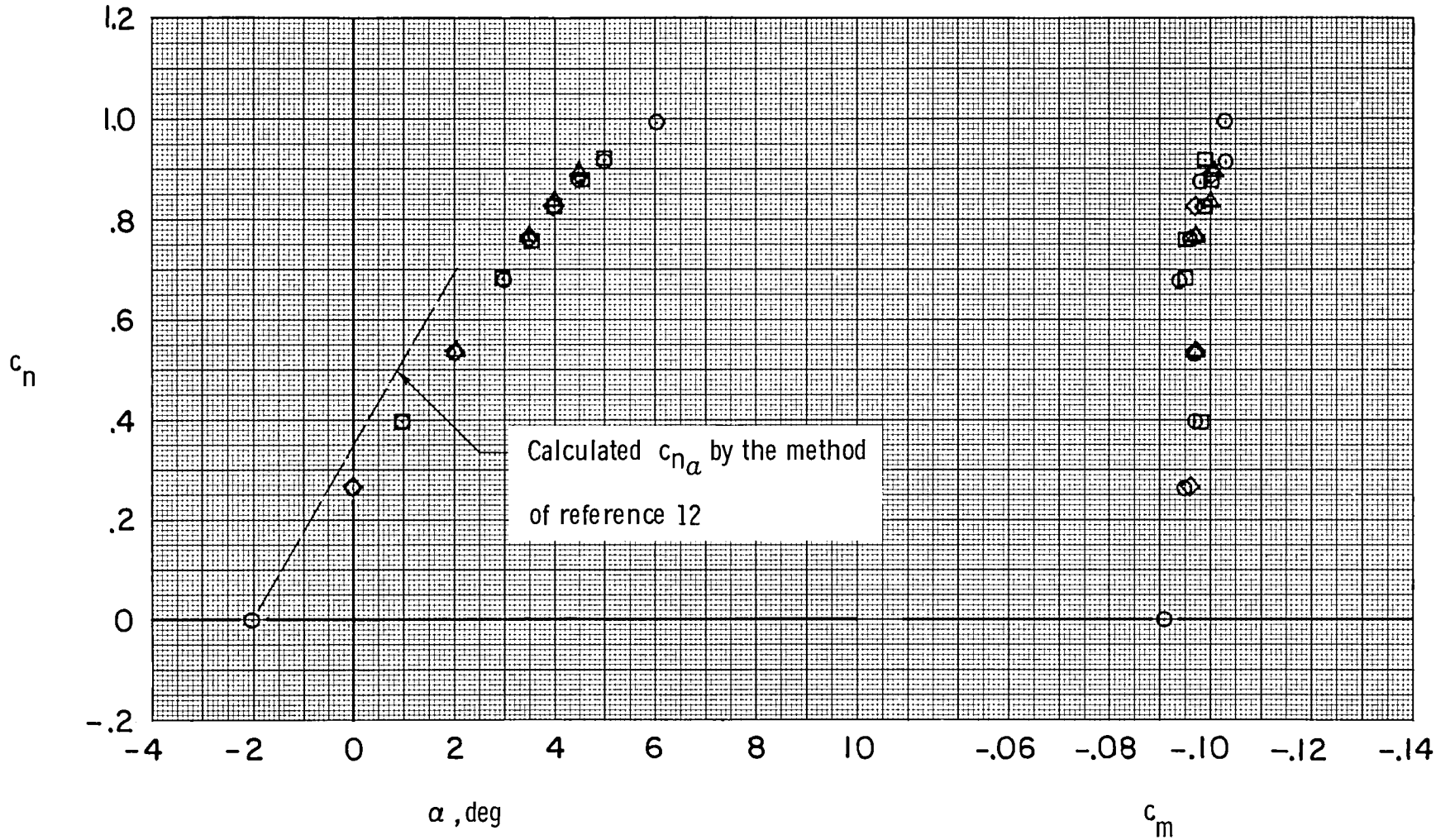

(a) c_n vs α and c_m.

Figure 9.- Repeatability of four sets of data $(\bigcirc, \square, \diamond, \triangle)$ with free transition at $M \approx 0.76$ and $R \approx 7.7 \times 10^6$.

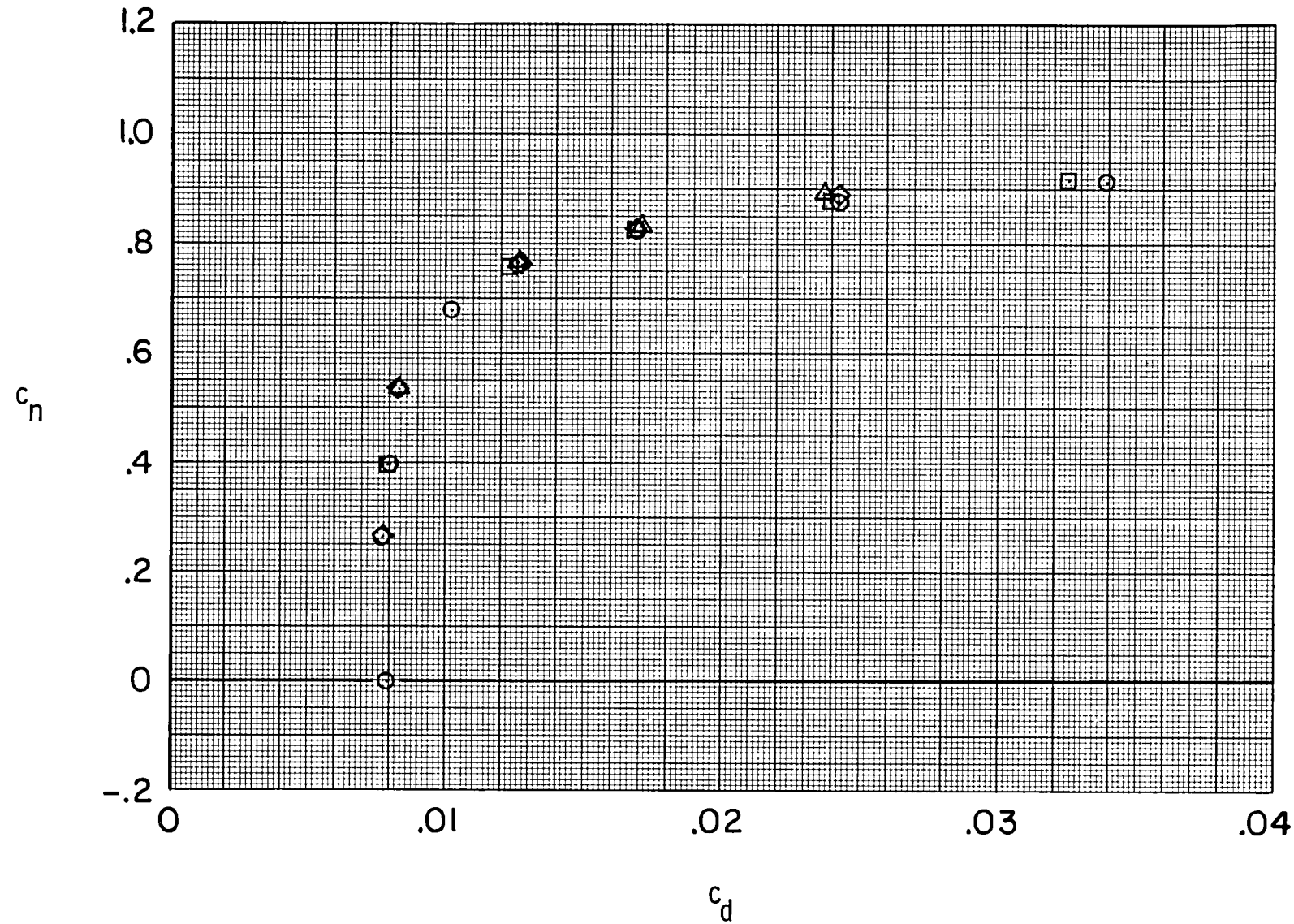

(b) c_n vs c_d.

Figure 9.- Concluded.

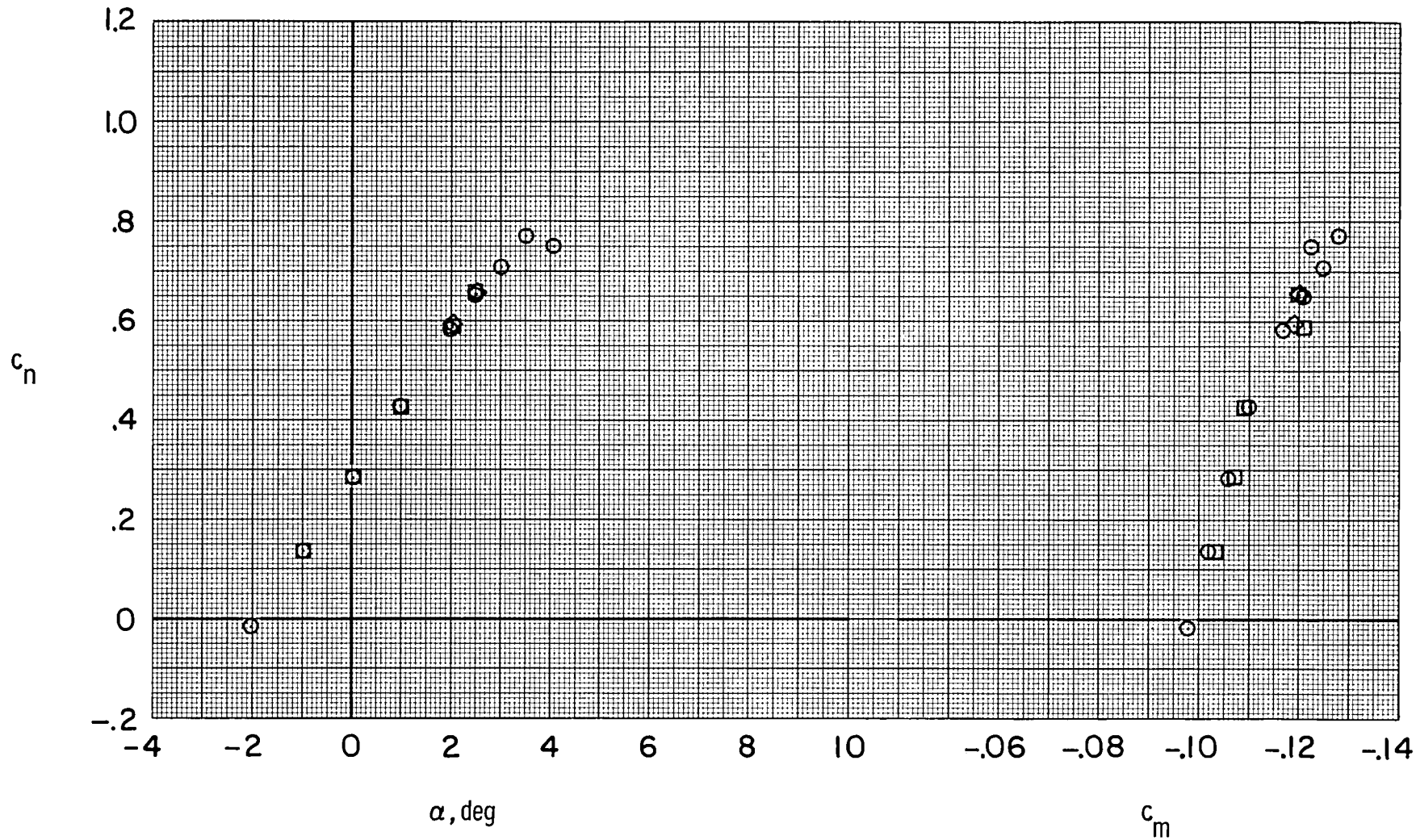

(a) c_n vs α and c_m.

Figure 10.- Repeatability of three sets of data $(\bigcirc, \square, \diamond)$ with free transition at $M \approx 0.80$ and $R \approx 14.0 \times 10^6$.

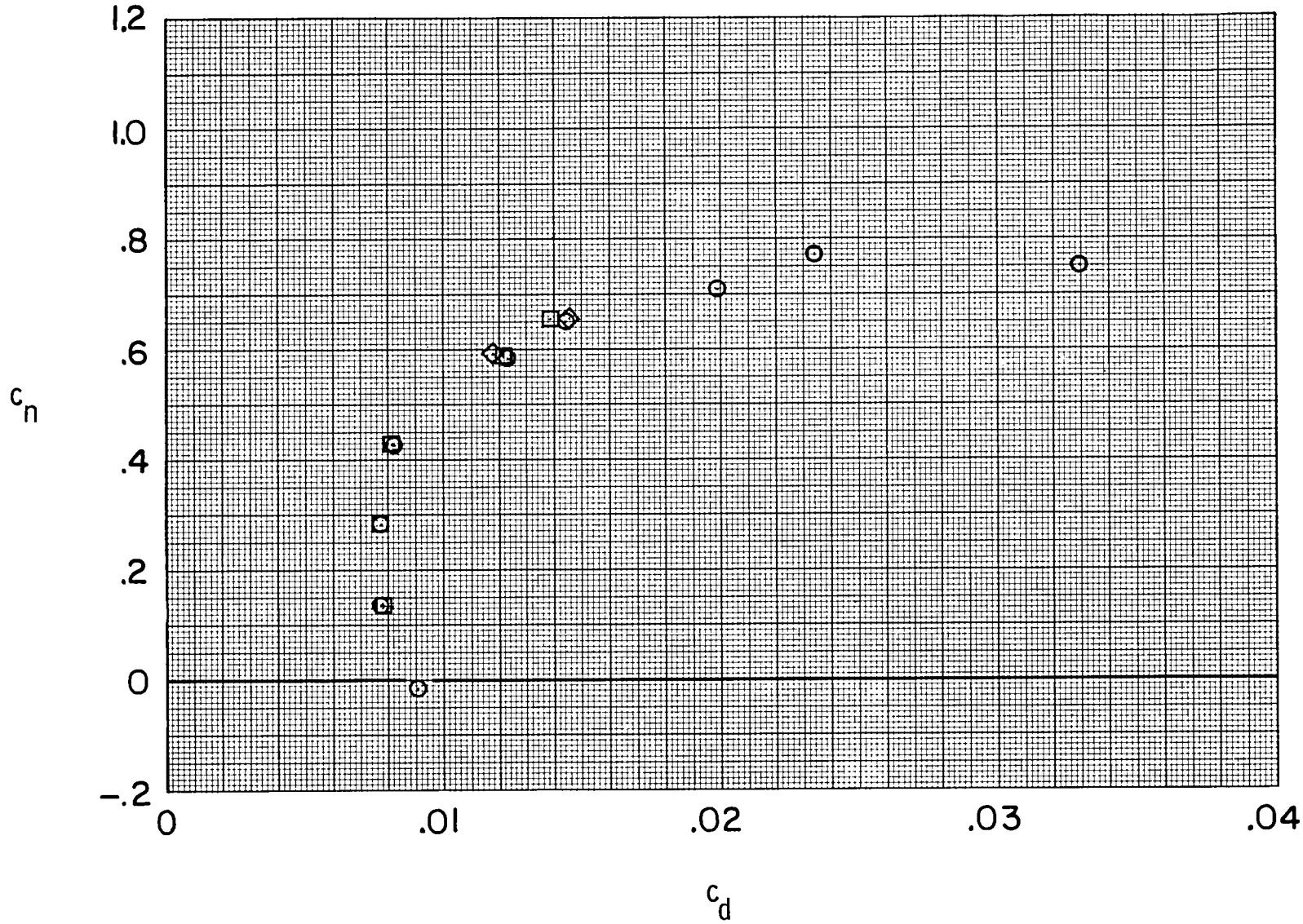

(b) c_n vs c_d.

Figure 10.- Concluded.

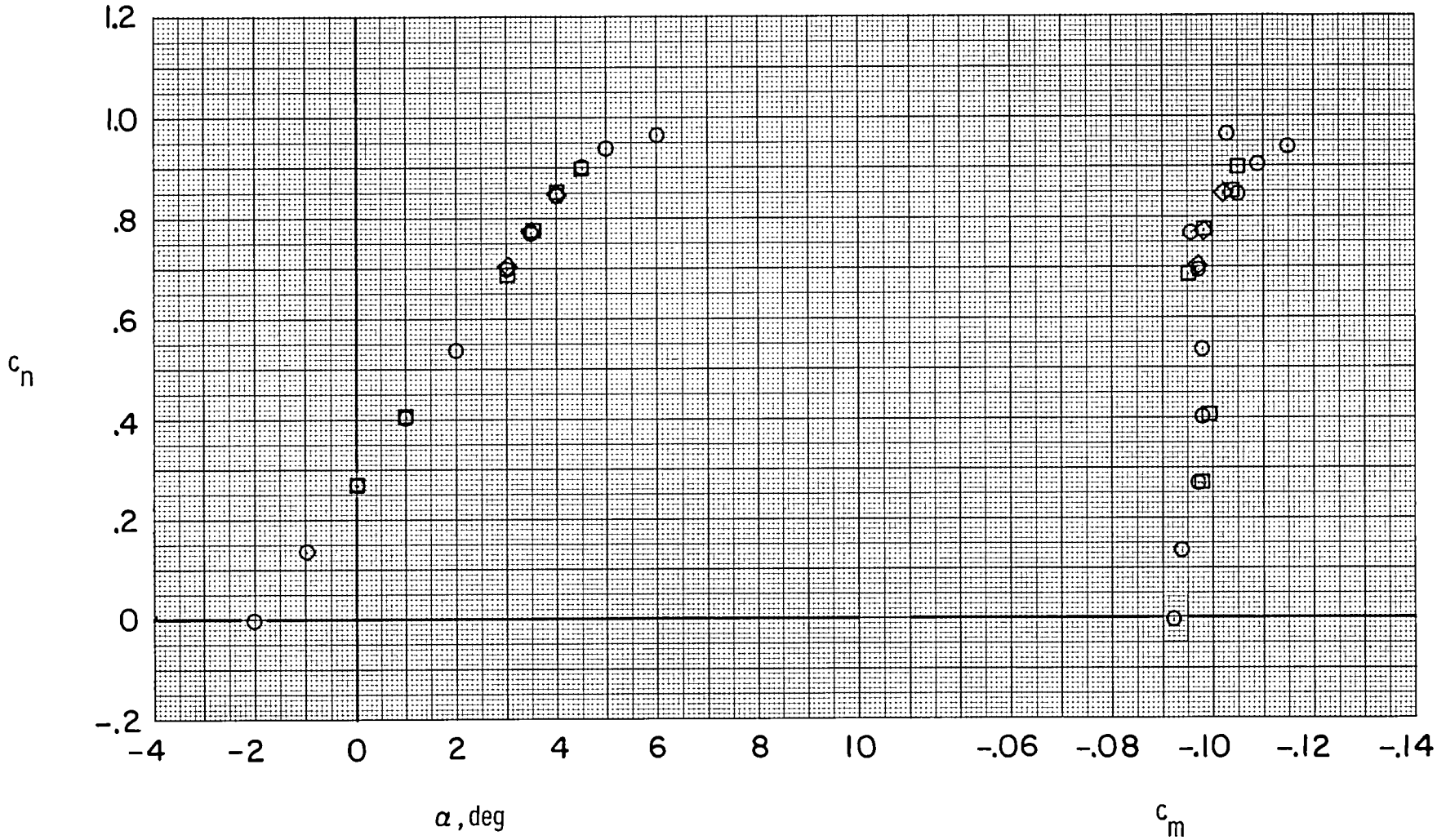

(a) c_n vs α and c_m.

Figure 11.- Repeatability of three sets of data $(\bigcirc, \square, \diamond)$ with fixed transition at $M \approx 0.76$ and $R \approx 7.7 \times 10^6$.

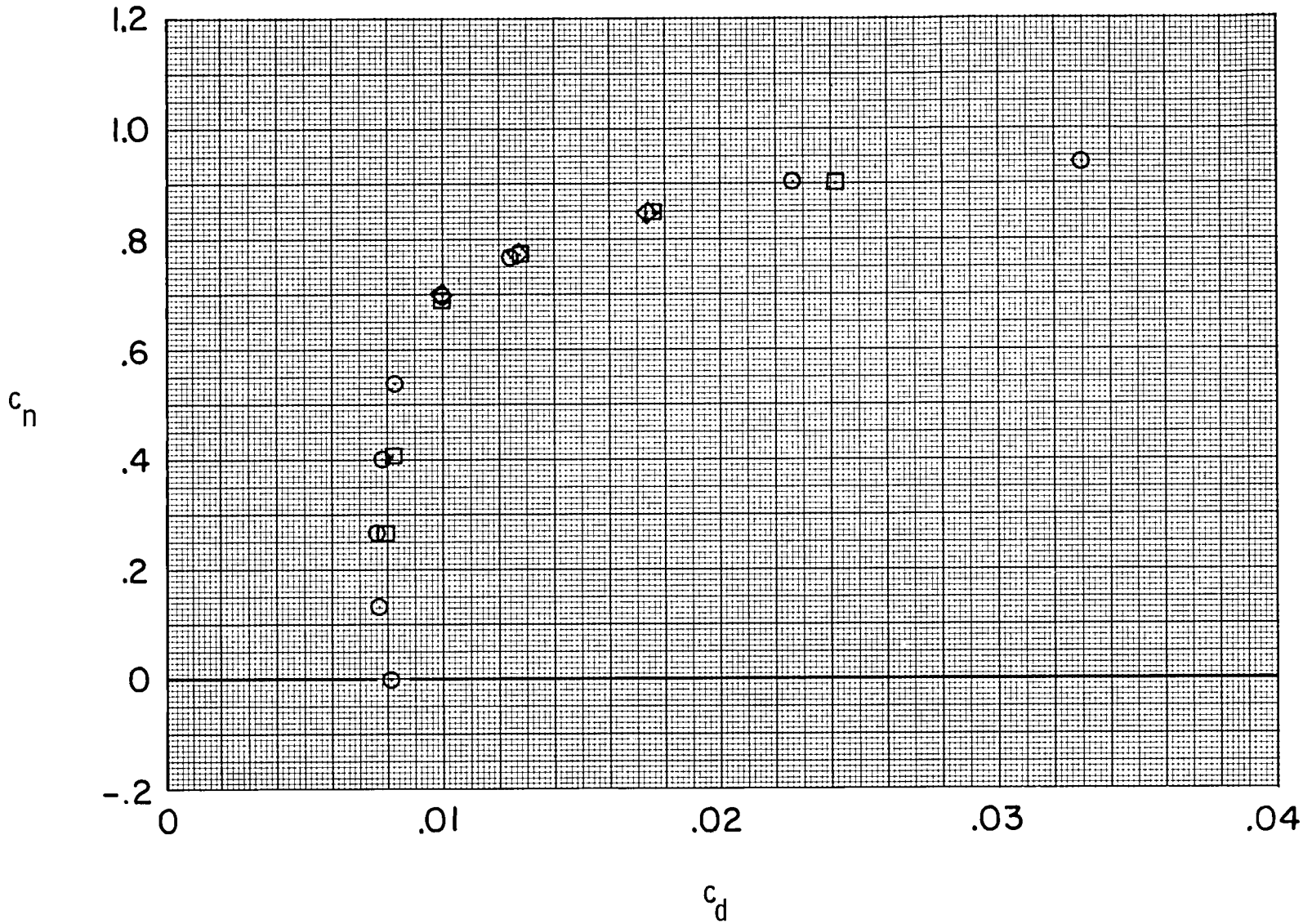

(b) c_n vs c_d.

Figure 11.- Concluded.

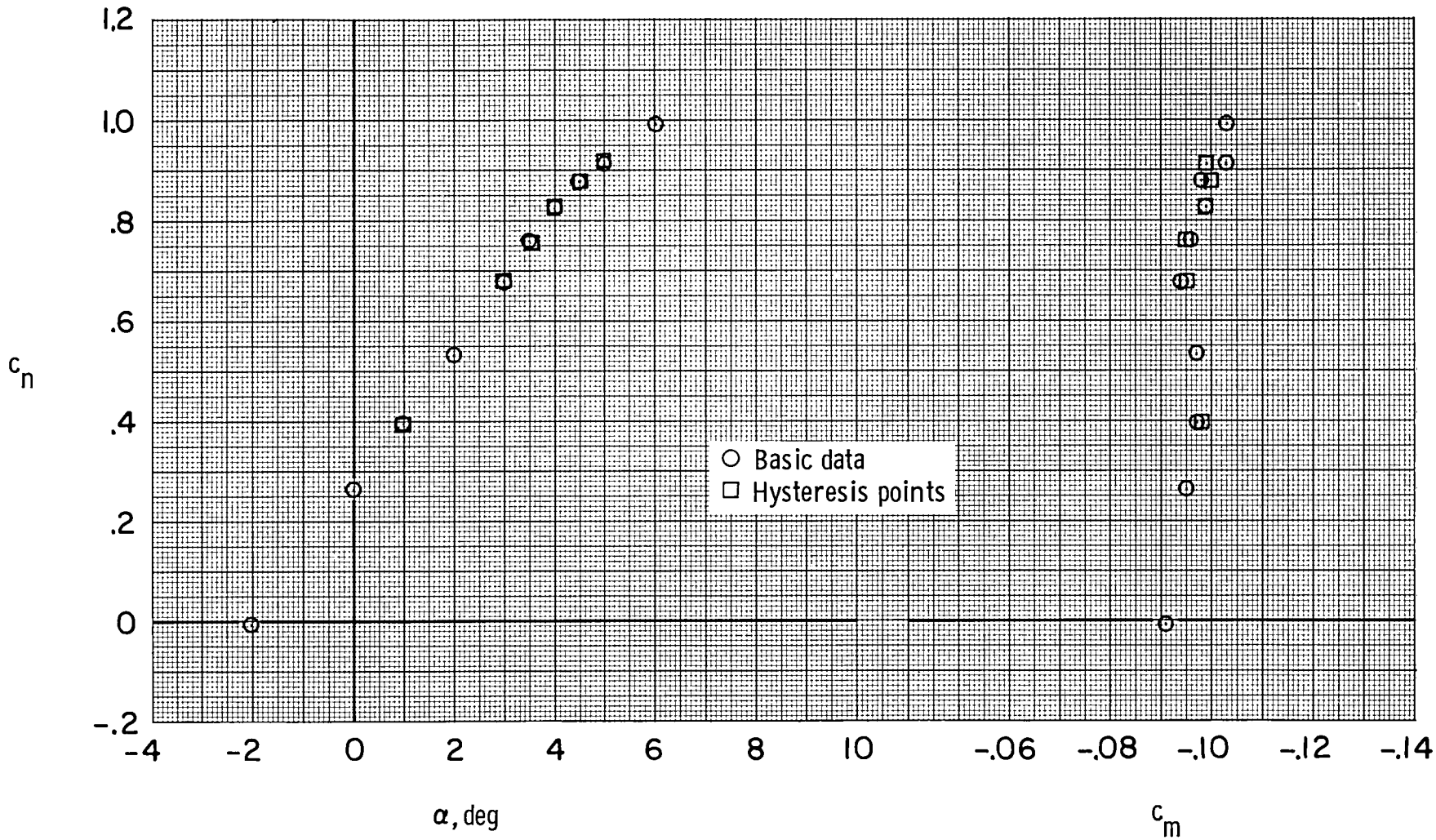

(a) c_n vs α and c_m.

Figure 12.- Hysteresis characteristics of data with free transition at $M \approx 0.76$ and $R \approx 7.7 \times 10^6$.

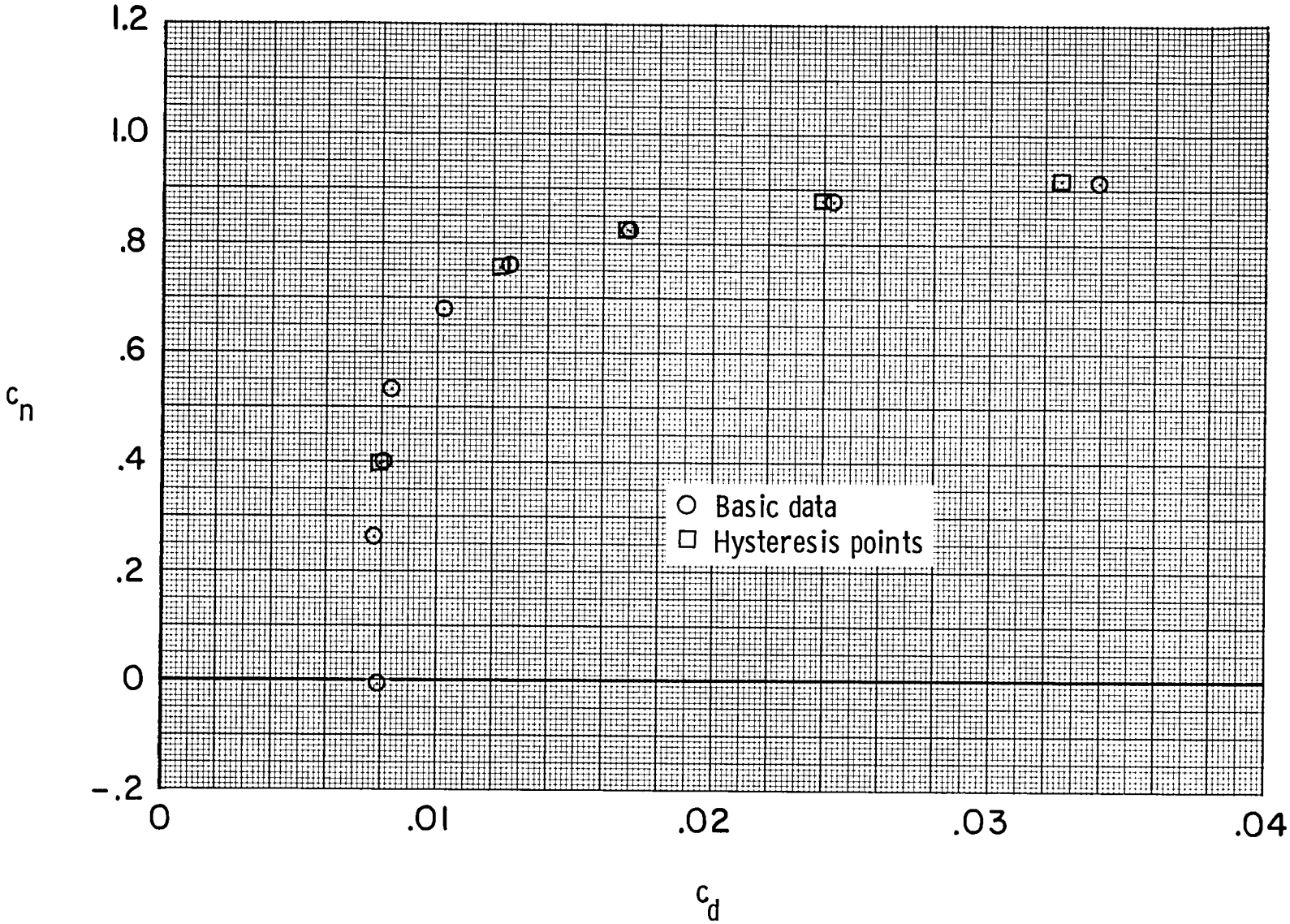

(b) c_n vs c_d.

Figure 12.- Concluded.

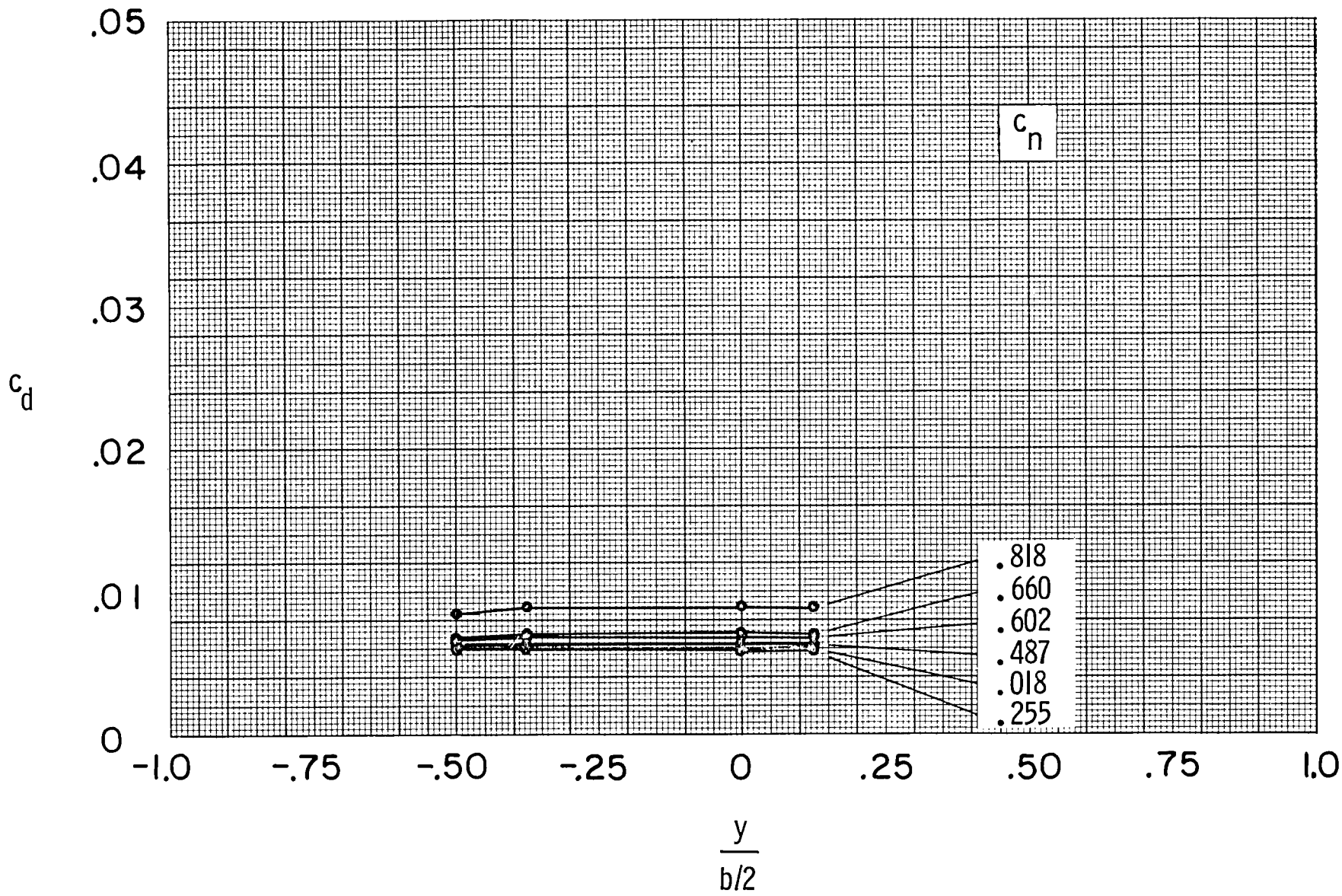

(a) M ≈ 0.60.

Figure 13.- Spanwise drag of airfoil with free transition for several Mach numbers at R ≈ 30.0 × 10^6.

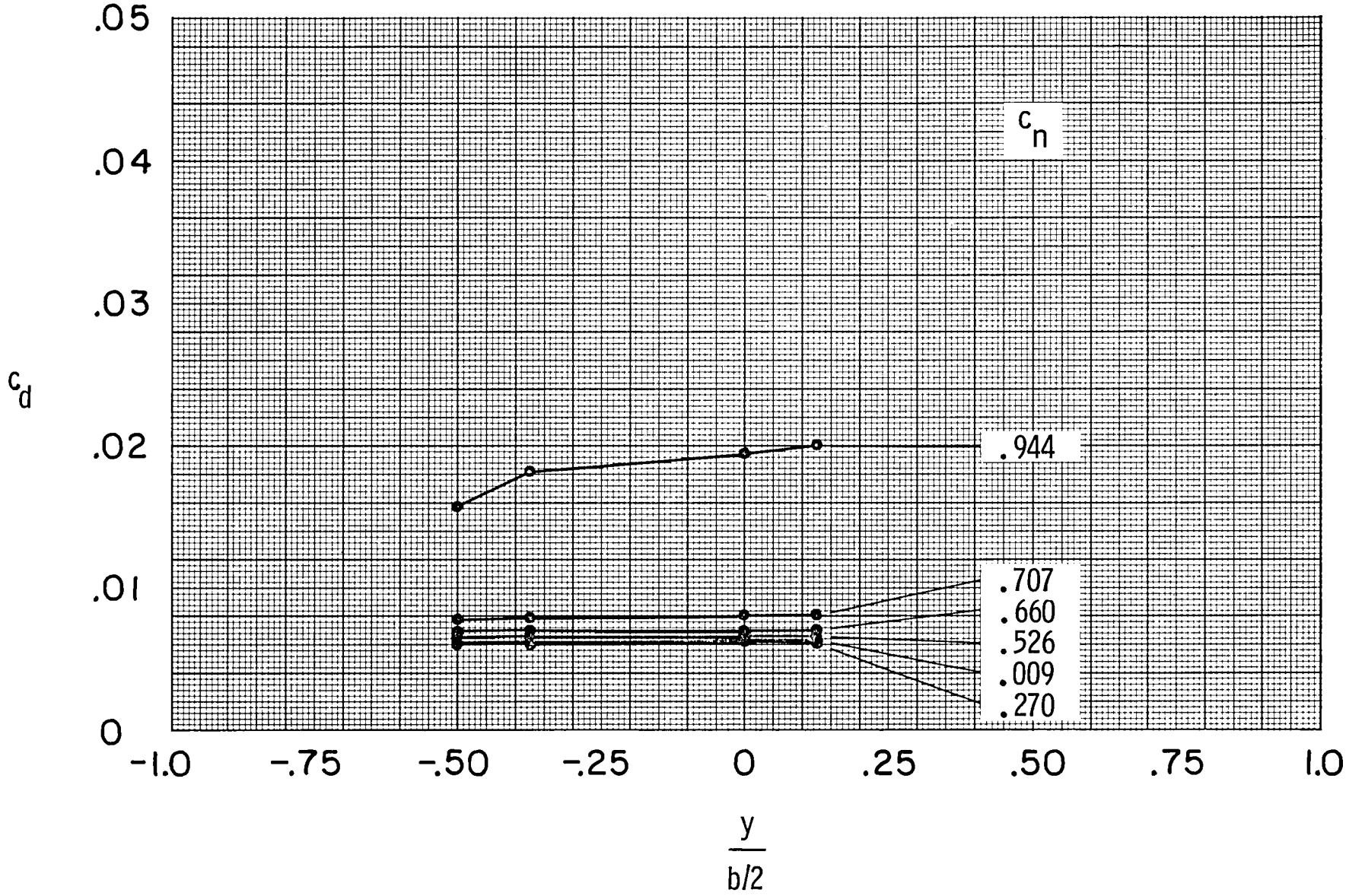

(b) M ≈ 0.70.

Figure 13.- Continued.

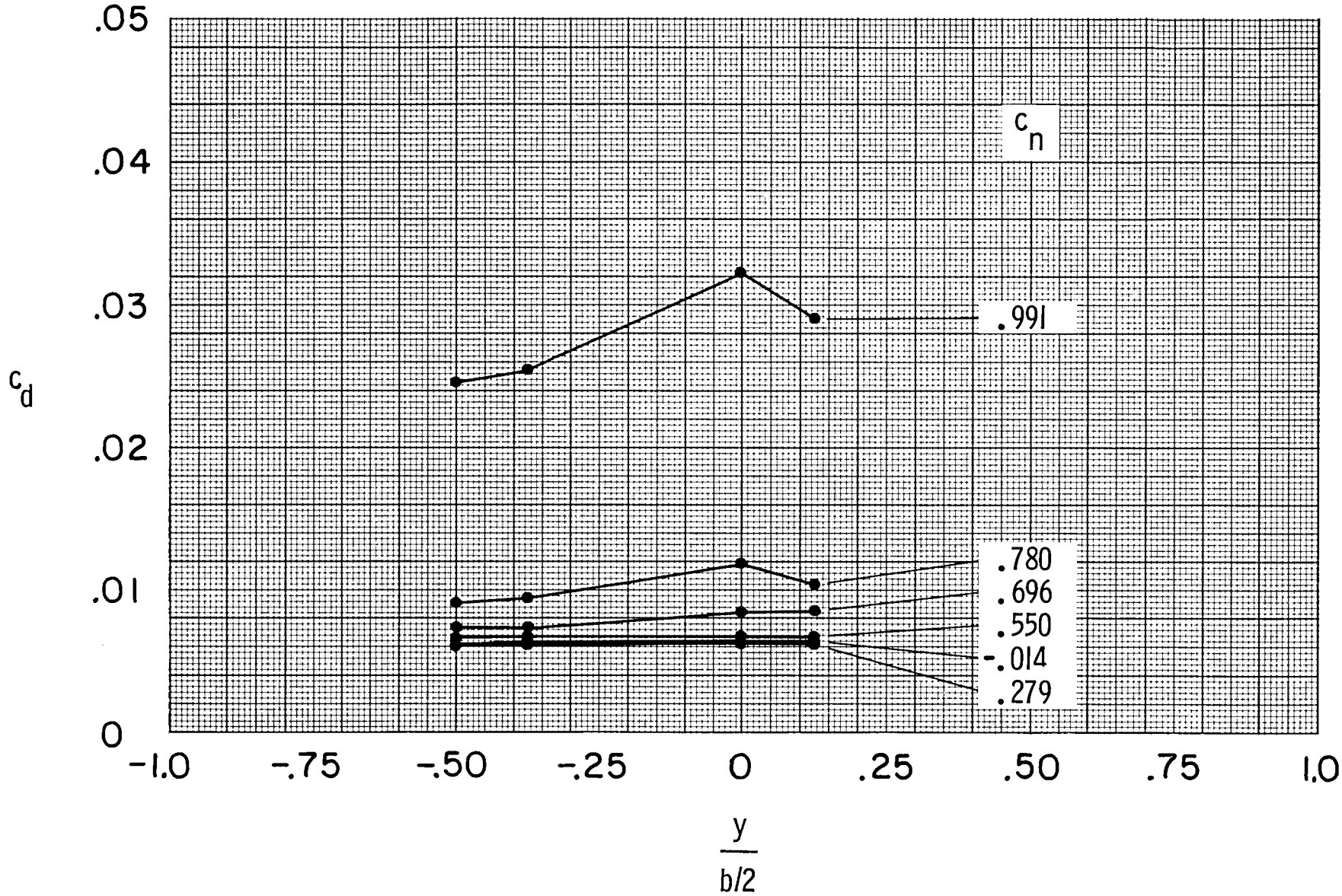

(c) M ≈ 0.74.

Figure 13.- Continued.

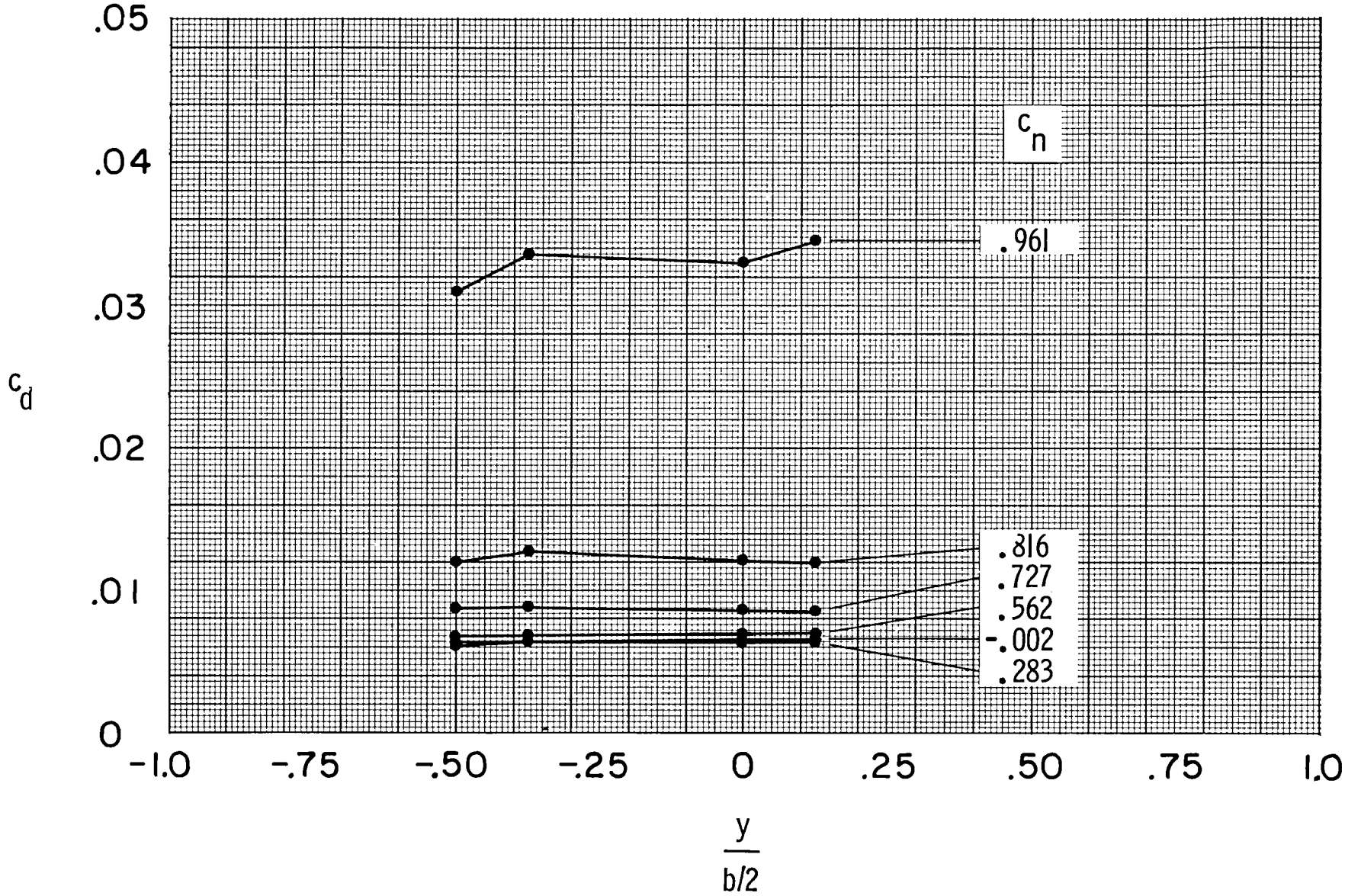

(d) M ≈ 0.76.

Figure 13.- Continued.

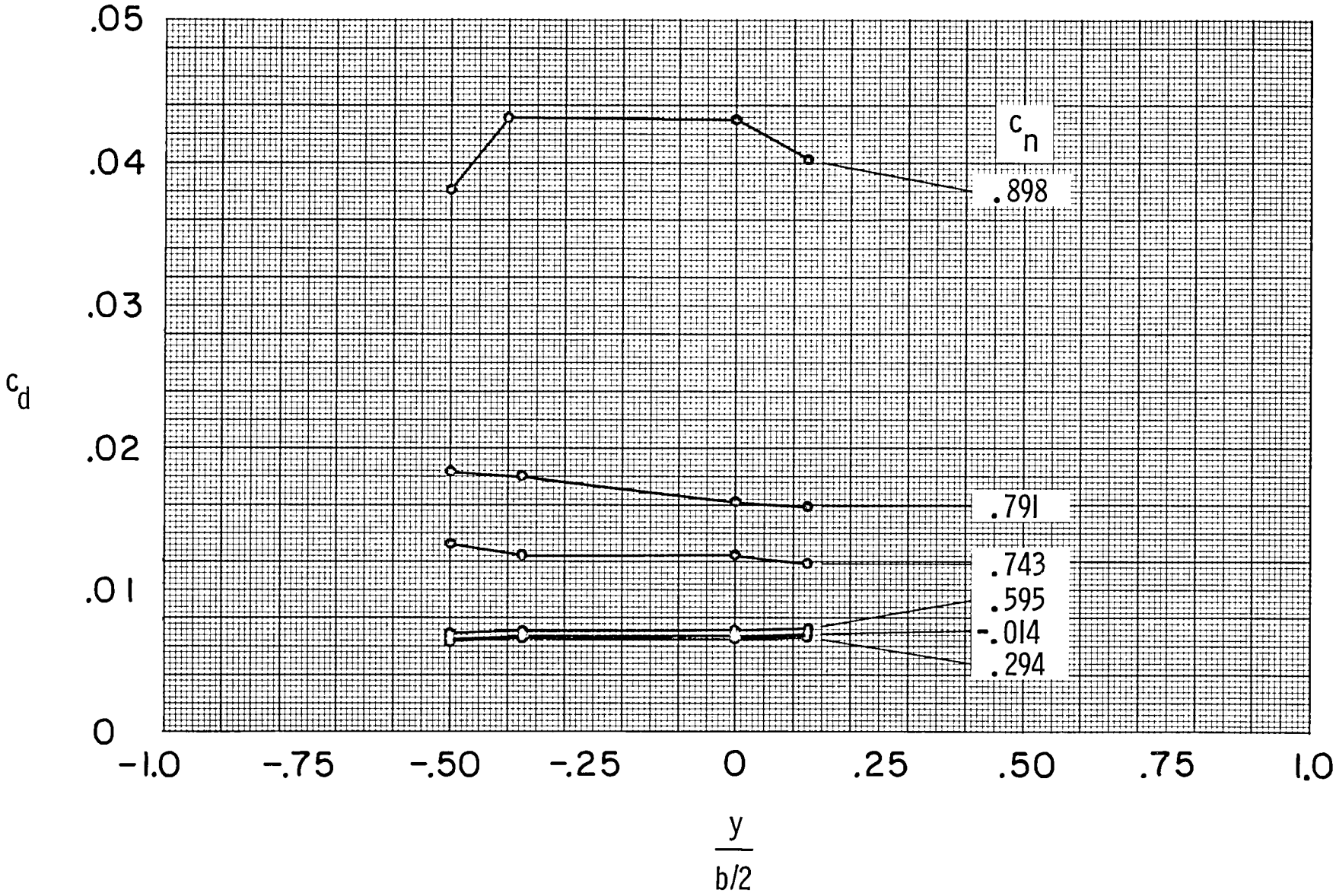

(e) M ≈ 0.78.

Figure 13.- Continued.

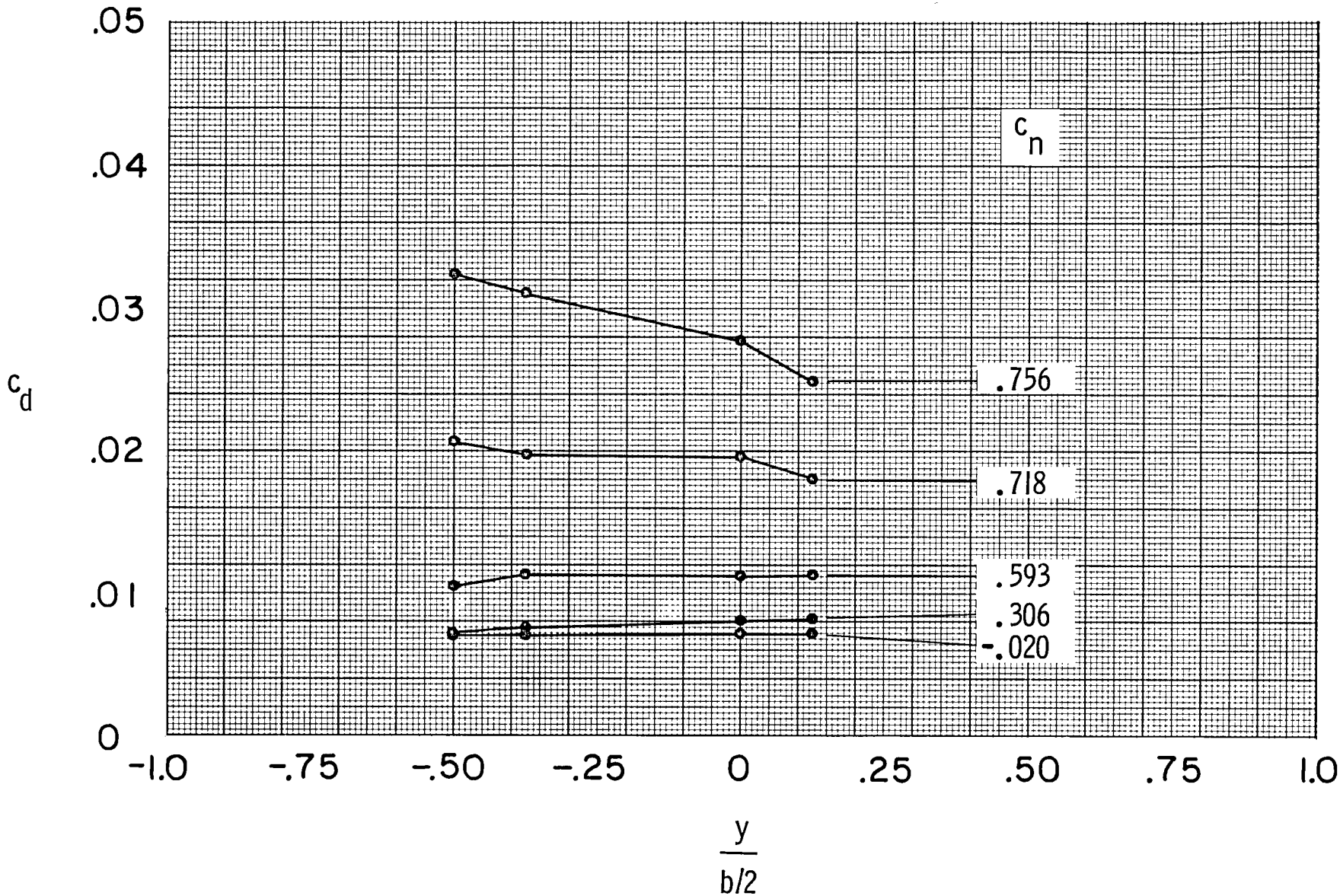

(f) M ≈ 0.80.

Figure 13.- Concluded.

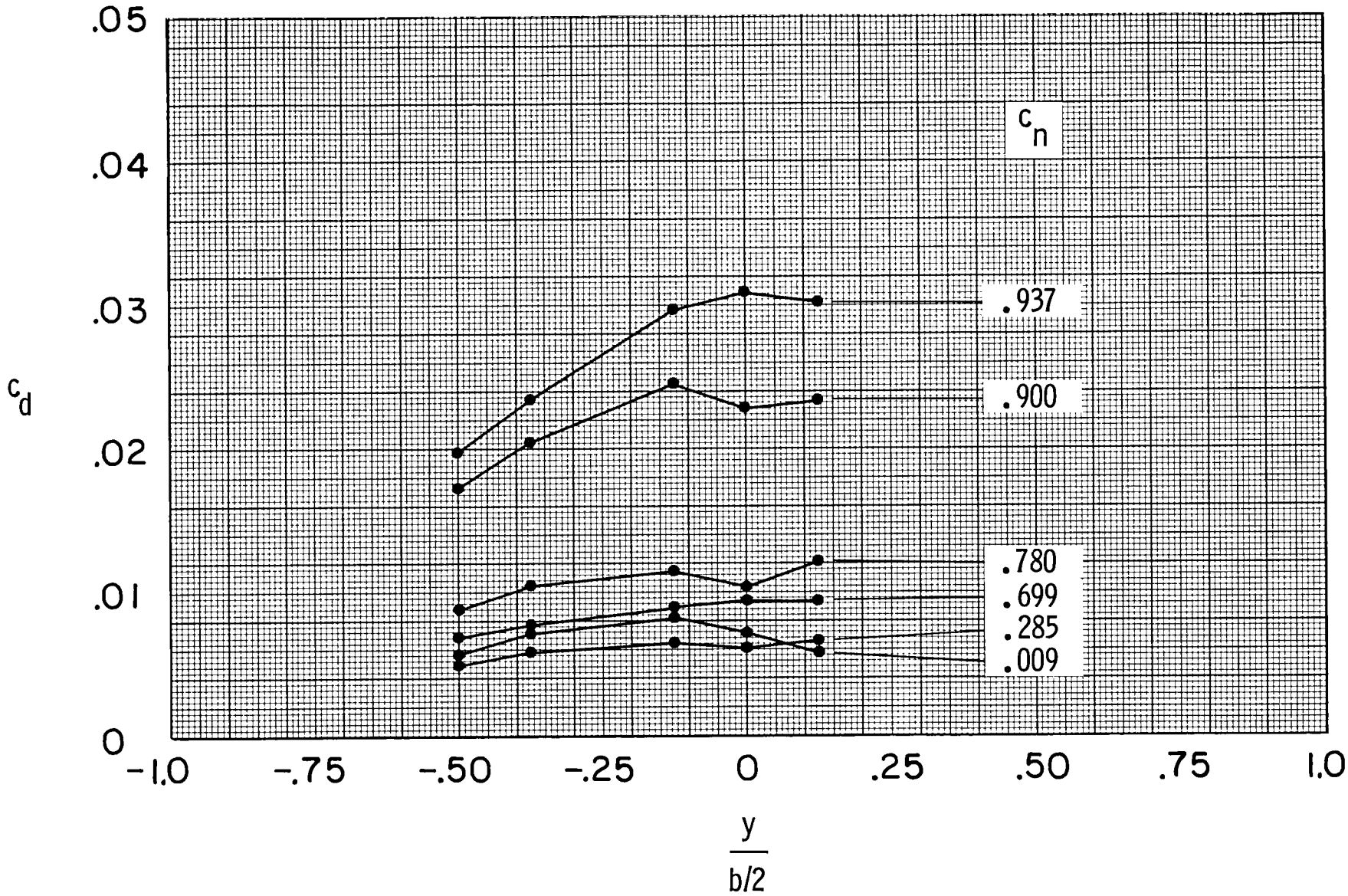

(a) $R \approx 4.4 \times 10^6$.

Figure 14.- Spanwise drag of airfoil with free transition for several Reynolds numbers at $M \approx 0.76$.

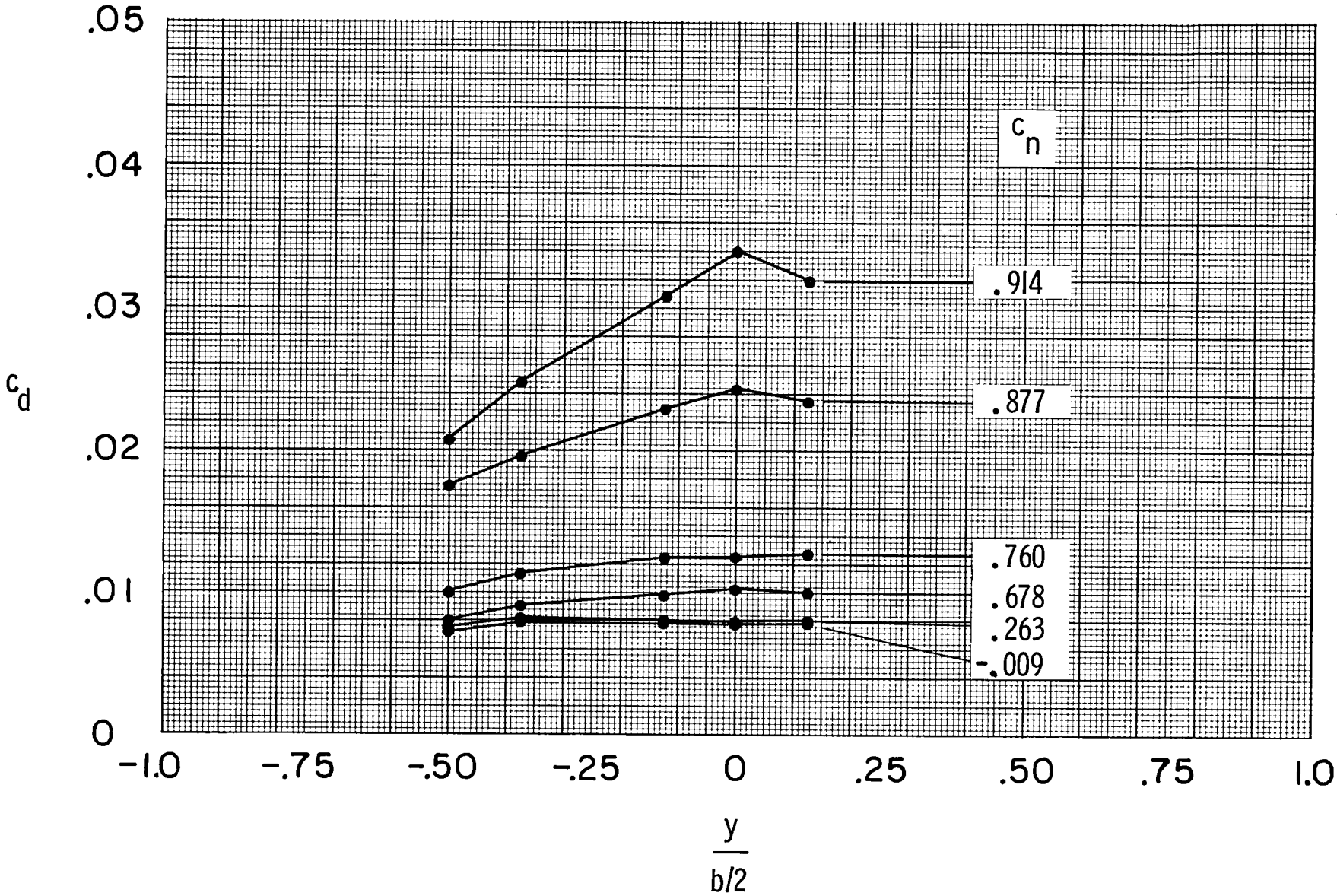

(b) $R \approx 7.7 \times 10^6$.

Figure 14.- Continued.

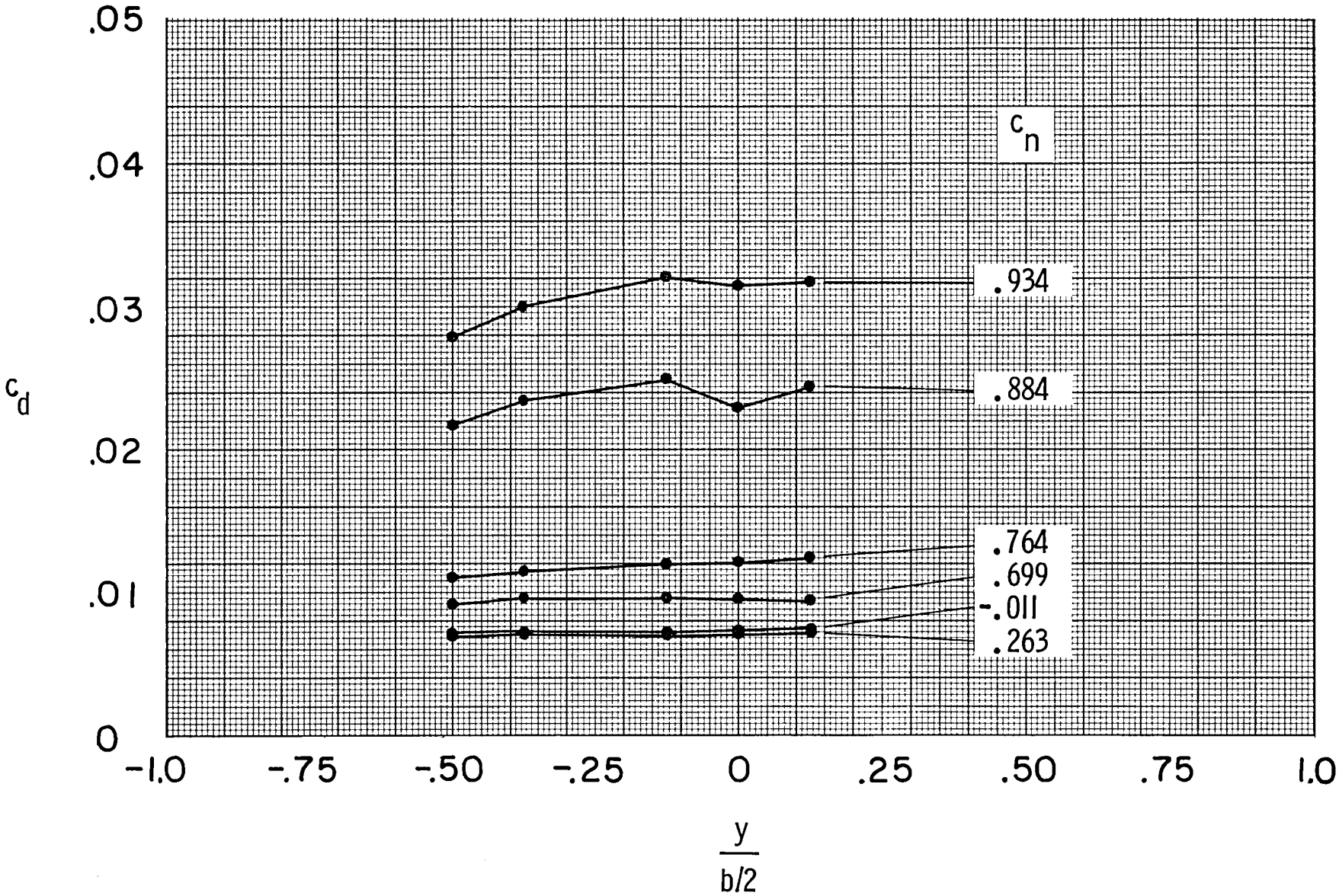

(c) $R \approx 14.0 \times 10^6$.

Figure 14.- Continued.

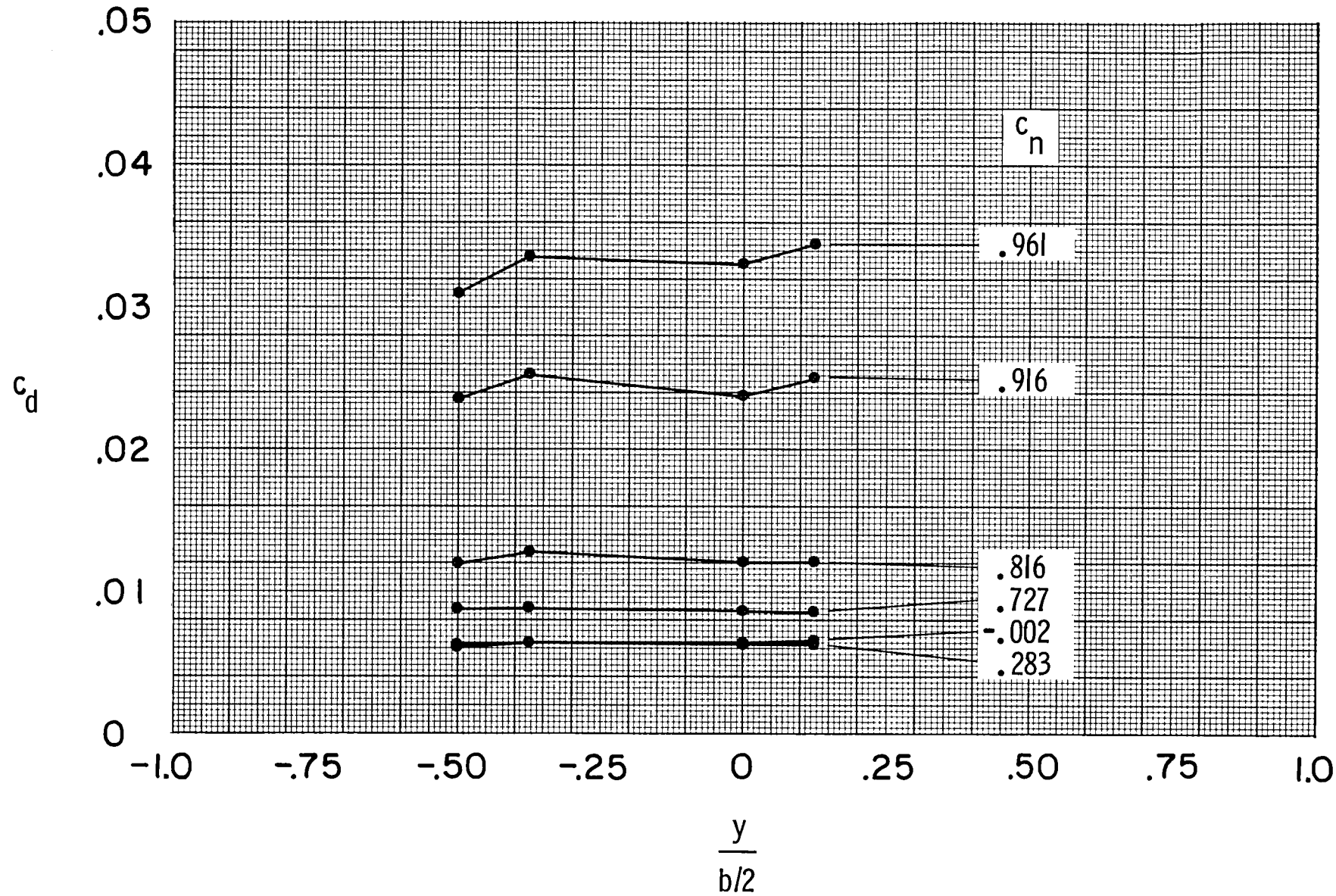

(d) $R \approx 30.0 \times 10^6$.

Figure 14.- Continued.

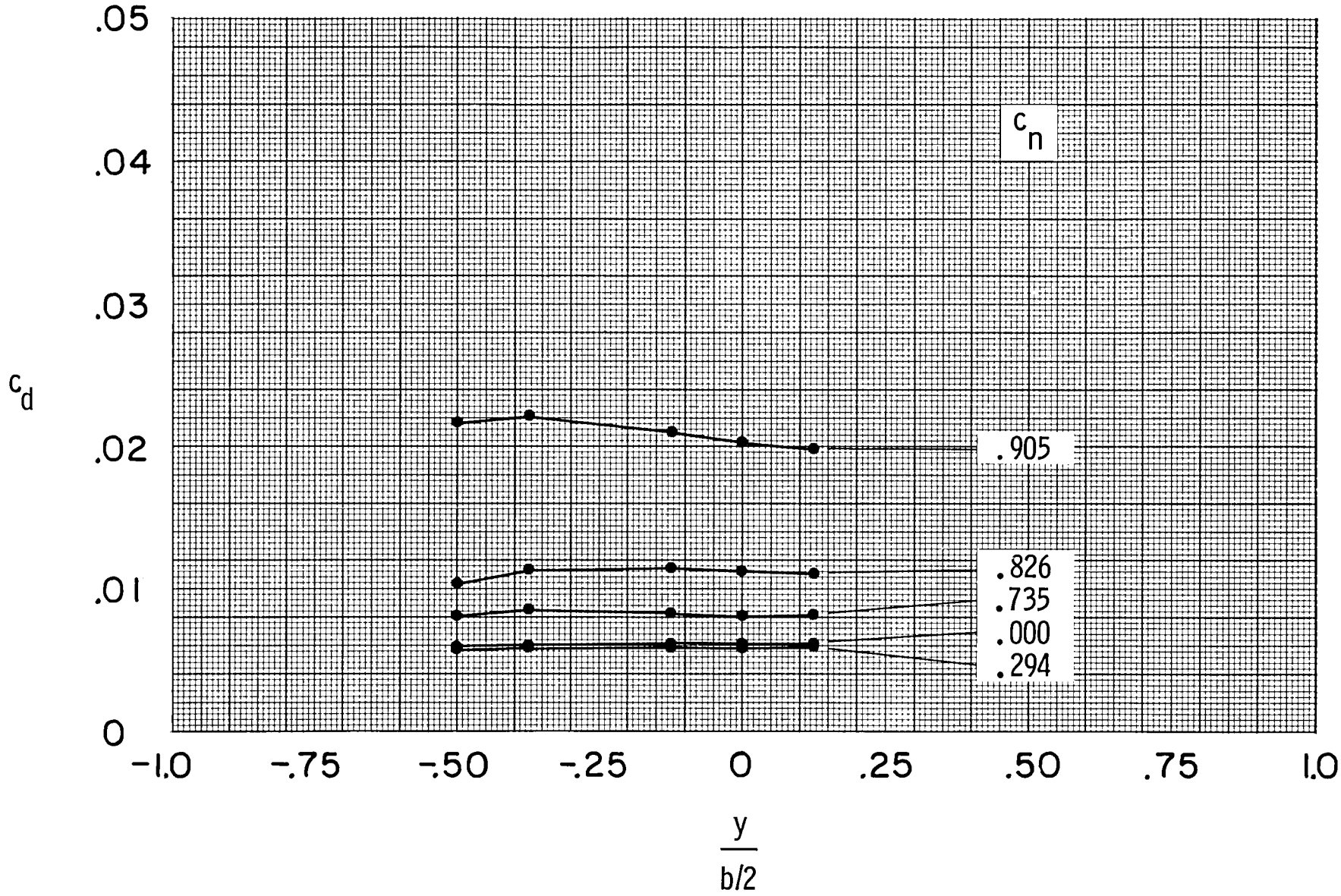

(e) $R \approx 45.0 \times 10^6$.

Figure 14.- Concluded.

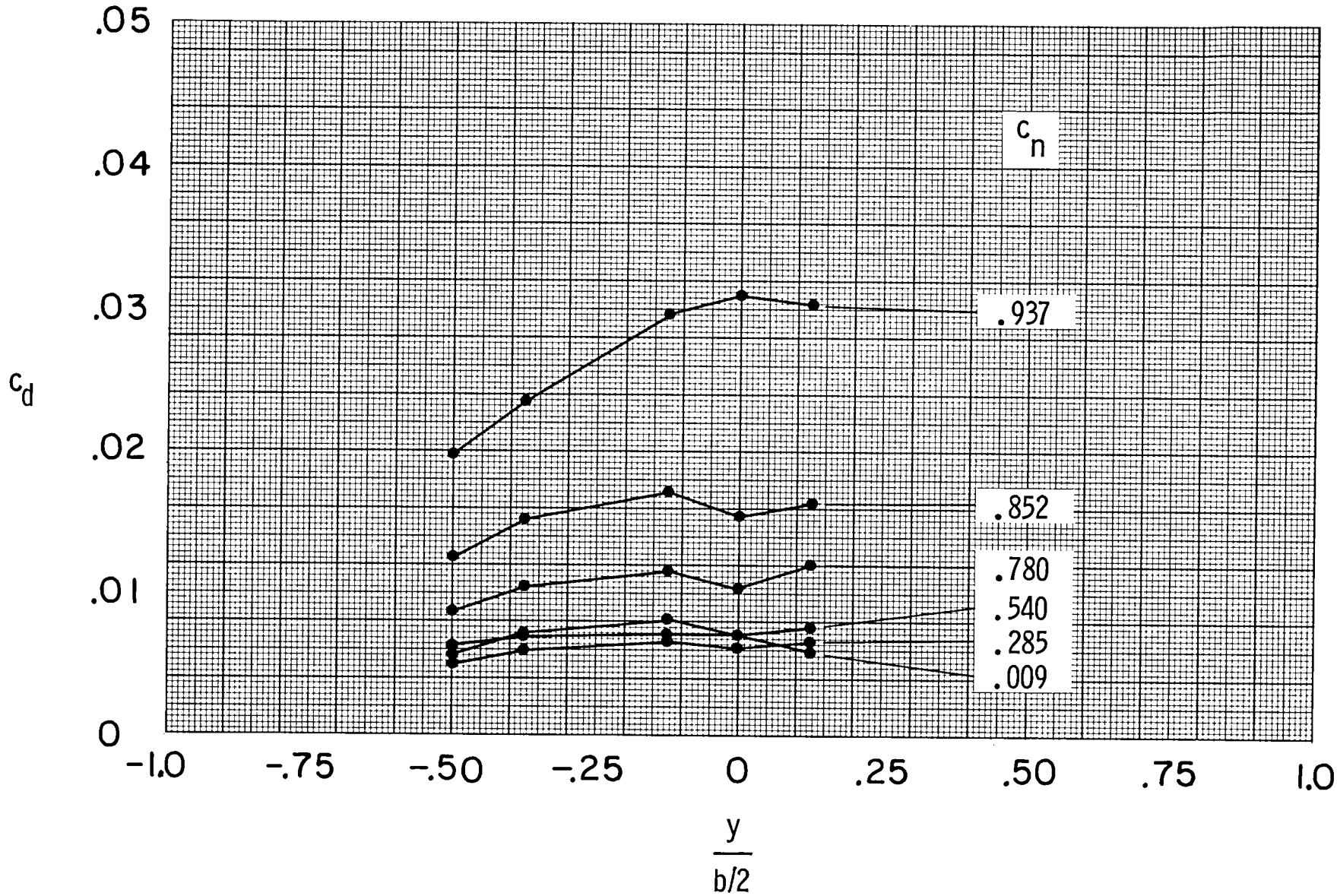

(a) Free transition.

Figure 15.- Spanwise drag of airfoil with free and fixed transition at $M \approx 0.76$ and $R \approx 4.4 \times 10^6$.

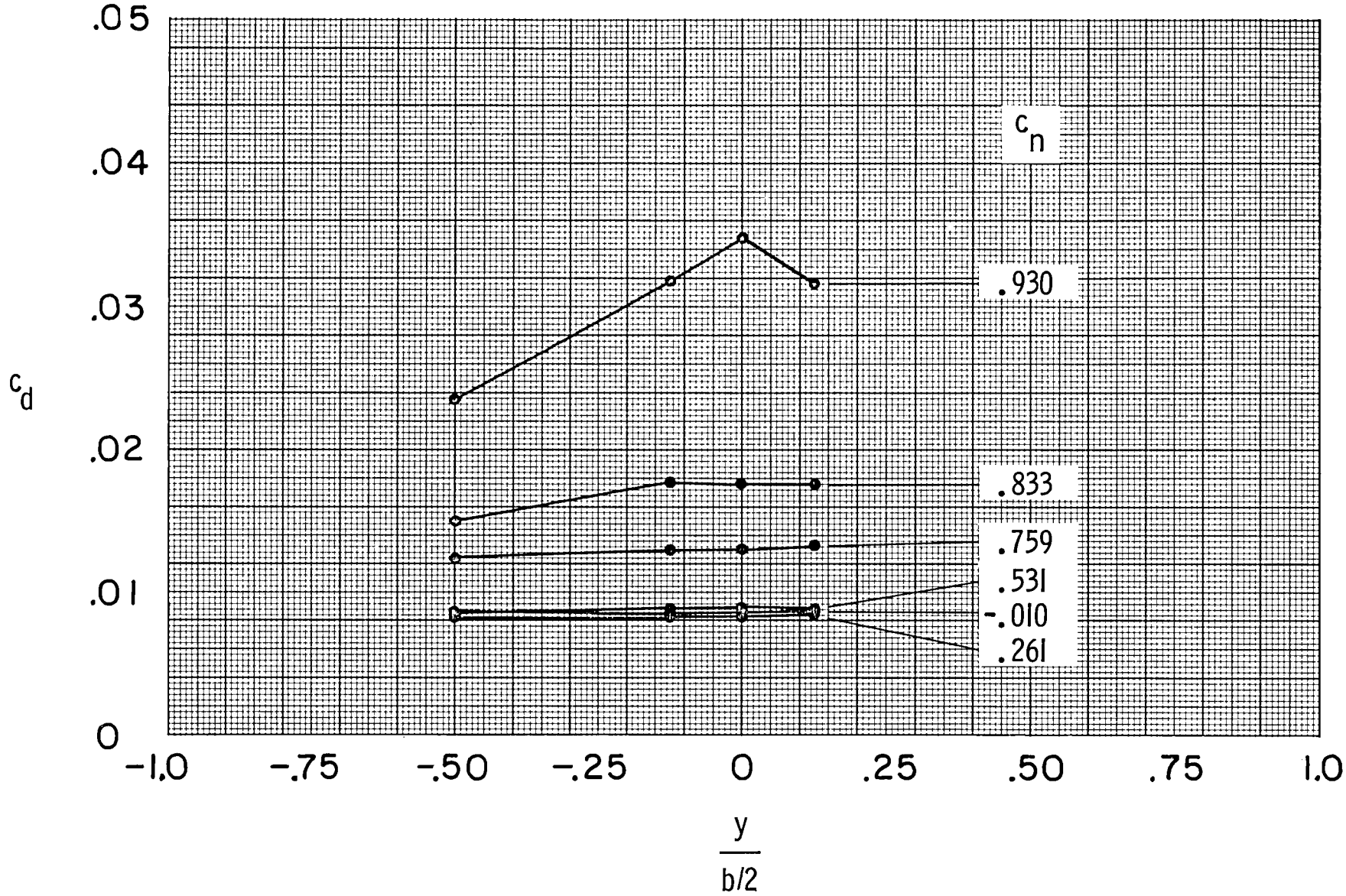

(b) Fixed transition.

Figure 15.- Concluded.

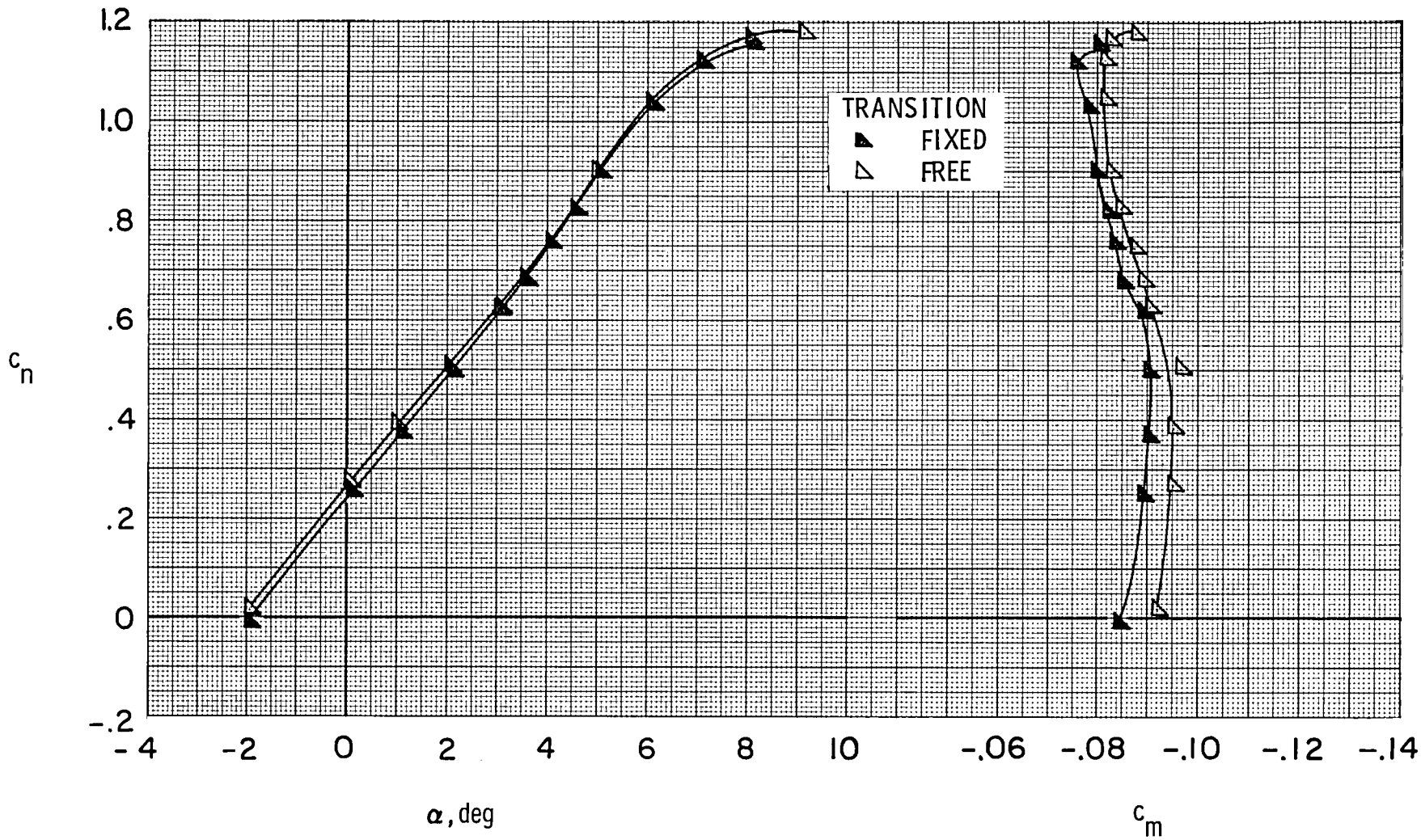

(a) c_n vs α and c_m.

Figure 16.- Effect of fixing transition on aerodynamic characteristics of airfoil at $M \approx 0.70$ and $R \approx 4.4 \times 10^6$.

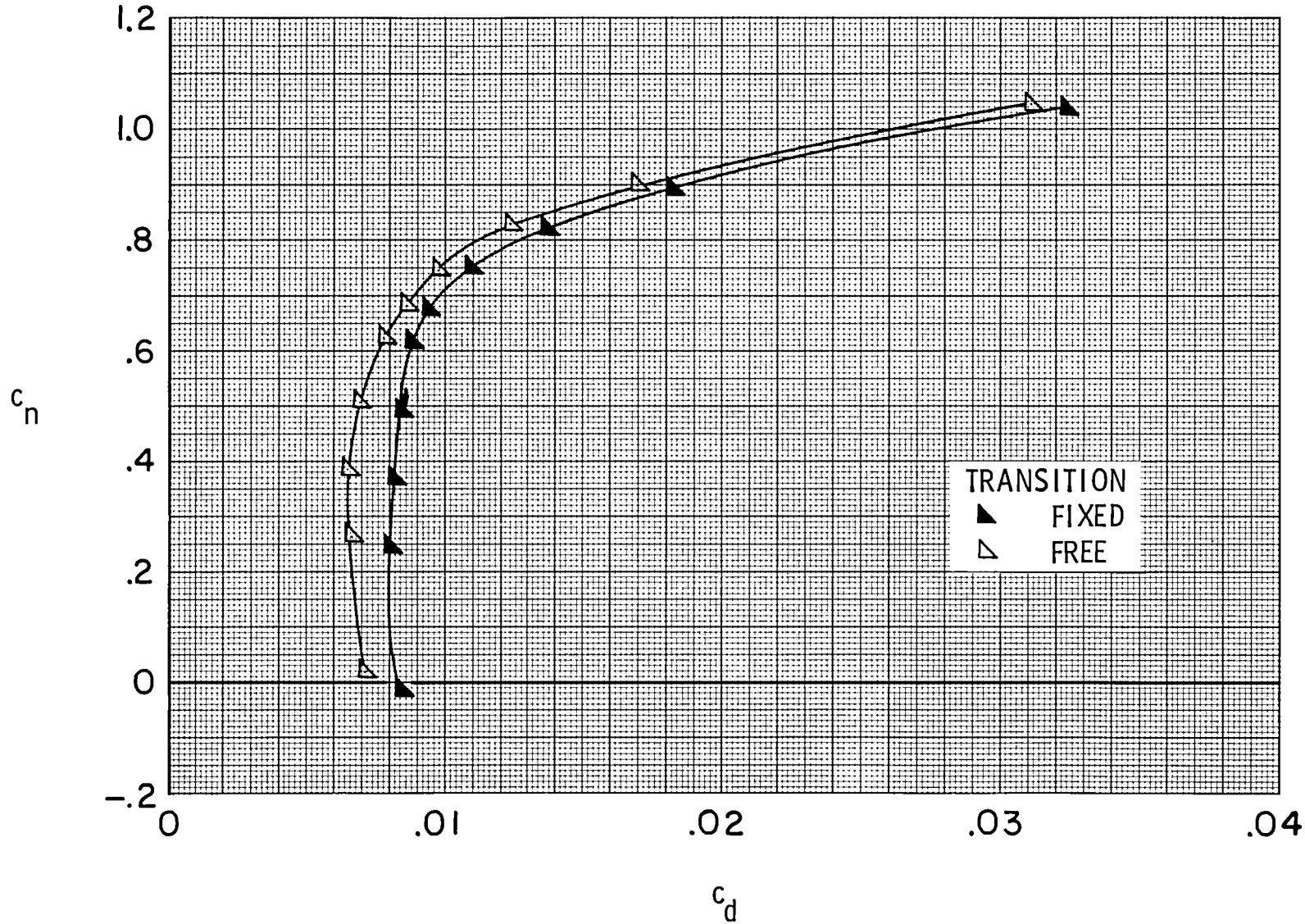

(b) c_n vs c_d.

Figure 16.- Concluded.

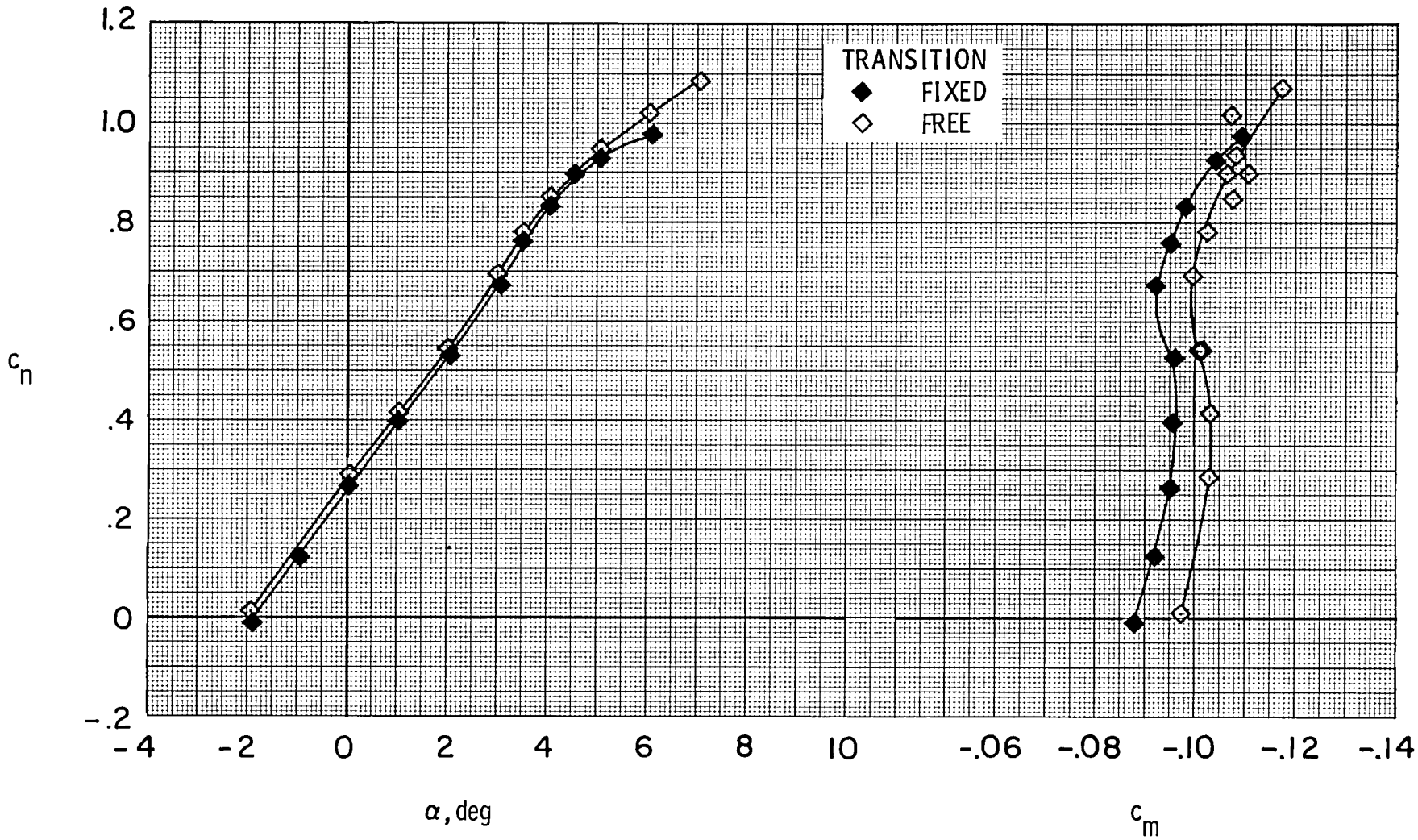

(a) c_n vs α and c_m.

Figure 17.- Effect of fixing transition on aerodynamic characteristics of airfoil at $M \approx 0.76$ and $R \approx 4.4 \times 10^6$.

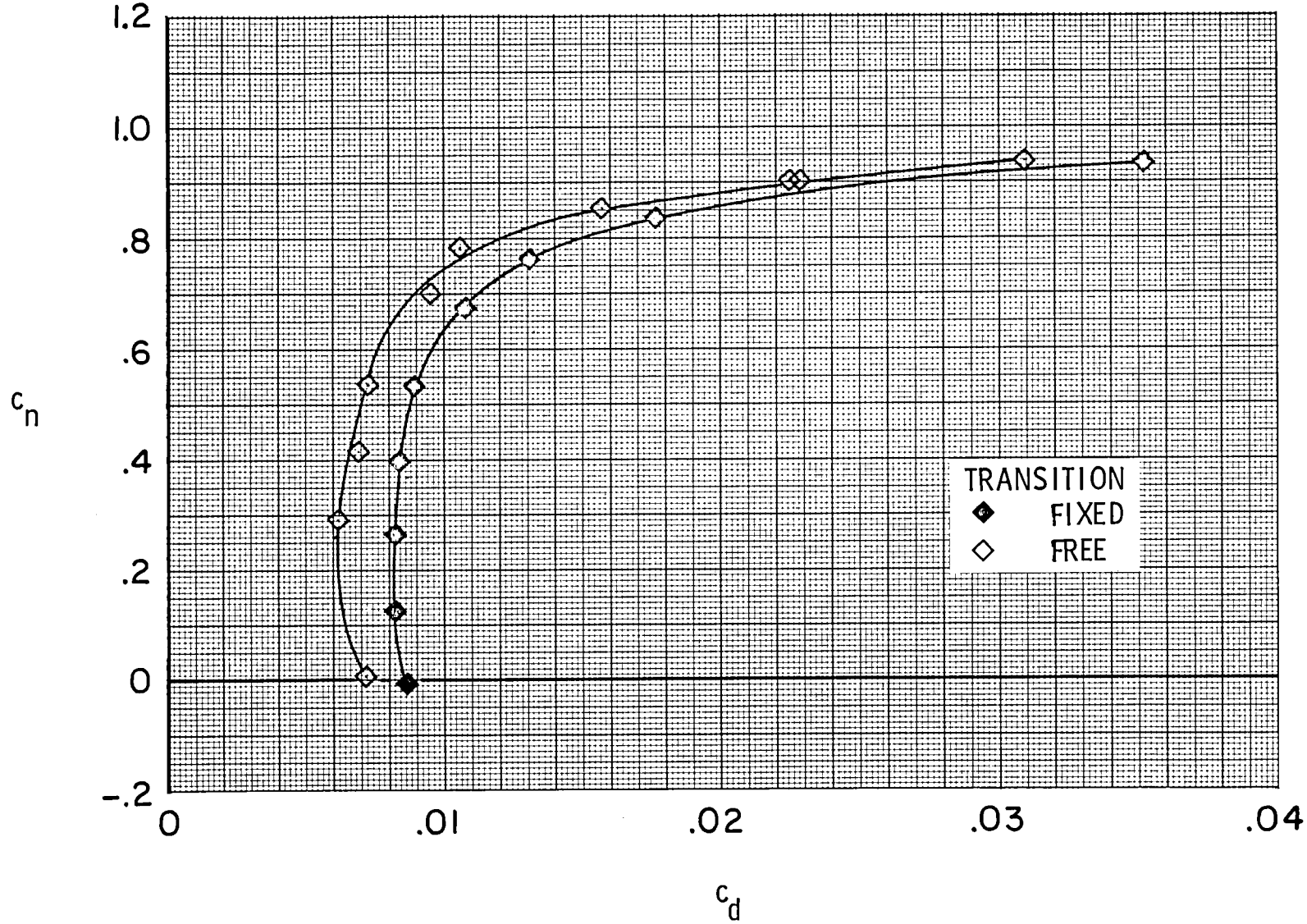

(b) c_n vs c_d.

Figure 17.- Concluded.

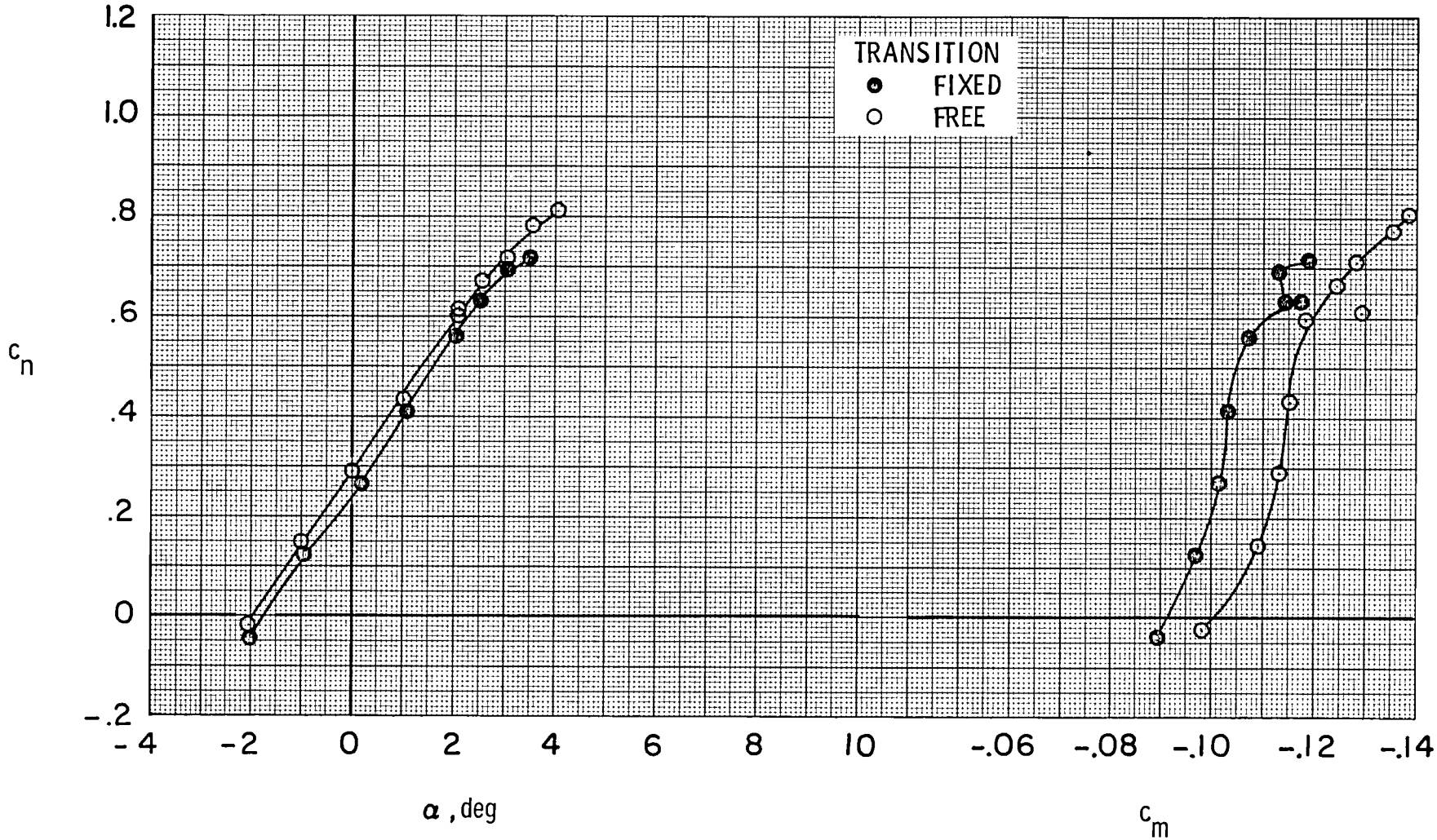

(a) c_n vs α and c_m.

Figure 18.- Effect of fixing transition on aerodynamic characteristics of airfoil at $M \approx 0.80$ and $R \approx 4.4 \times 10^6$.

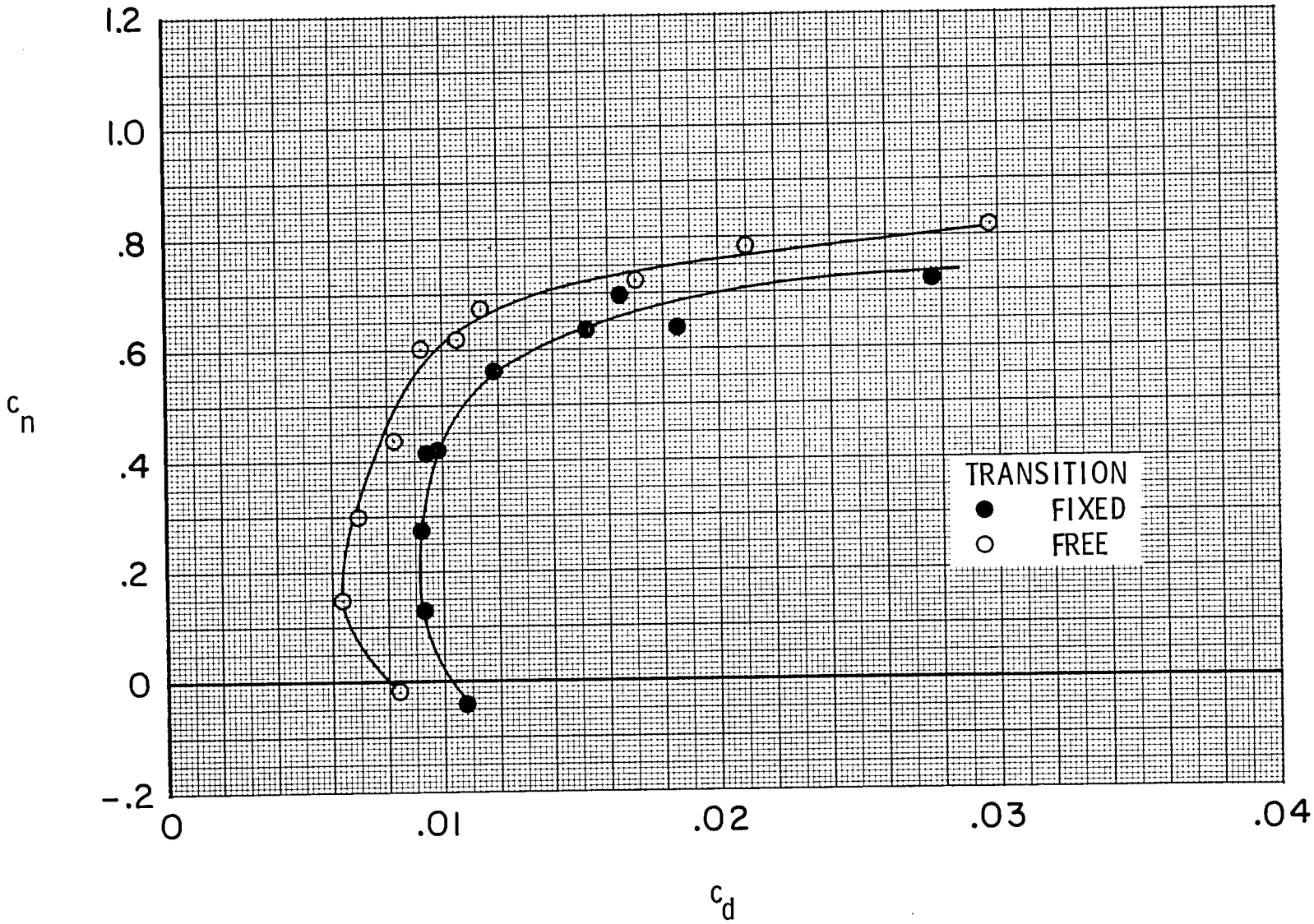

(b) c_n vs c_d.

Figure 18.- Concluded.

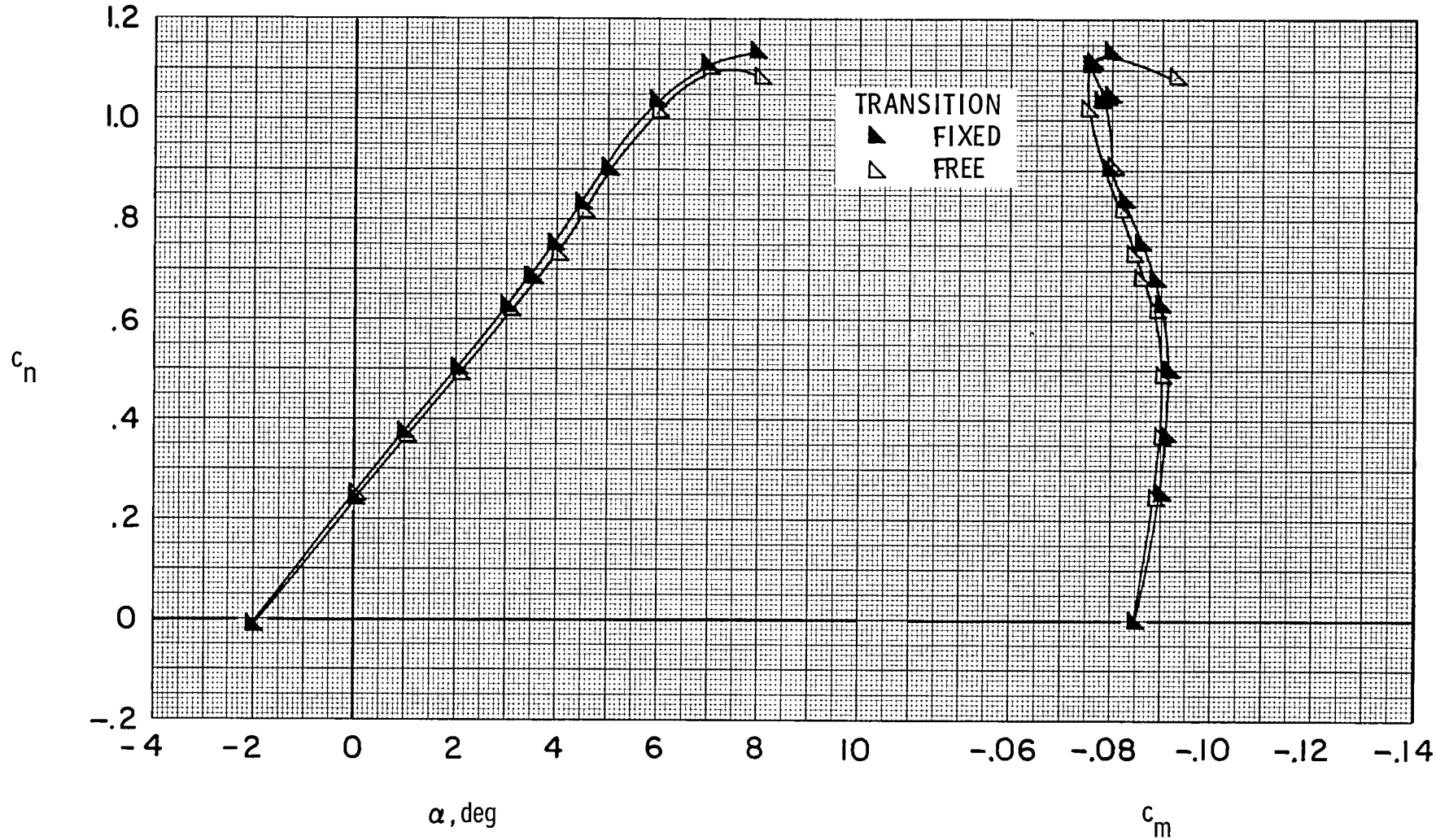

(a) c_n vs α and c_m.

Figure 19.- Effect of fixing transition on aerodynamic characteristics of airfoil at $M \approx 0.70$ and $R \approx 7.7 \times 10^6$.

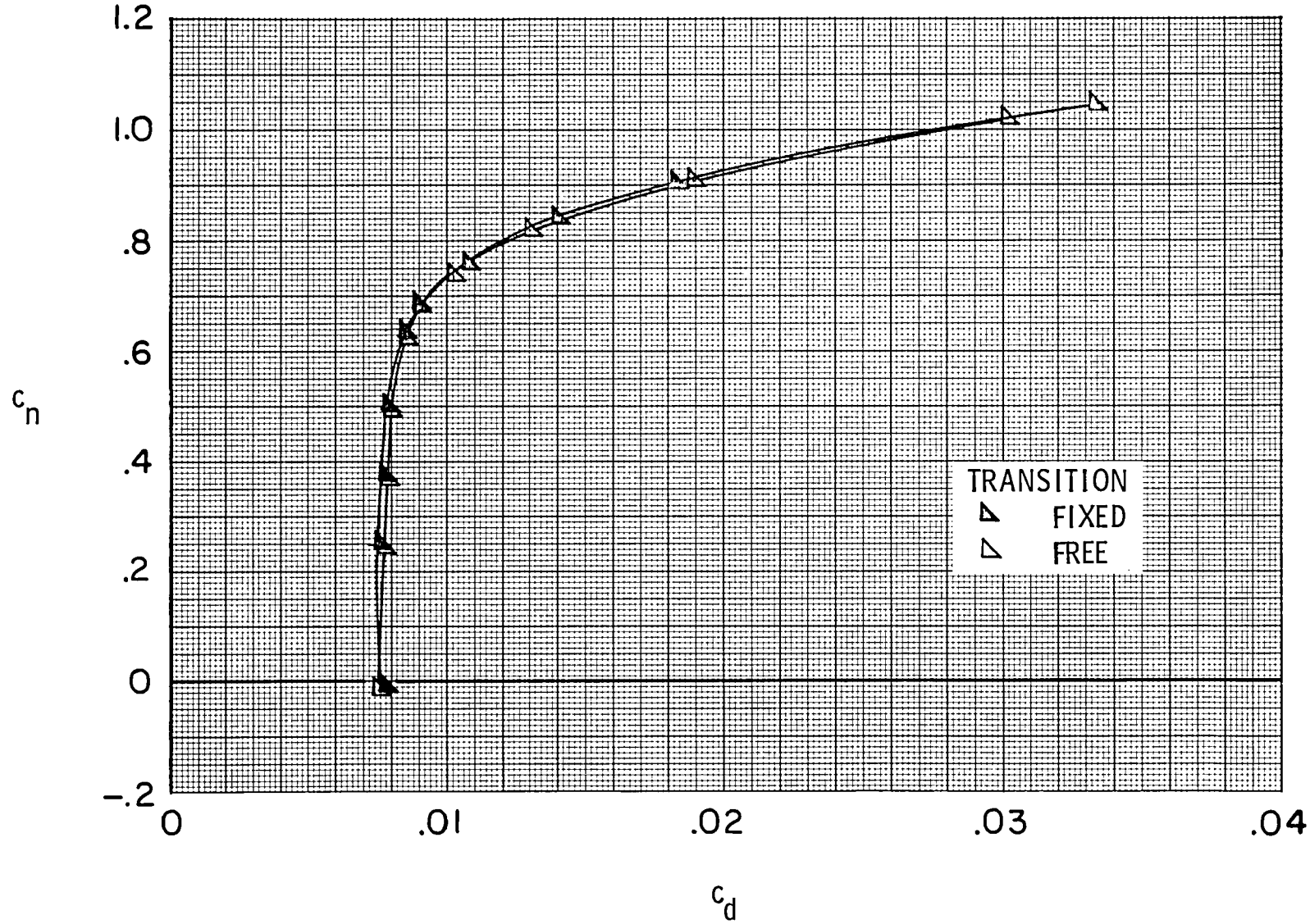

(b) c_n vs c_d.

Figure 19.- Concluded.

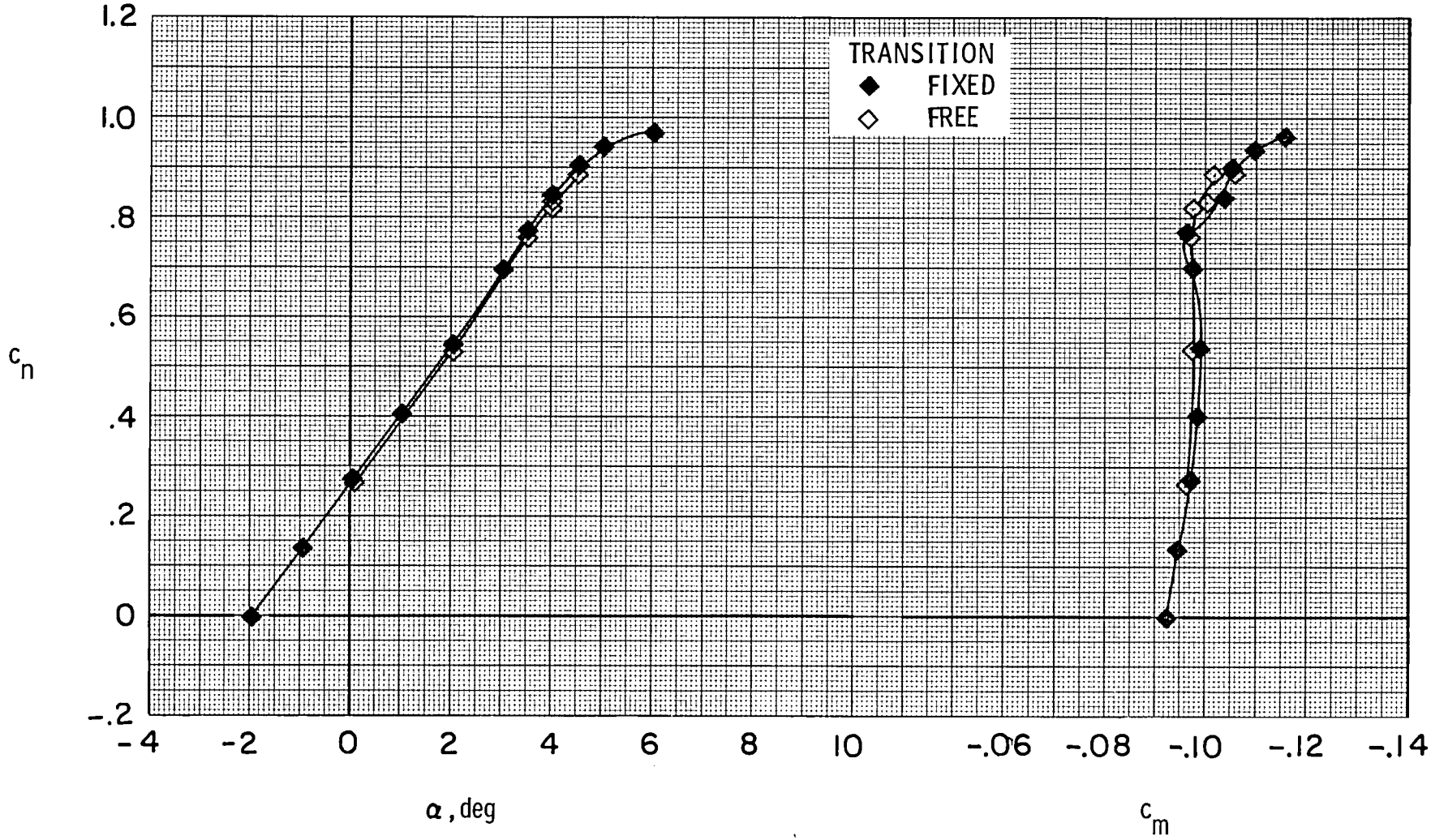

(a) c_n vs α and c_m.

Figure 20.- Effect of fixing transition on aerodynamic characteristics of airfoil at $M \approx 0.76$ and $R \approx 7.7 \times 10^6$.

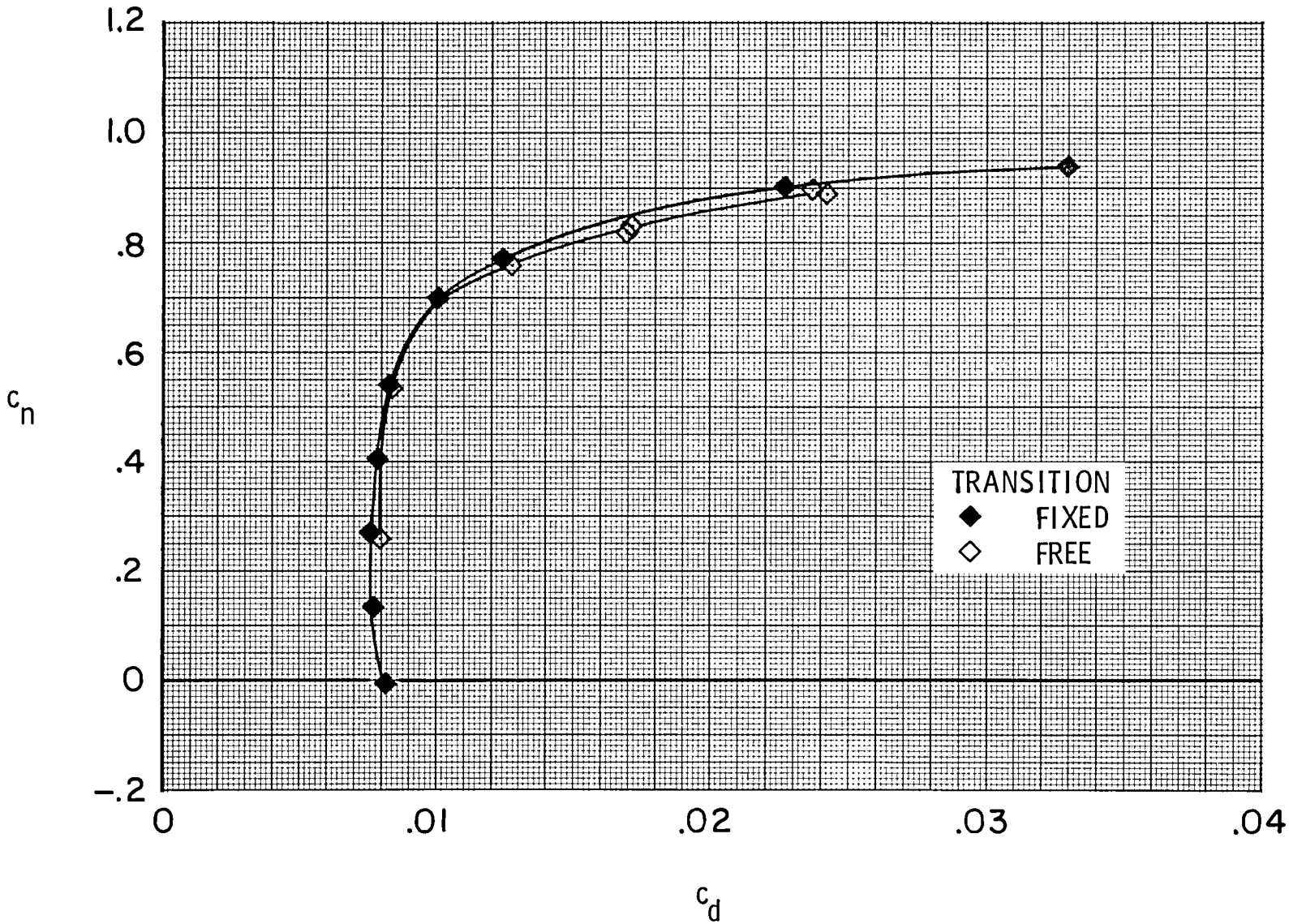

(b) c_n vs c_d.

Figure 20.- Concluded.

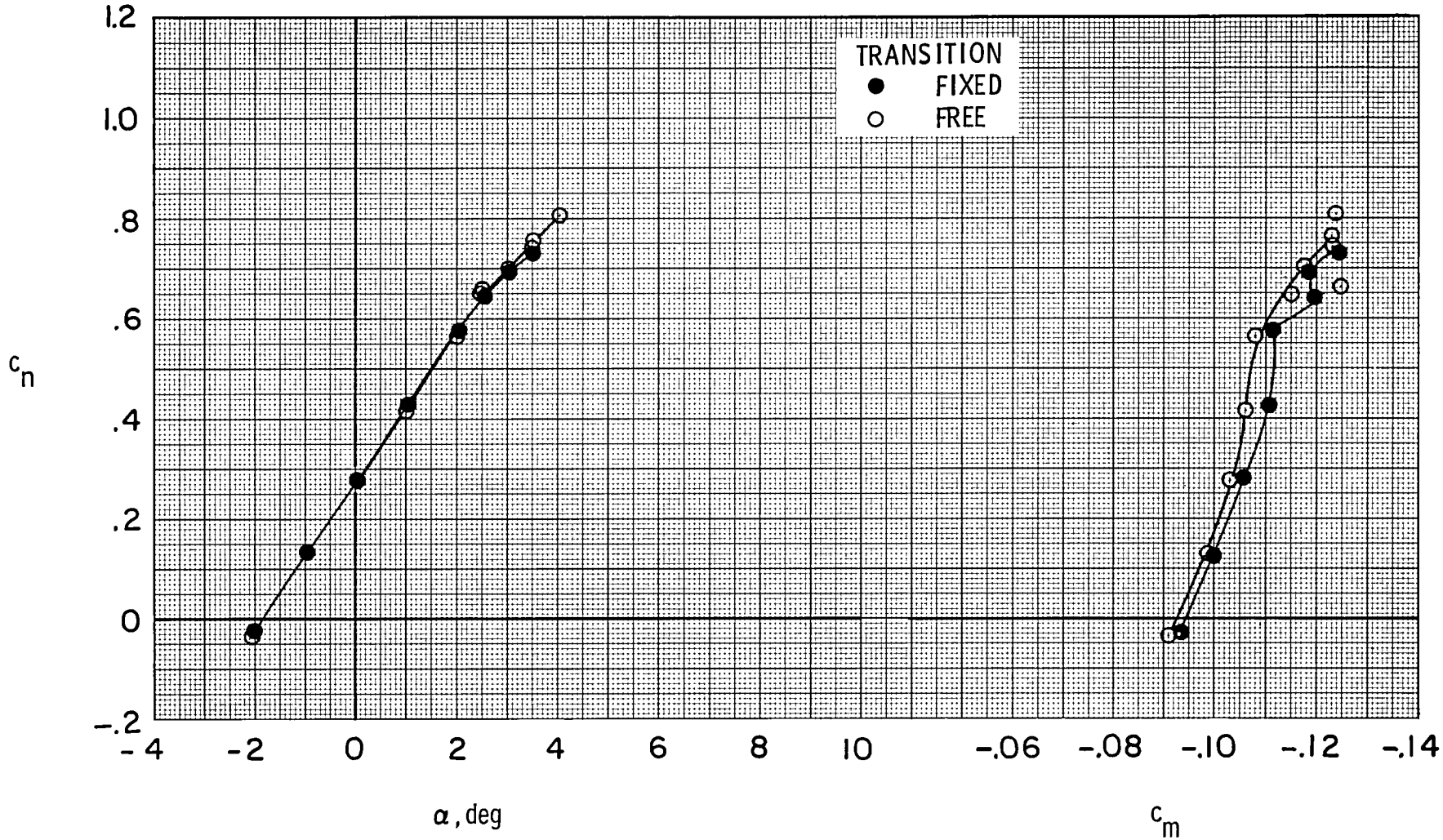

(a) c_n vs α and c_m.

Figure 21.- Effect of fixing transition on aerodynamic characteristics of airfoil at $M \approx 0.80$ and $R \approx 7.7 \times 10^6$.

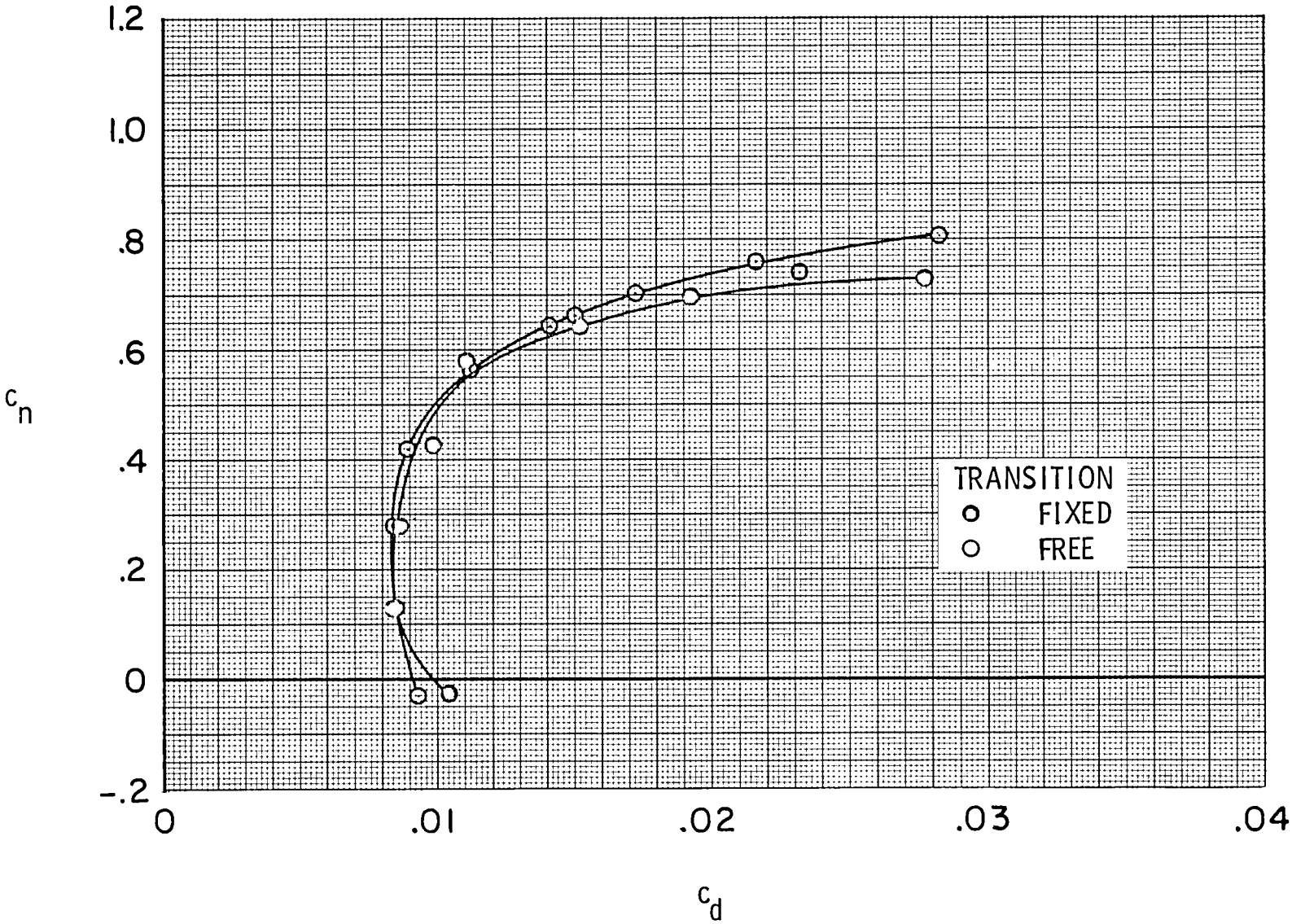

(b) c_n vs c_d.

Figure 21.- Concluded.

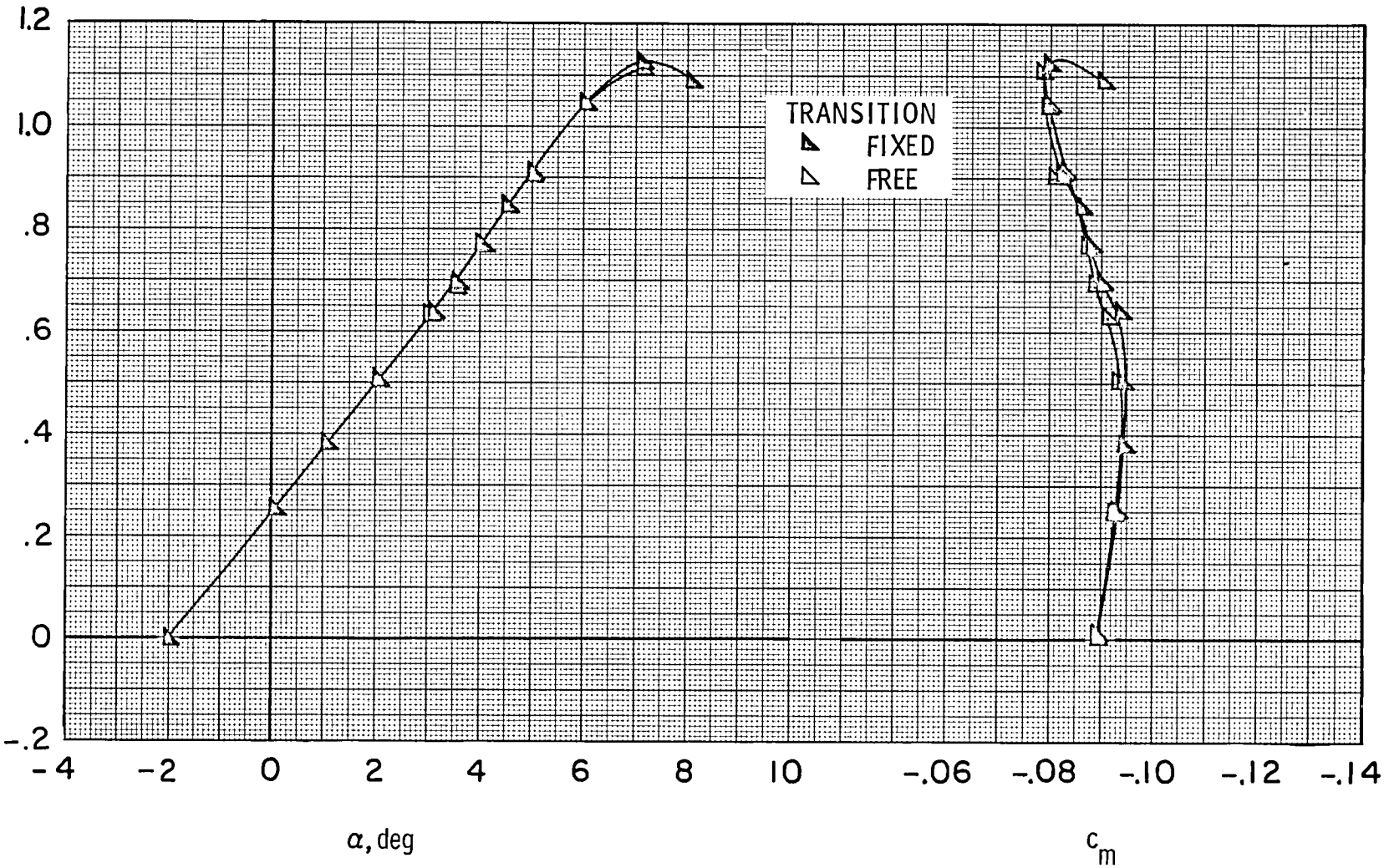

(a) c_n vs α and c_m.

Figure 22.- Effect of fixing transition on aerodynamic characteristics of airfoil at $M \approx 0.70$ and $R \approx 14.0 \times 10^6$.

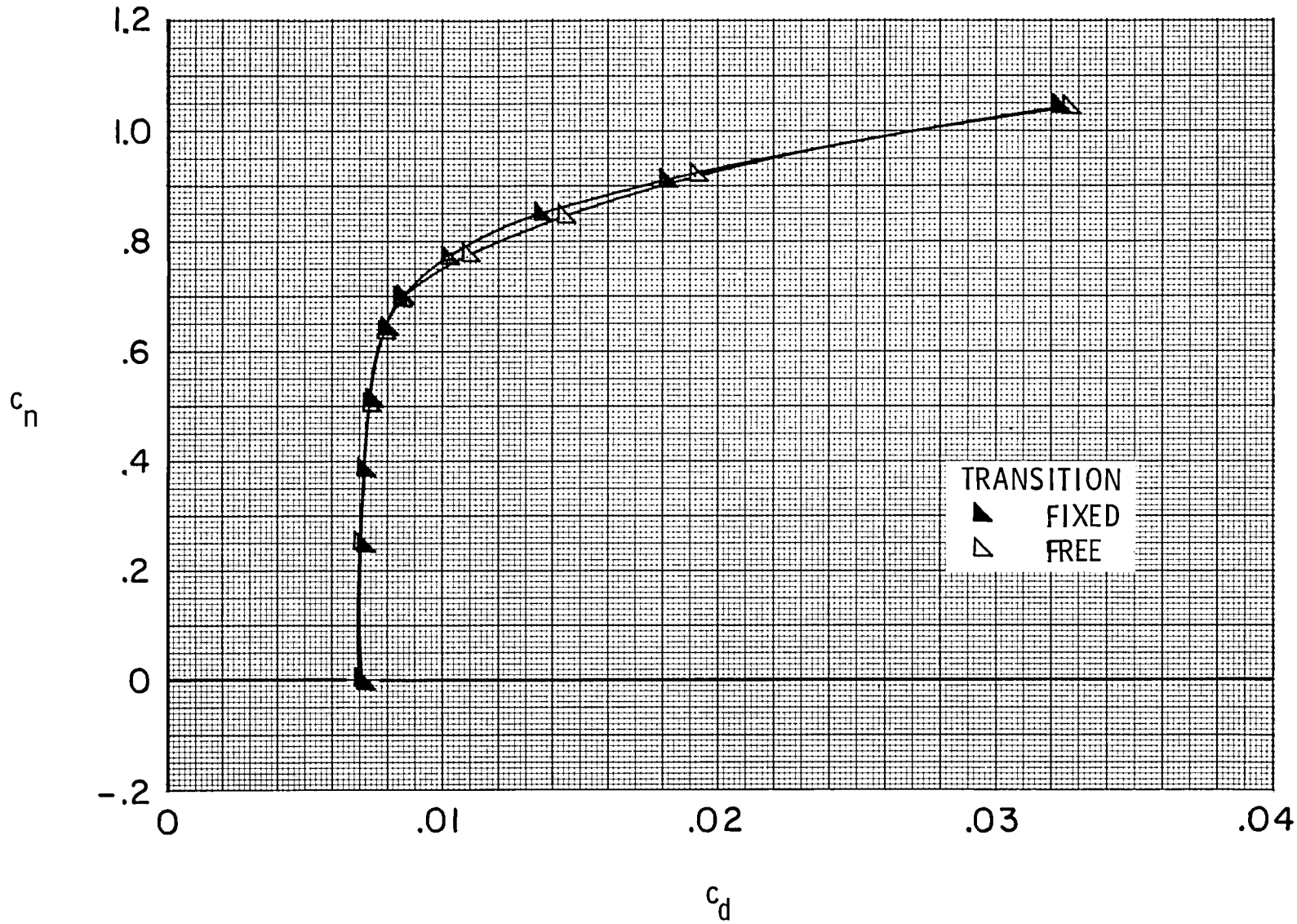

(b) c_n vs c_d.

Figure 22.- Concluded.

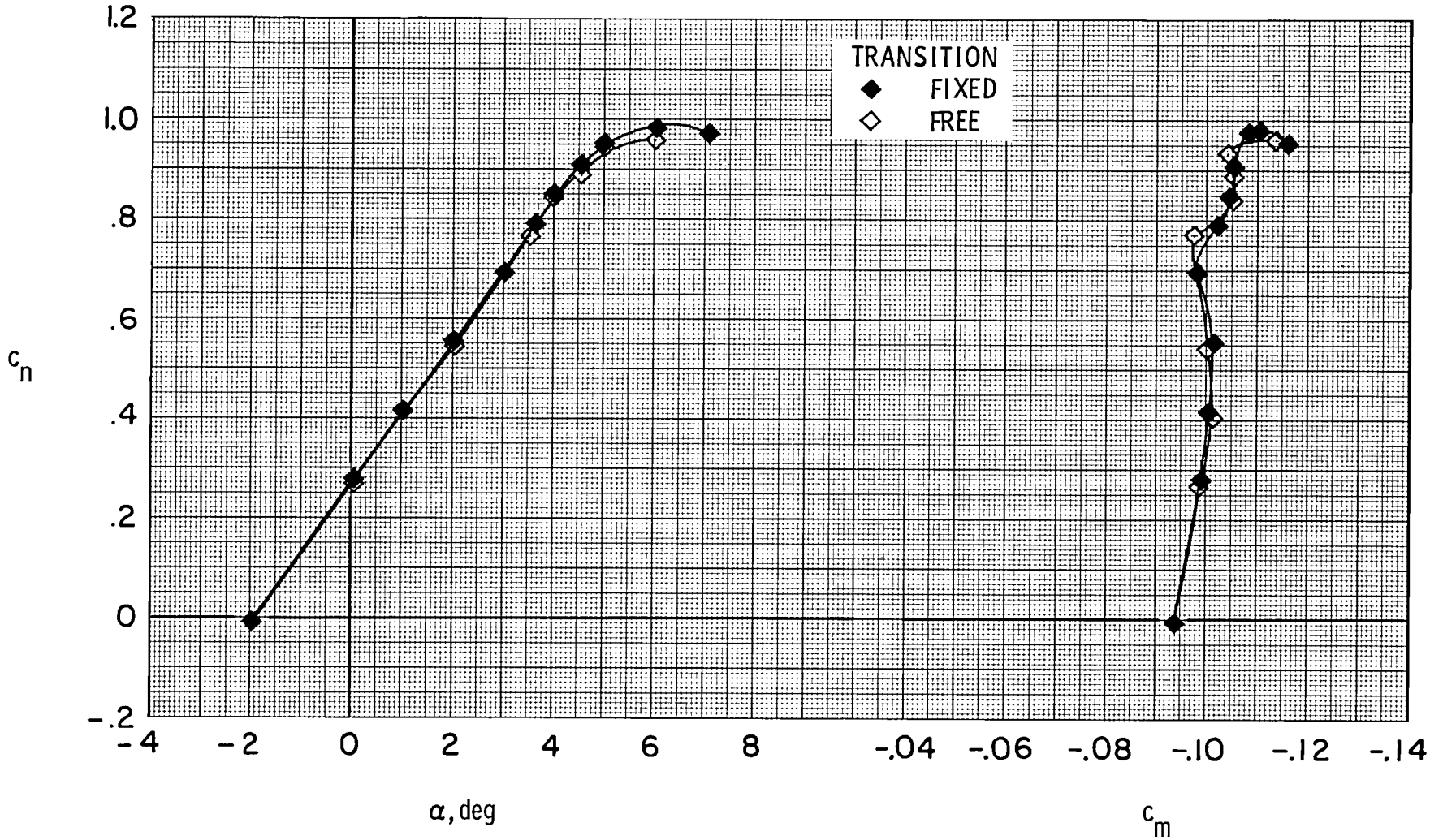

(a) c_n vs α and c_m.

Figure 23.- Effect of fixing transition on aerodynamic characteristics of airfoil at $M \approx 0.76$ and $R \approx 14.0 \times 10^6$.

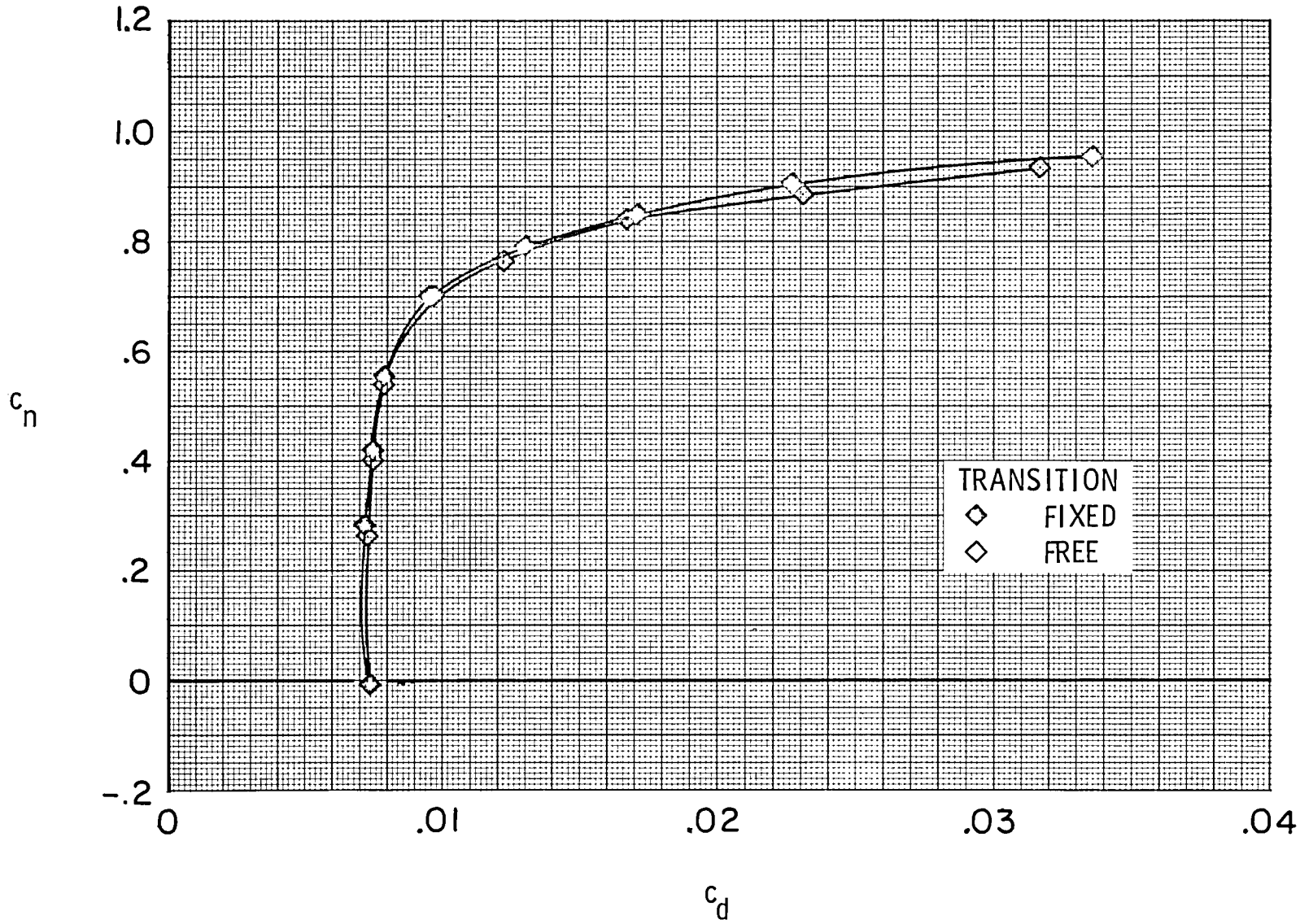

(b) c_n vs c_d.

Figure 23.- Concluded.

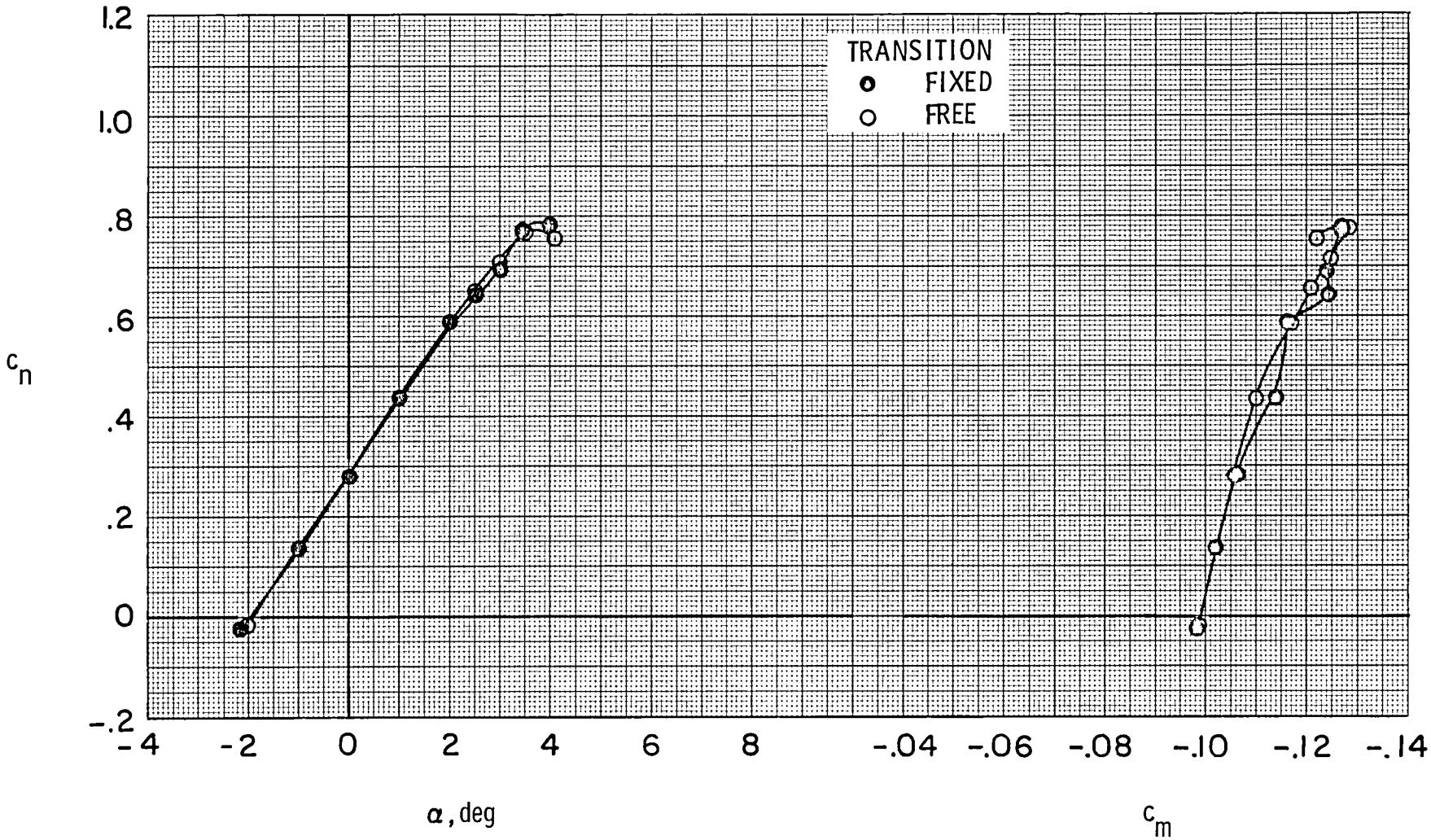

(a) c_n vs α and c_m.

Figure 24.- Effect of fixing transition on aerodynamic characteristics of airfoil at $M \approx 0.80$ and $R \approx 14.0 \times 10^6$.

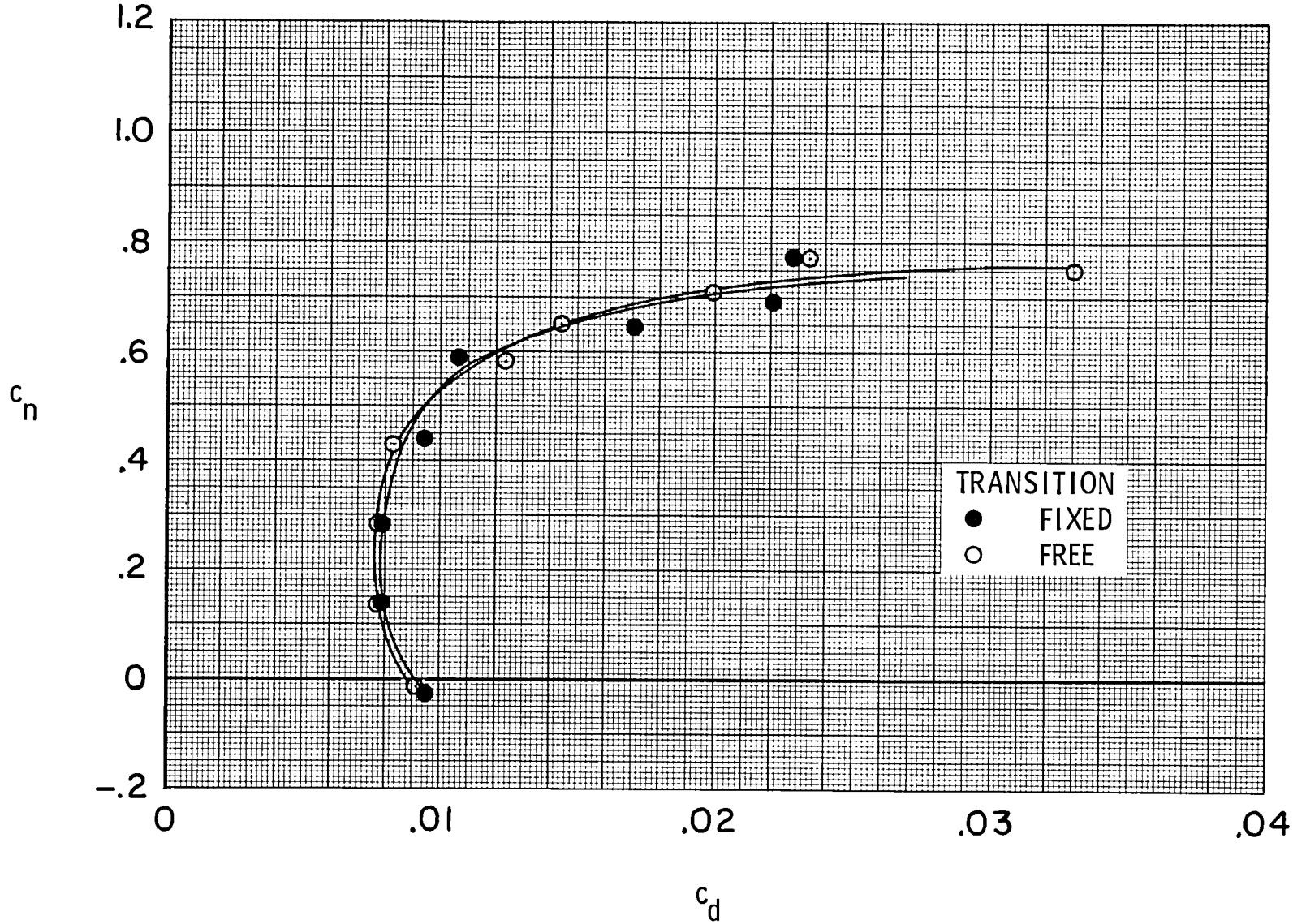

(b) c_n vs c_d.

Figure 24.- Concluded.

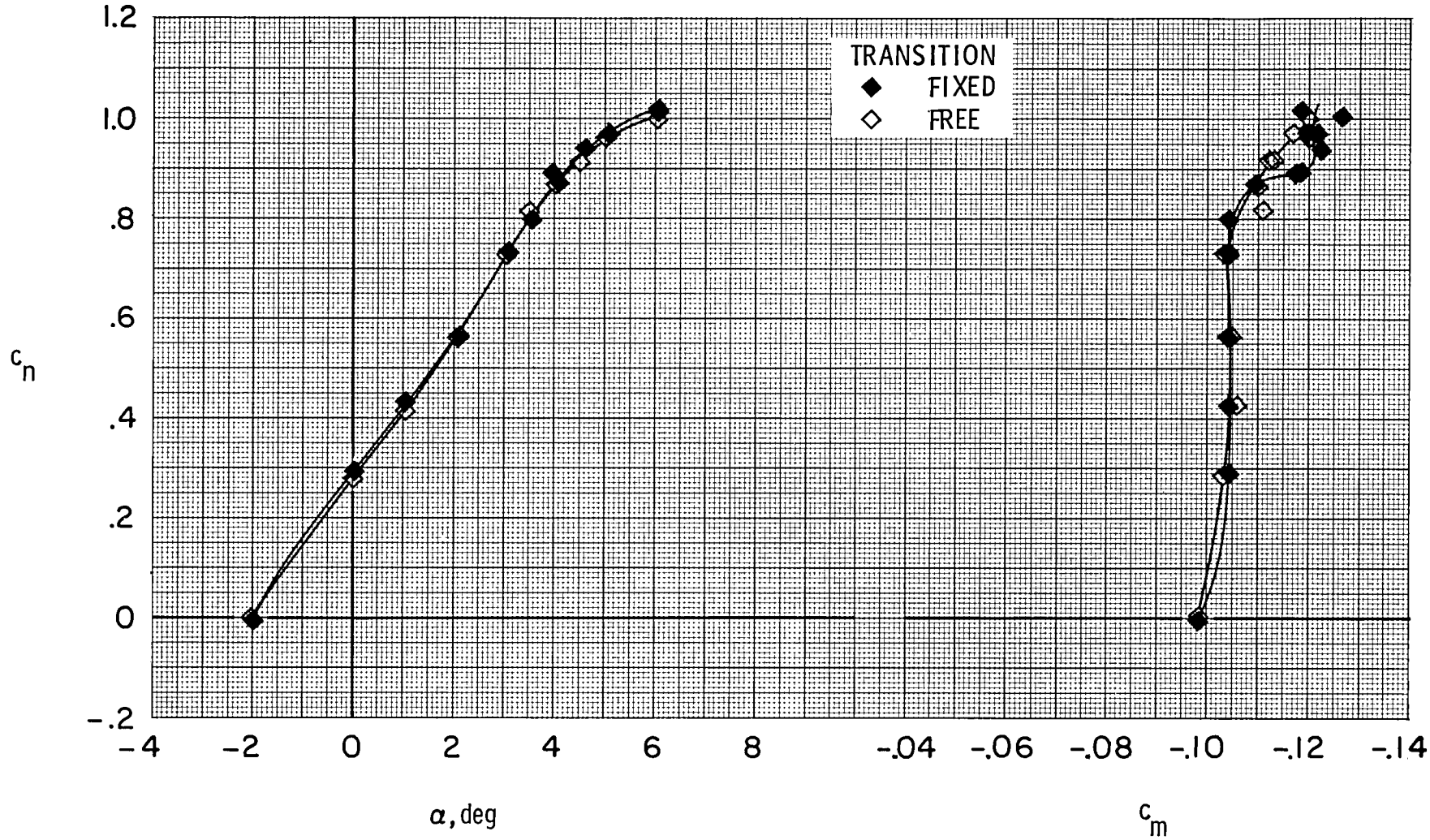

(a) c_n vs α and c_m.

Figure 25.- Effect of fixing transition on aerodynamic characteristics of airfoil at $M \approx 0.76$ and $R \approx 30.0 \times 10^6$.

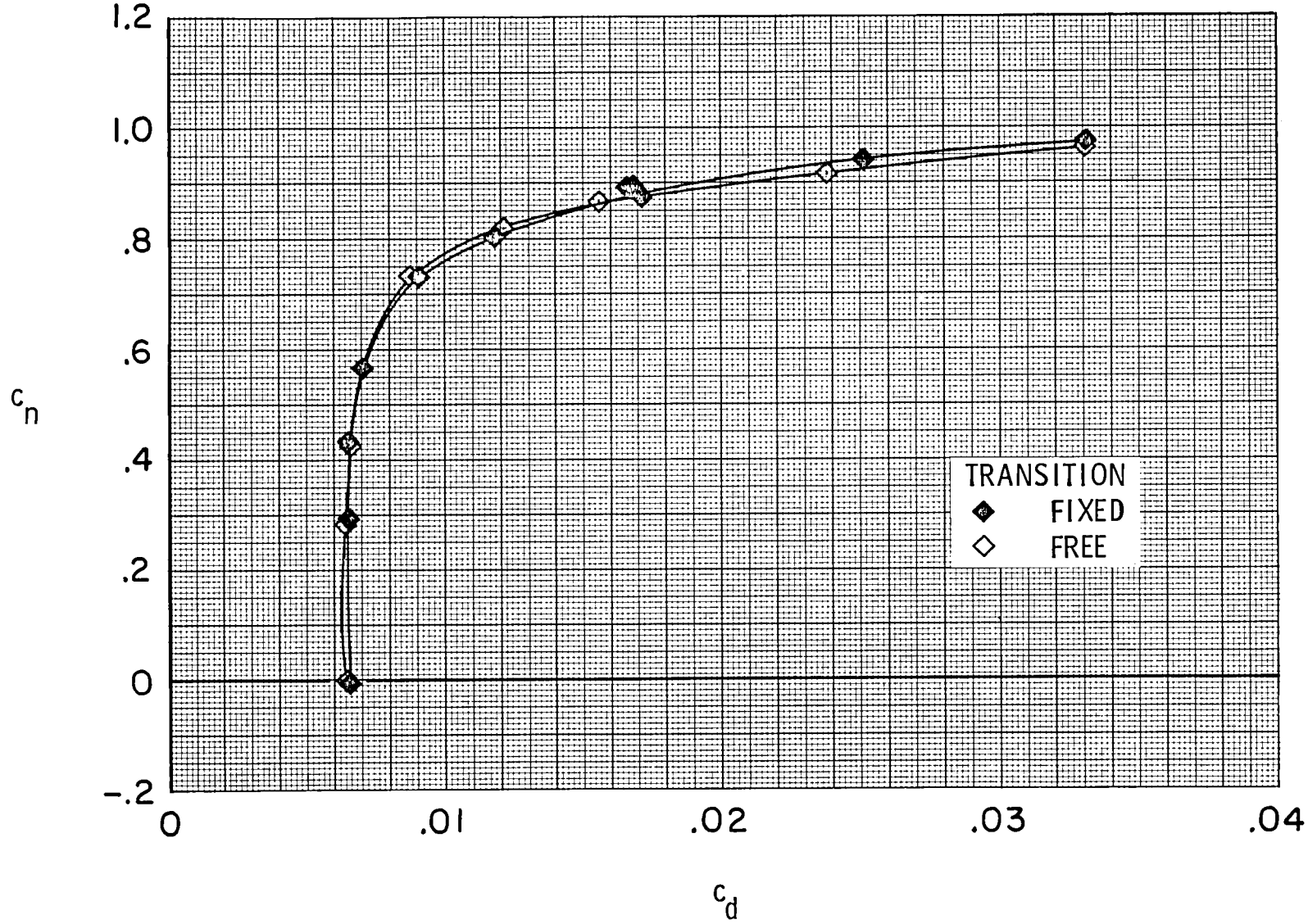

(b) c_n vs c_d.

Figure 25.- Concluded.

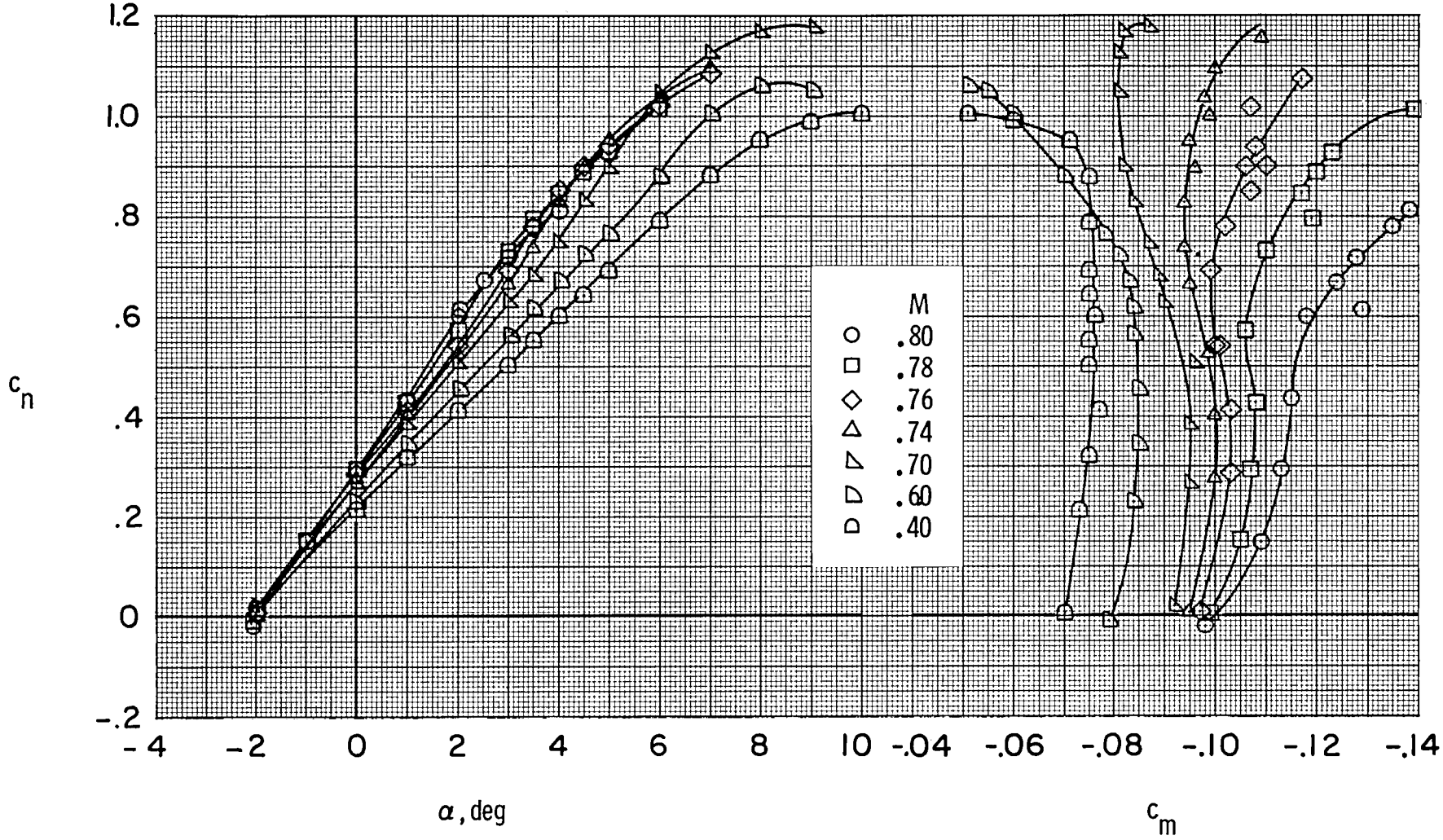

(a) c_n vs α and c_m.

Figure 26.- Effect of Mach number on aerodynamic characteristics of airfoil with free transition at $R \approx 4.4 \times 10^6$.

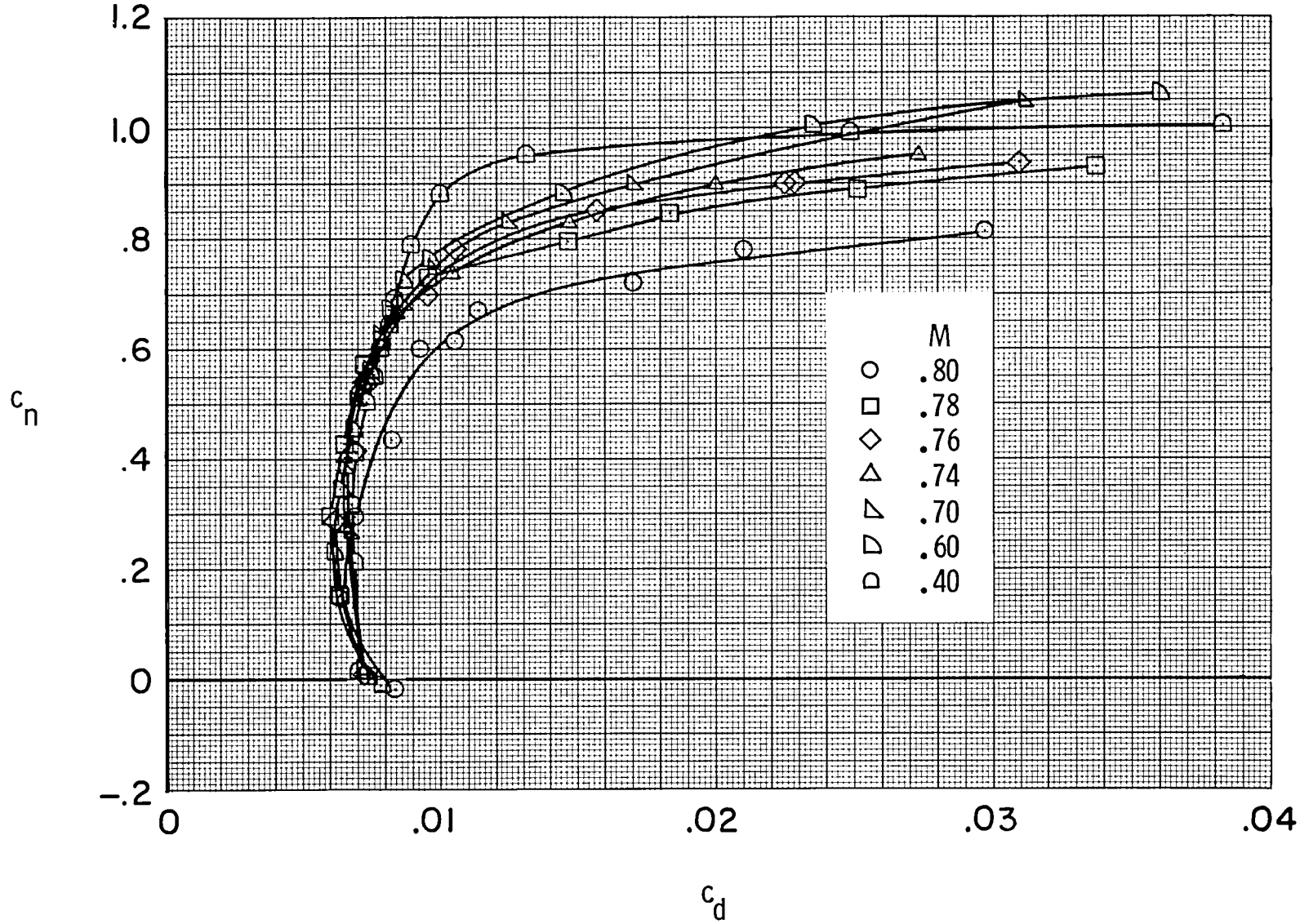

(b) c_n vs c_d.

Figure 26.- Concluded.

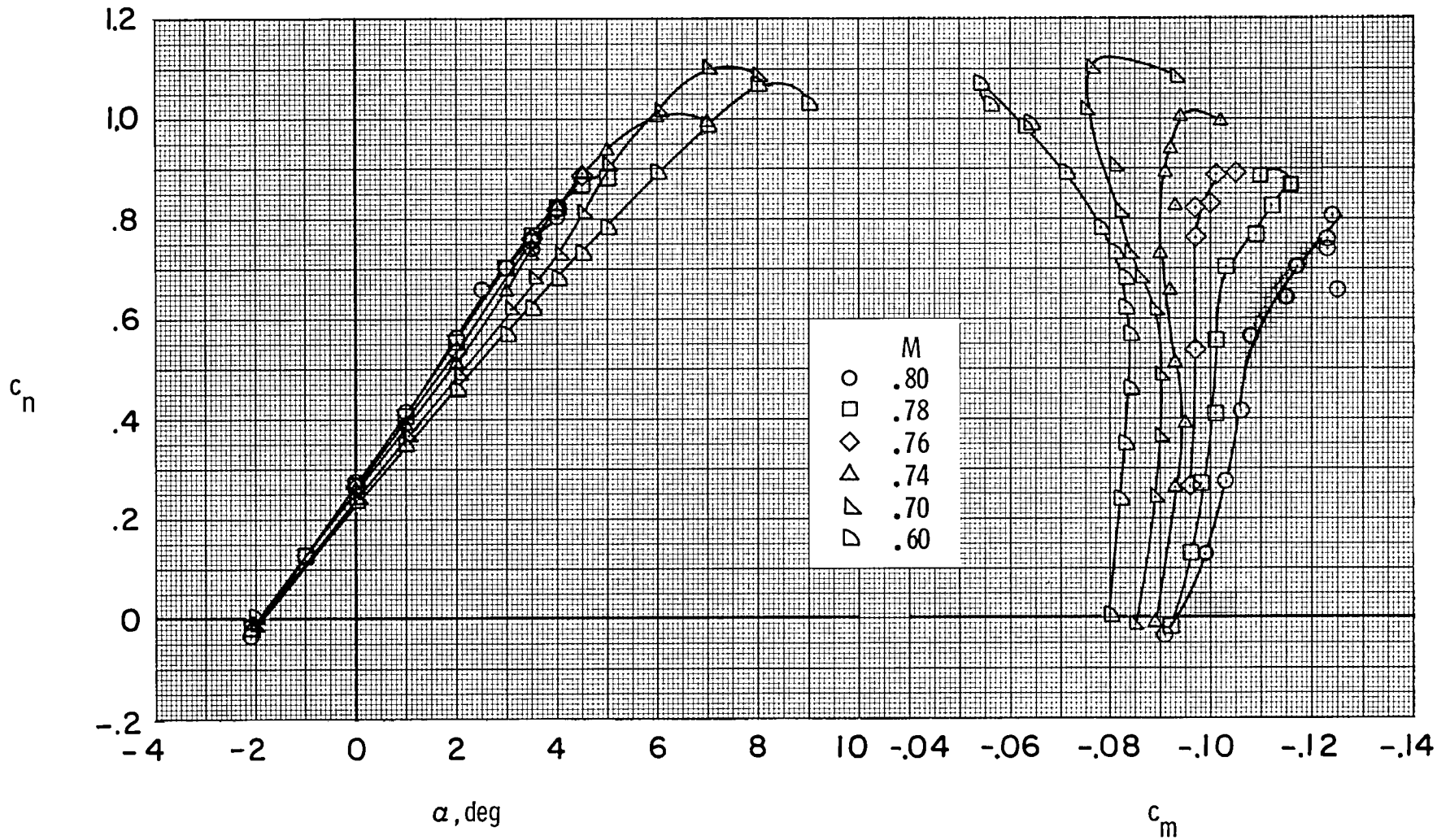

(a) c_n vs α and c_m.

Figure 27.- Effect of Mach number on aerodynamic characteristics of airfoil with free transition at $R \approx 7.7 \times 10^6$.

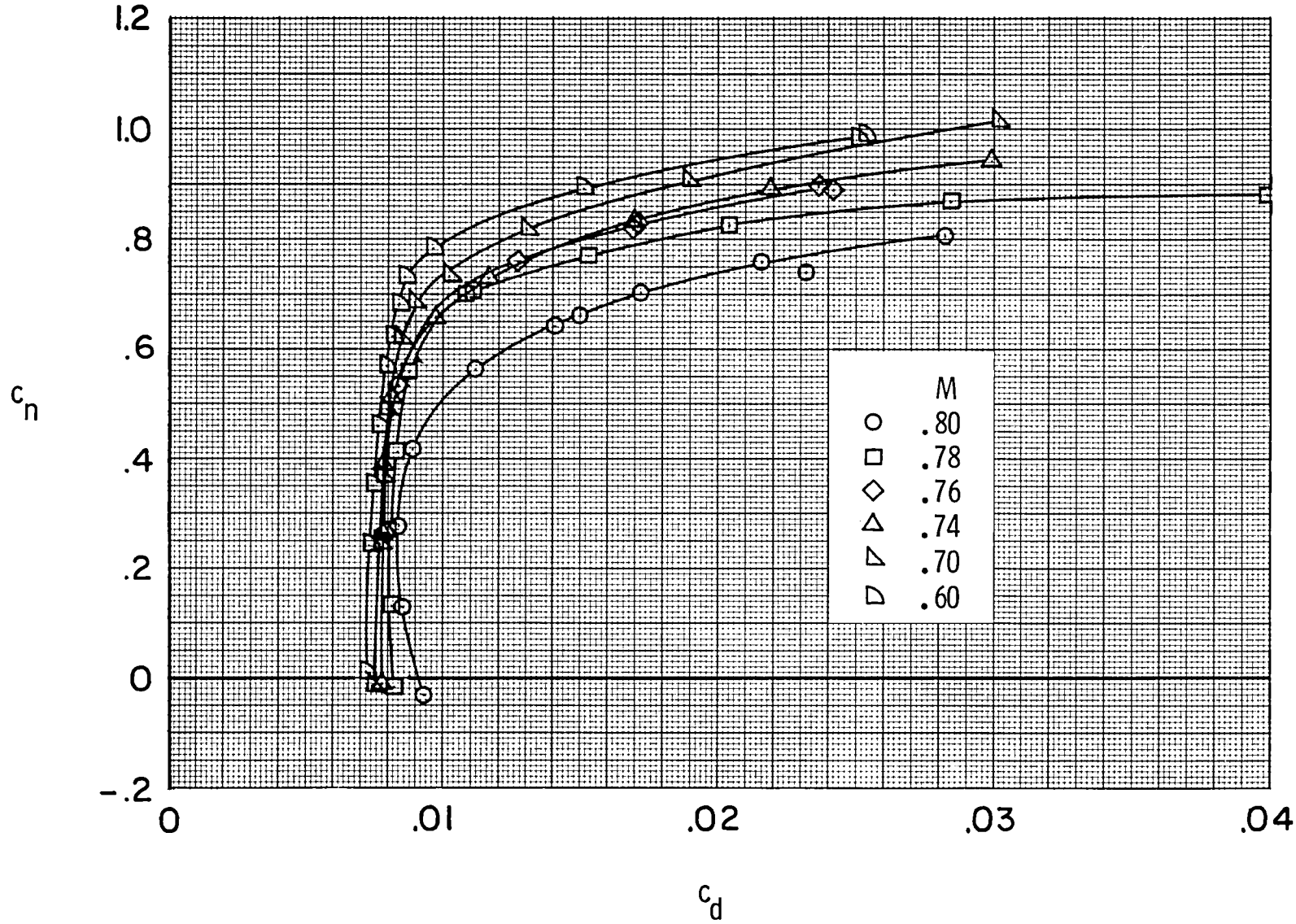

(b) c_n vs c_d.

Figure 27.- Concluded.

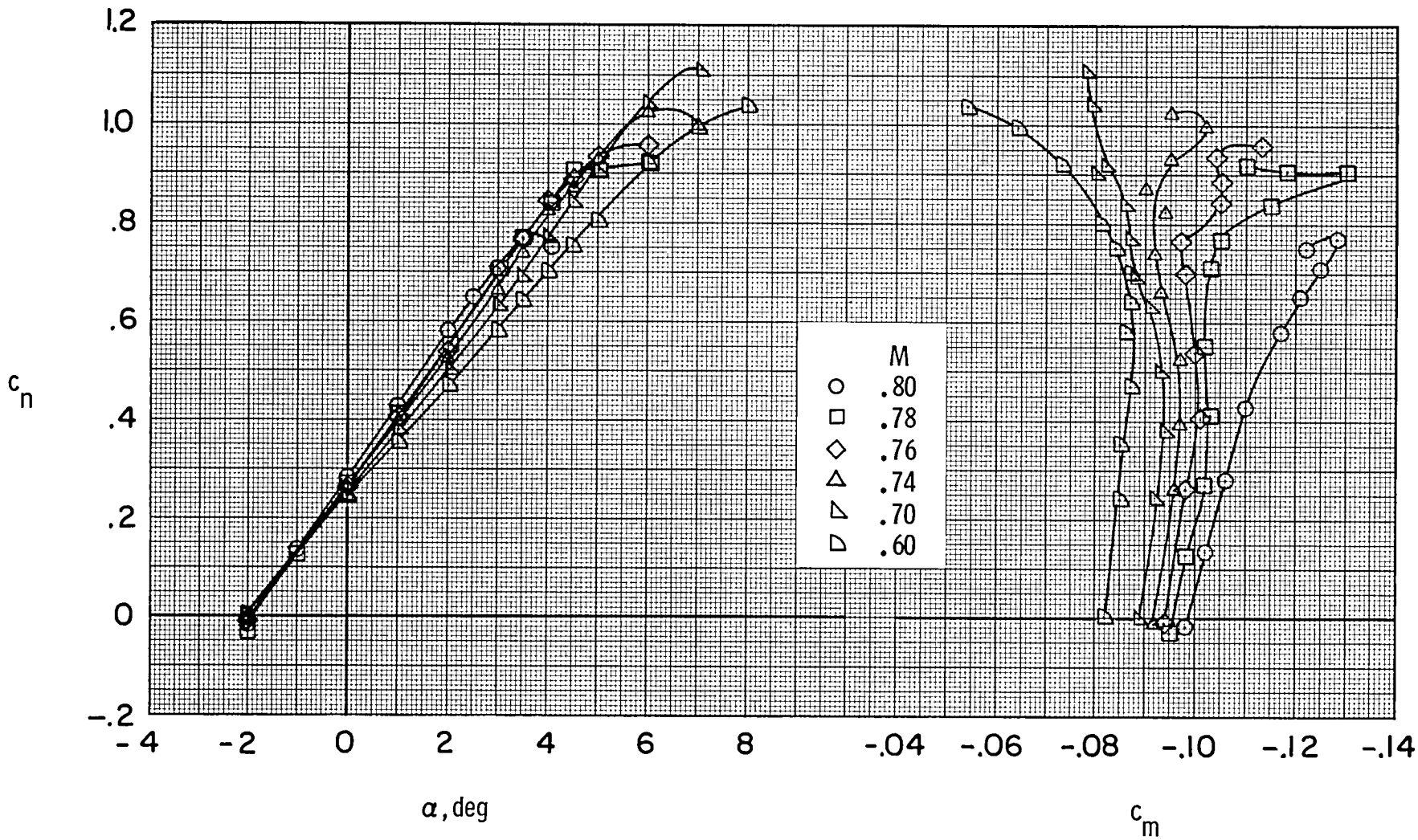

(a) c_n vs α and c_m.

Figure 28.- Effect of Mach number on aerodynamic characteristics of airfoil with free transition at $R \approx 14.0 \times 10^6$.

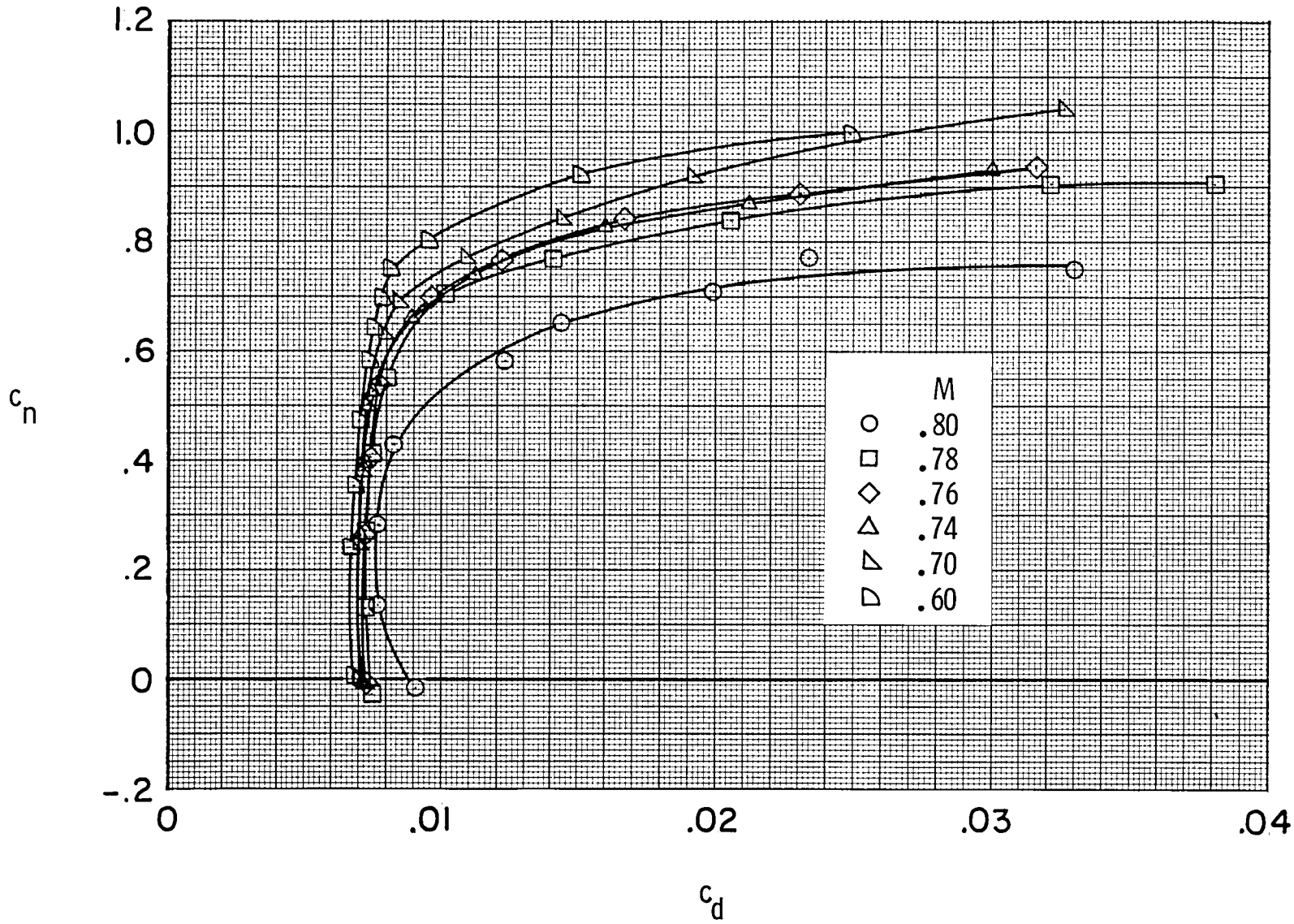

(b) c_n vs c_d.

Figure 28.- Concluded.

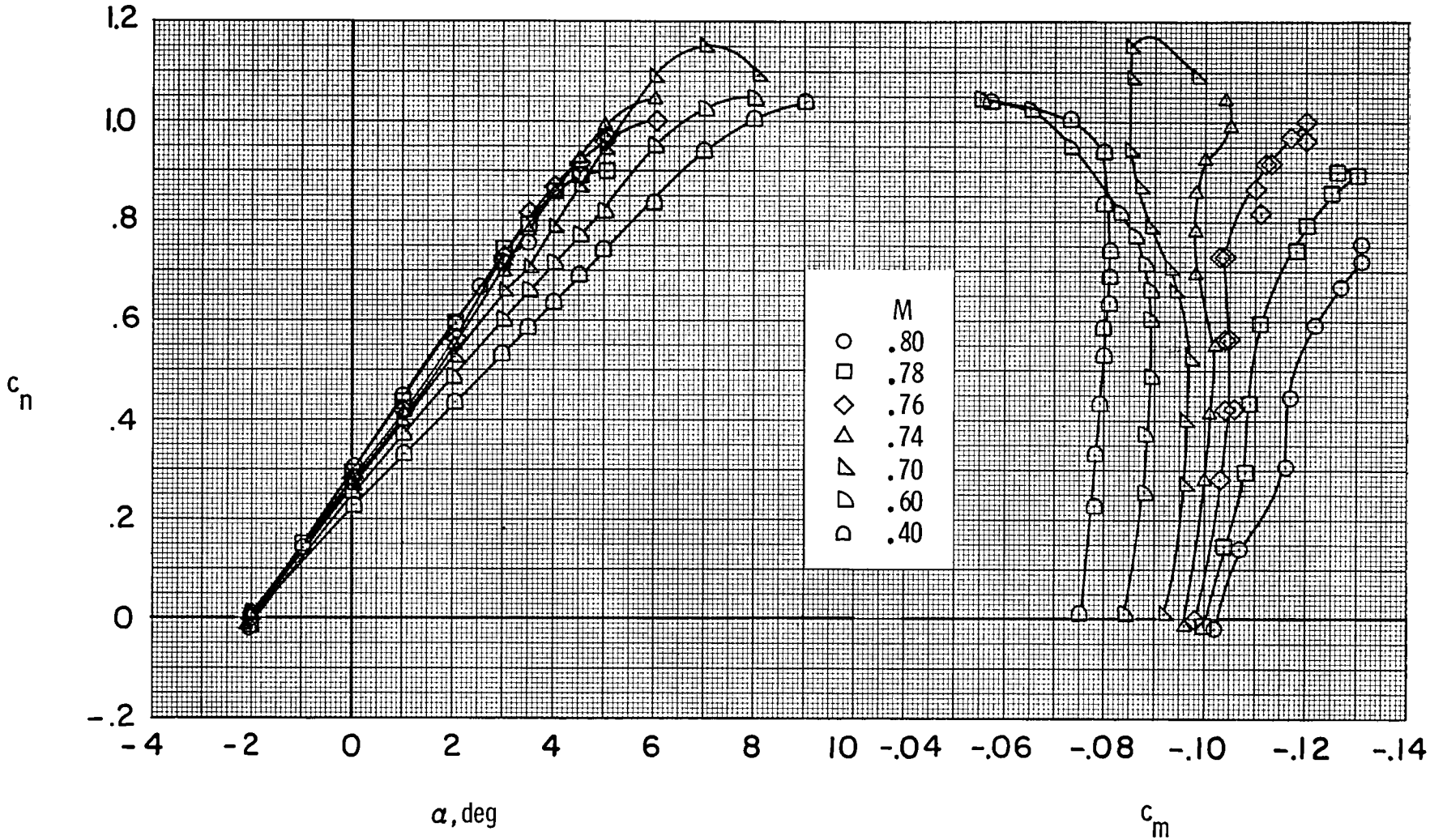

(a) c_n vs α and c_m.

Figure 29.- Effect of Mach number on aerodynamic characteristics of airfoil with free transition at $R \approx 30.0 \times 10^6$.

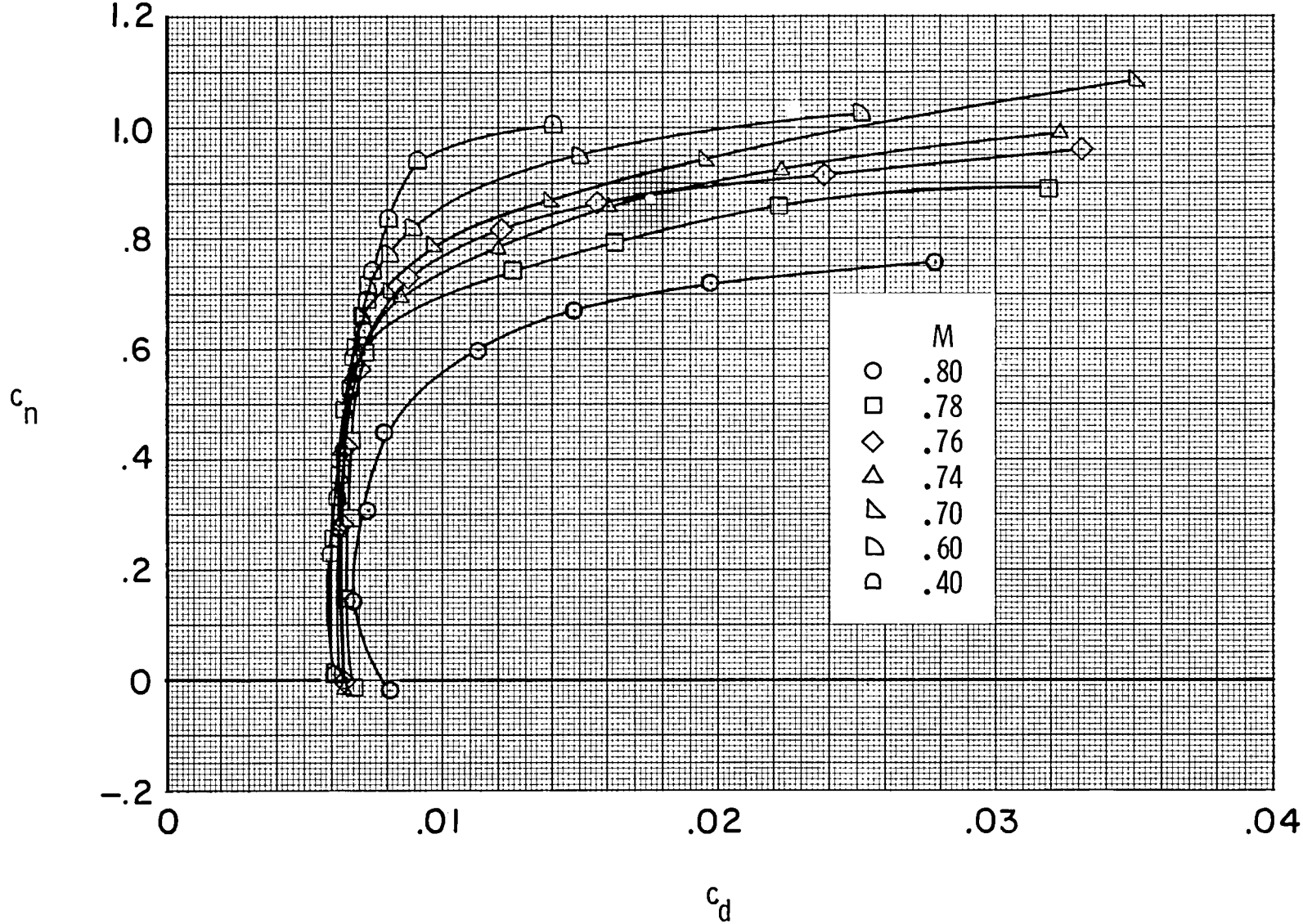

(b) c_n vs c_d.

Figure 29.- Concluded.

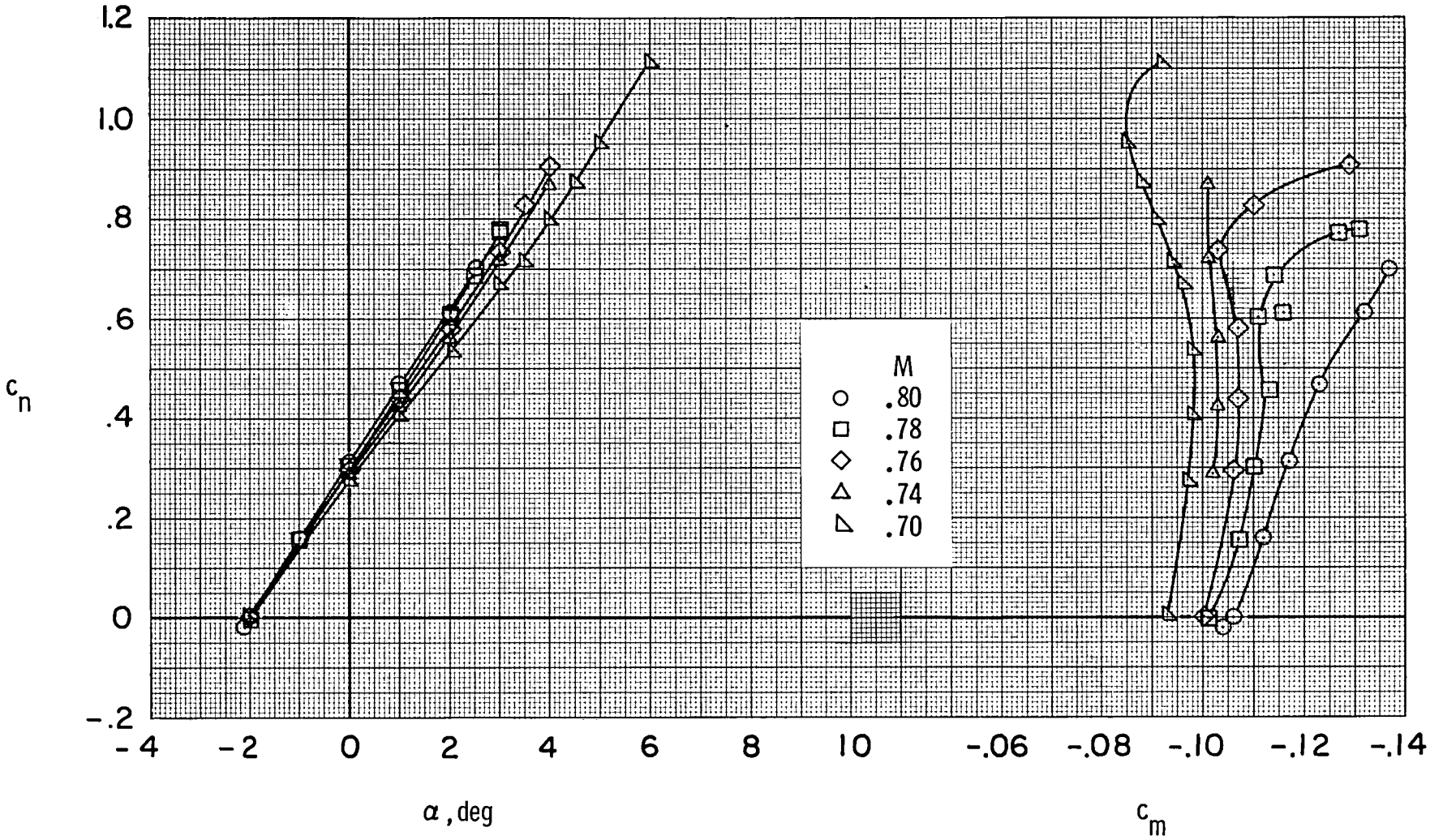

(a) c_n vs α and c_m.

Figure 30.- Effect of Mach number on aerodynamic characteristics of airfoil with free transition at $R \approx 45.0 \times 10^6$.

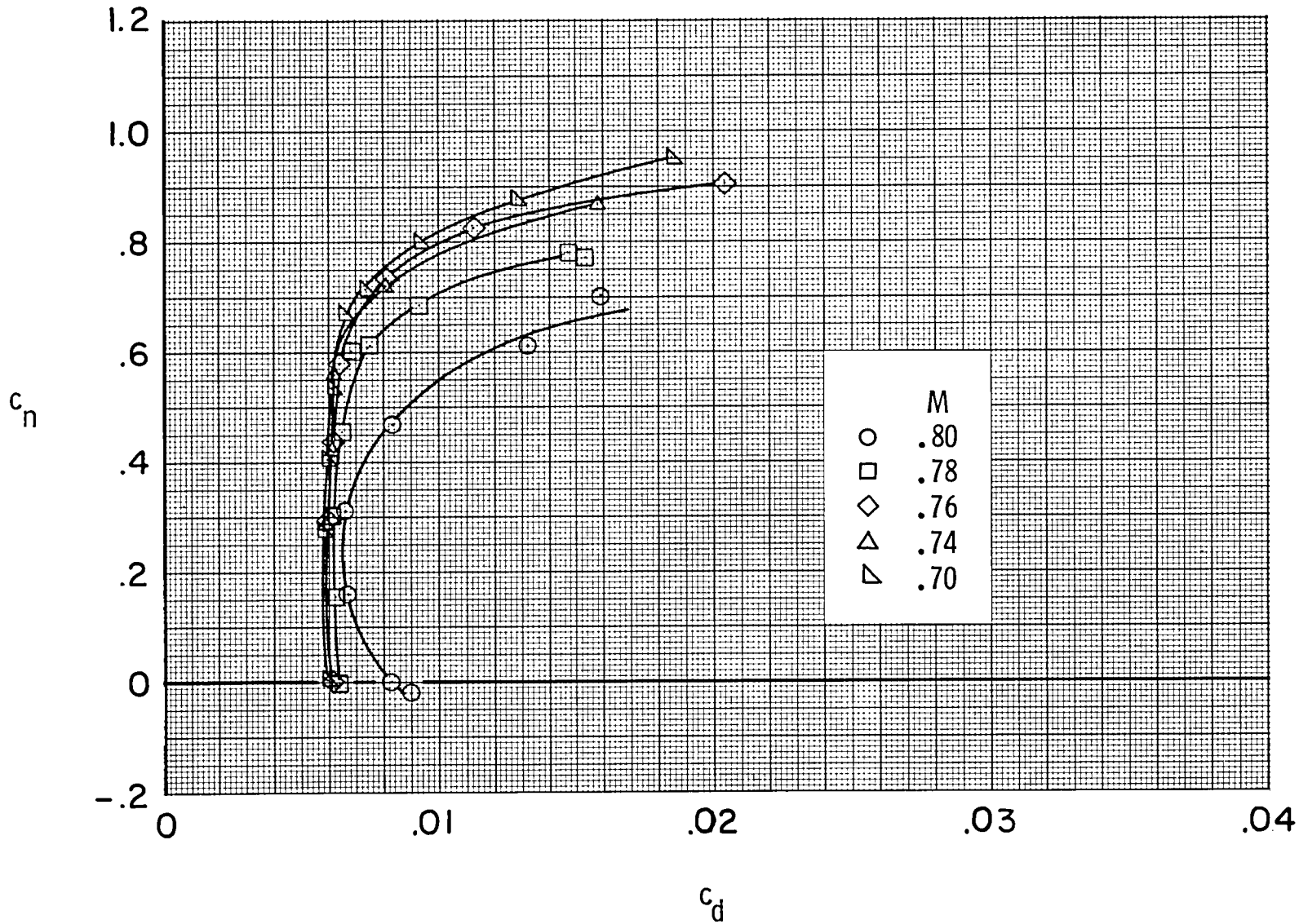

(b) c_n vs c_d.

Figure 30.- Concluded.

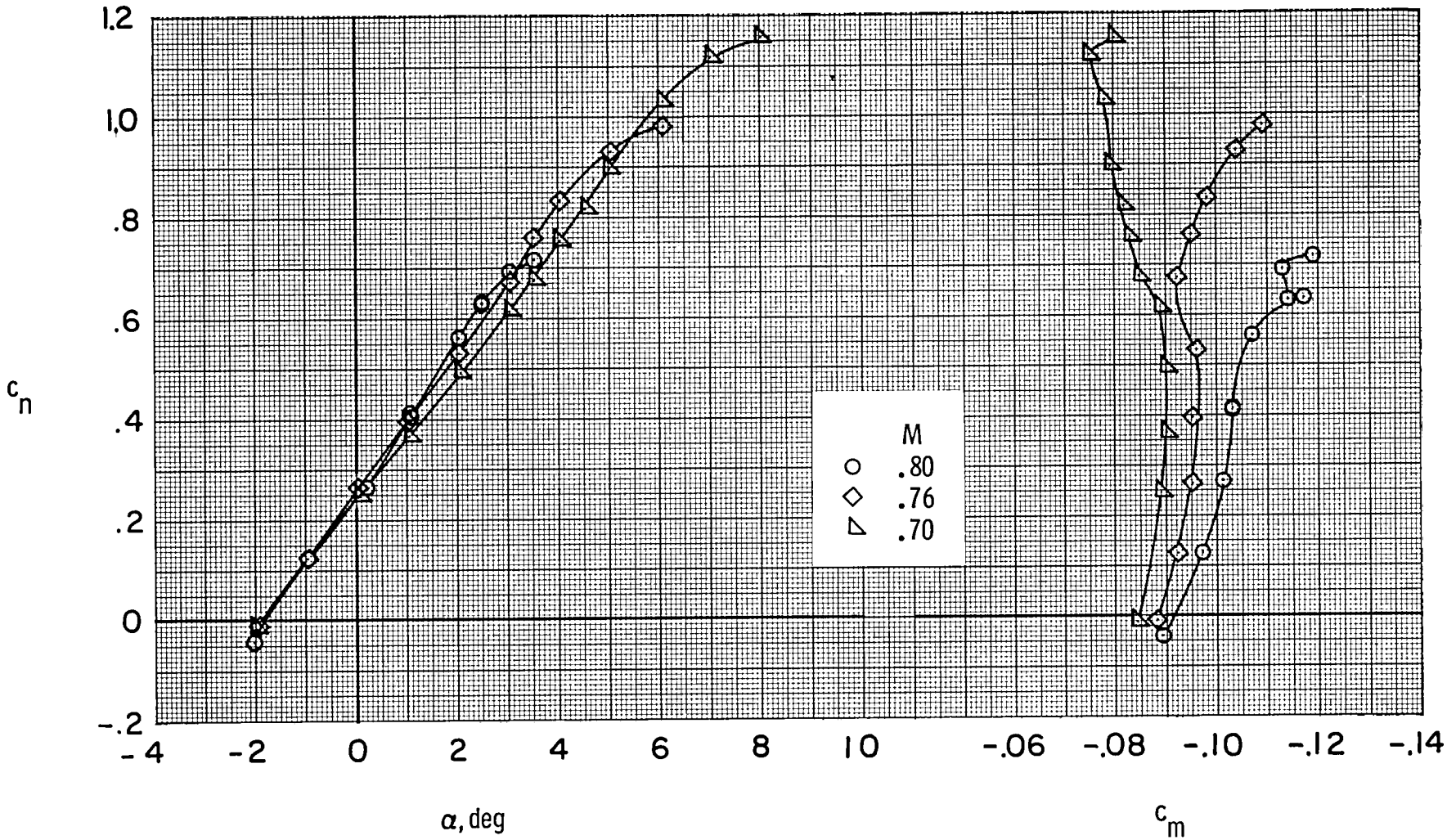

(a) c_n vs α and c_m.

Figure 31.- Effect of Mach number on aerodynamic characteristics of airfoil with fixed transition at $R \approx 4.4 \times 10^6$.

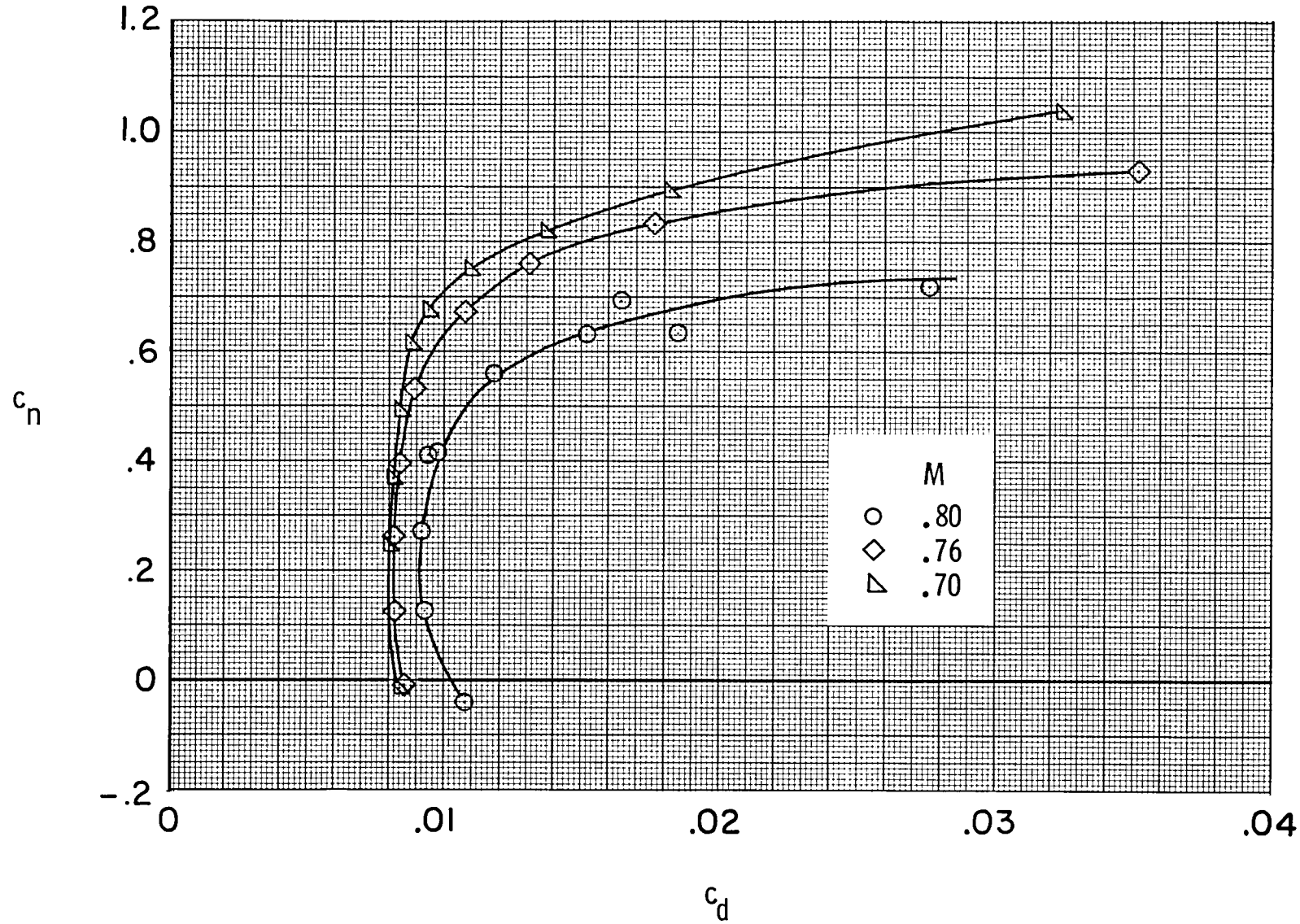

(b) c_n vs c_d.

Figure 31.- Concluded.

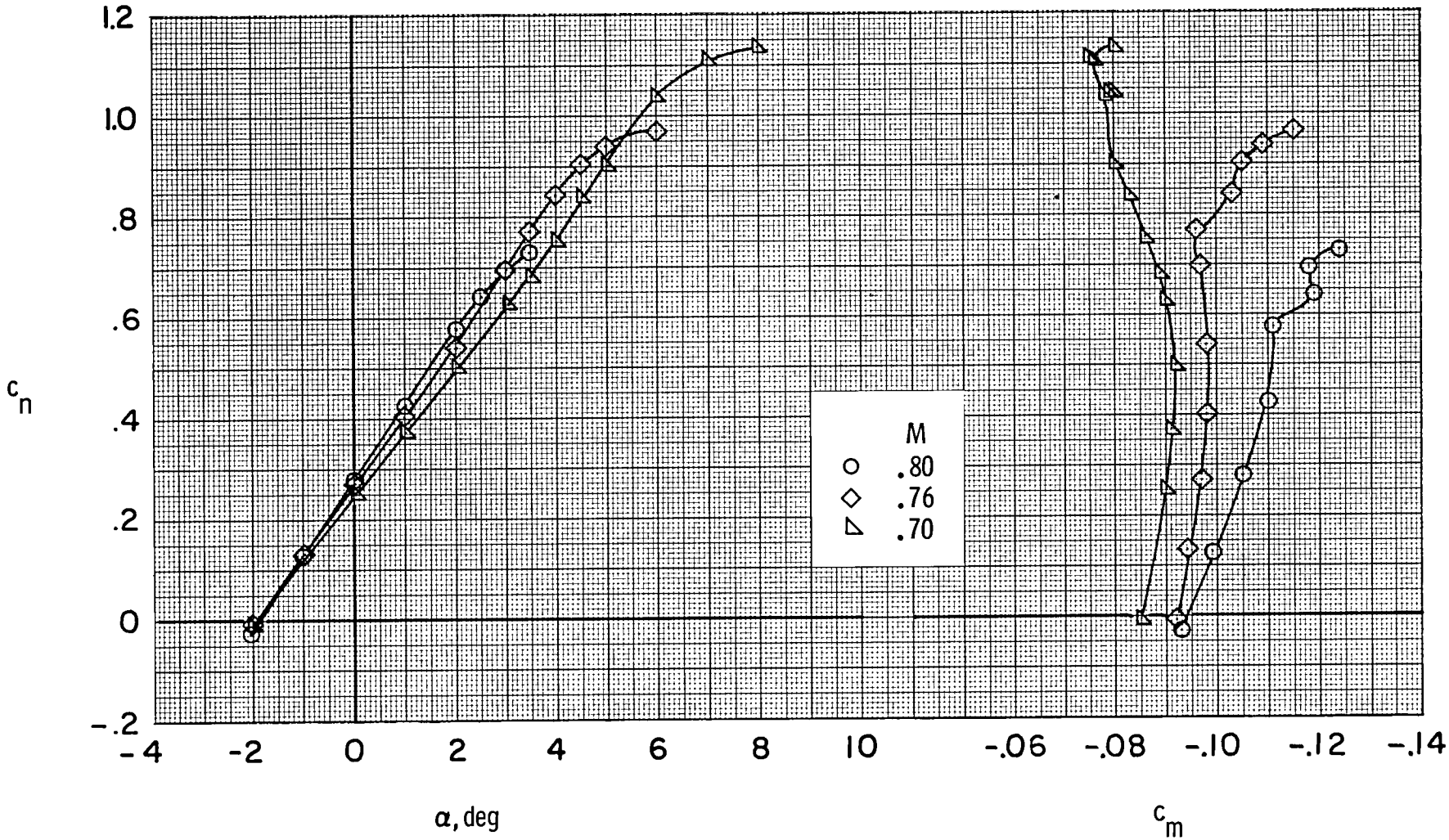

(a) c_n vs α and c_m.

Figure 32.- Effect of Mach number on aerodynamic characteristics of airfoil with fixed transition at $R \approx 7.7 \times 10^6$.

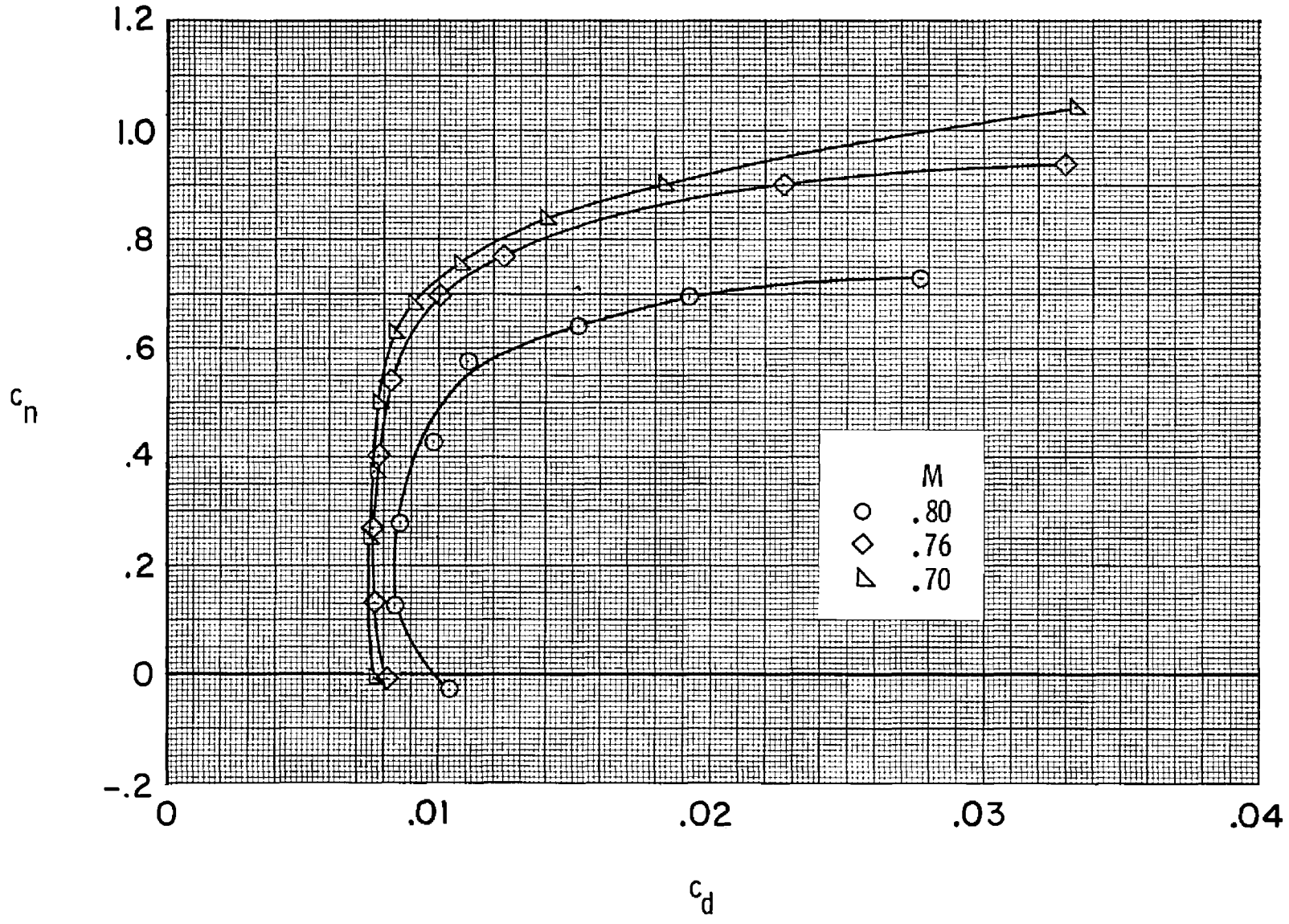

(b) c_n vs c_d.

Figure 32.- Concluded.

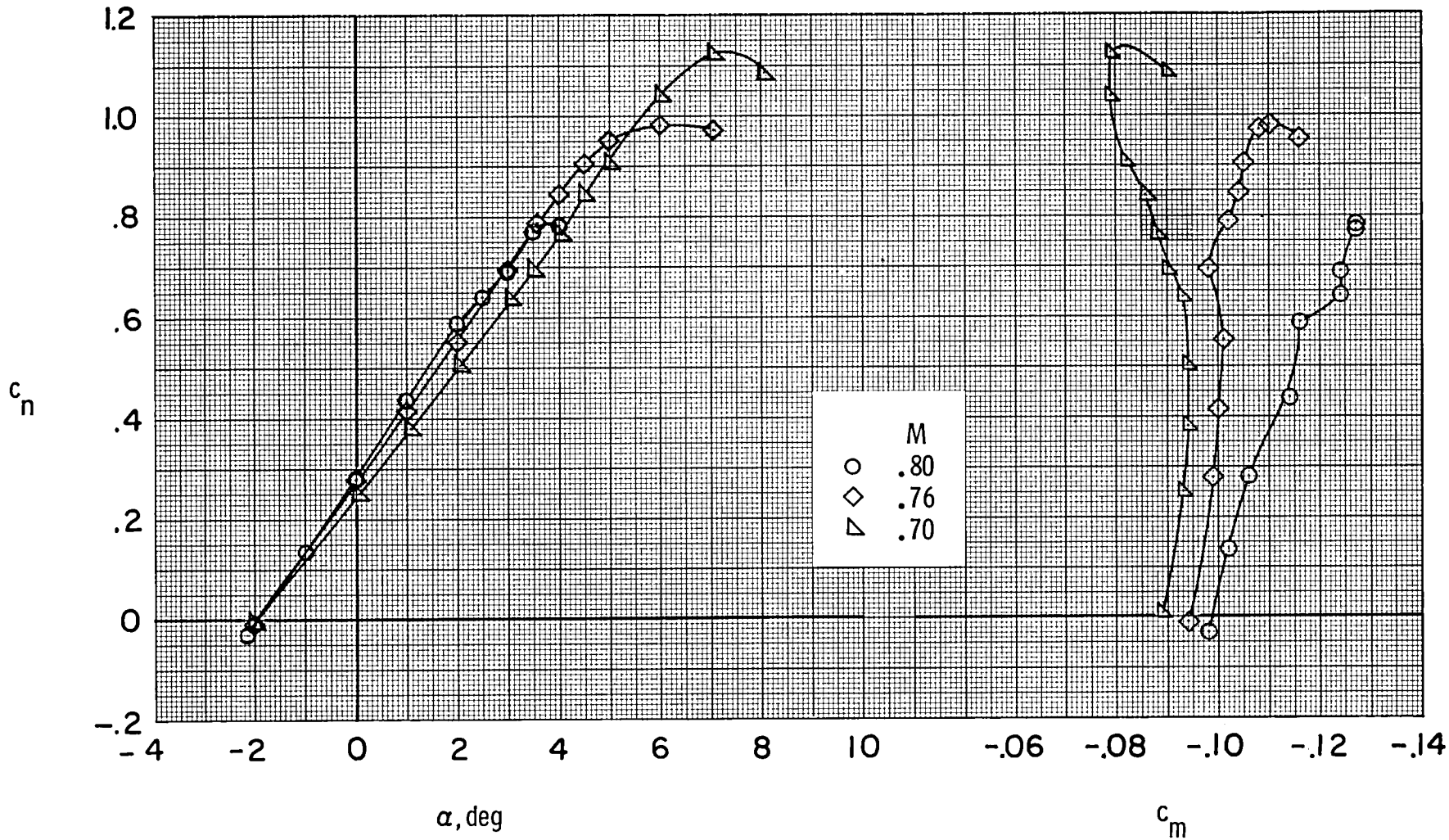

(a) c_n vs α and c_m.

Figure 33.- Effect of Mach number on aerodynamic characteristics of airfoil with fixed transition at $R \approx 14.0 \times 10^6$.

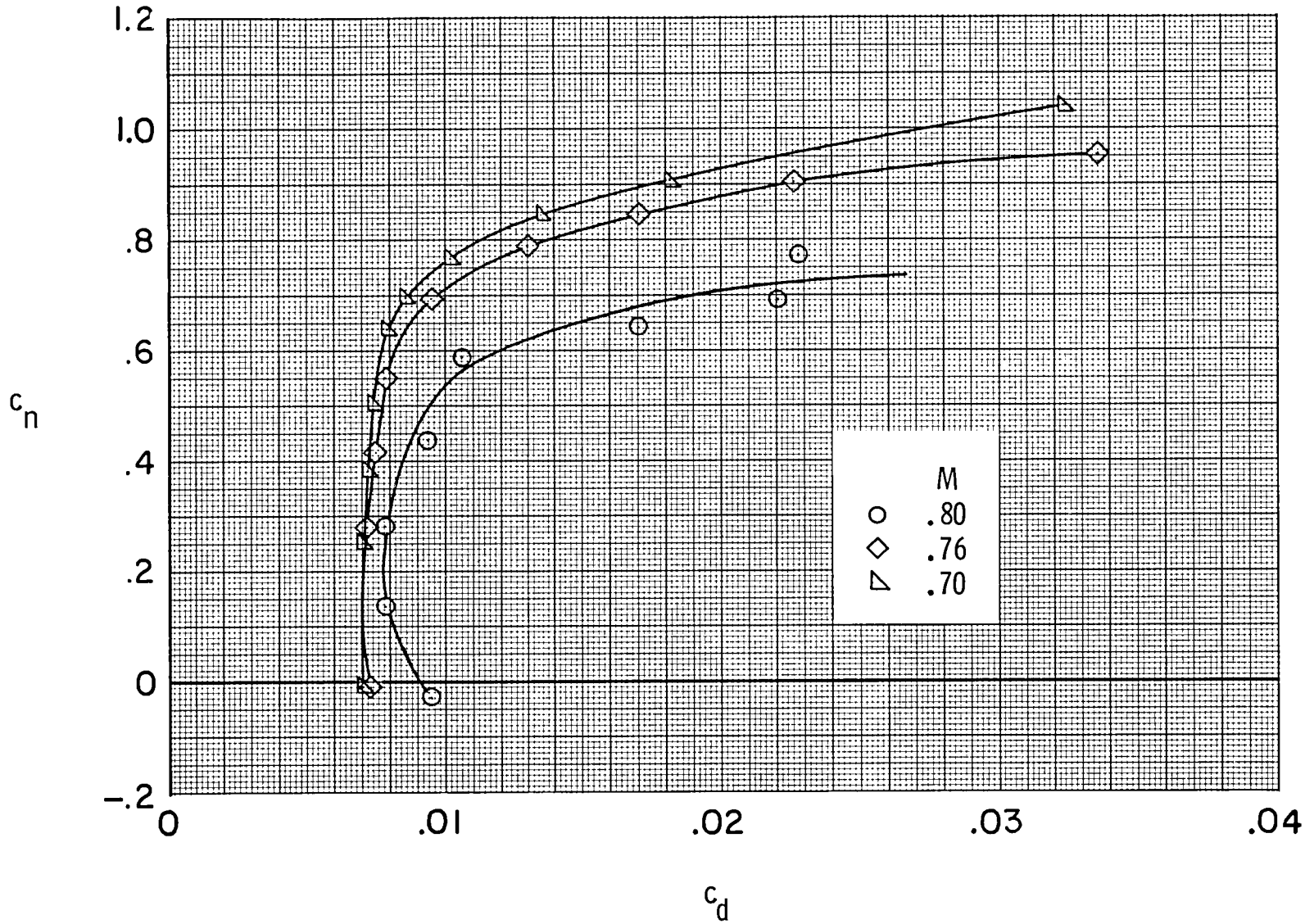

(b) c_n vs c_d.

Figure 33.- Concluded.

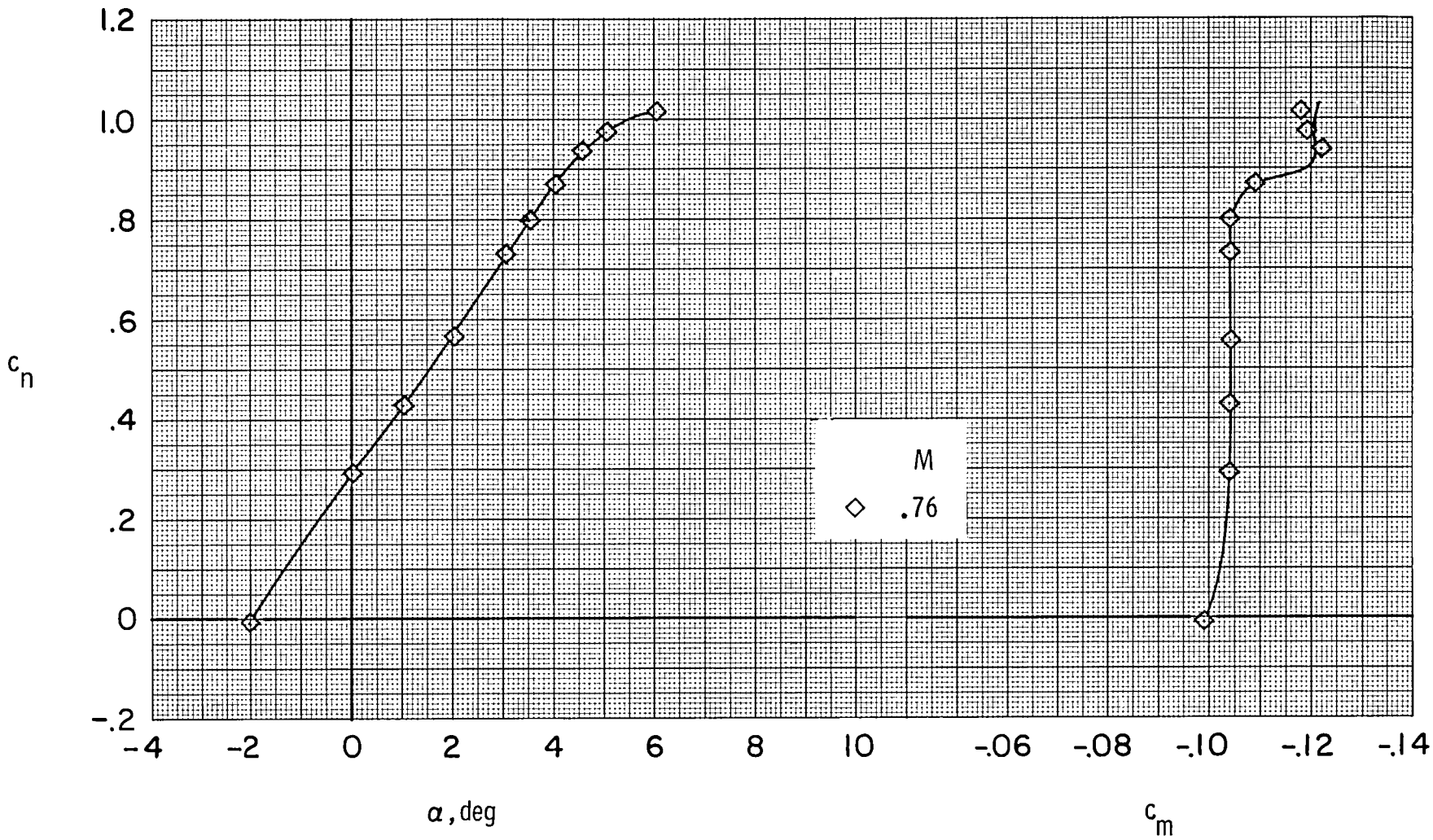

(a) c_n vs α and c_m.

Figure 34.- Effect of Mach number on aerodynamic characteristics of airfoil with fixed transition at $R \approx 30.0 \times 10^6$.

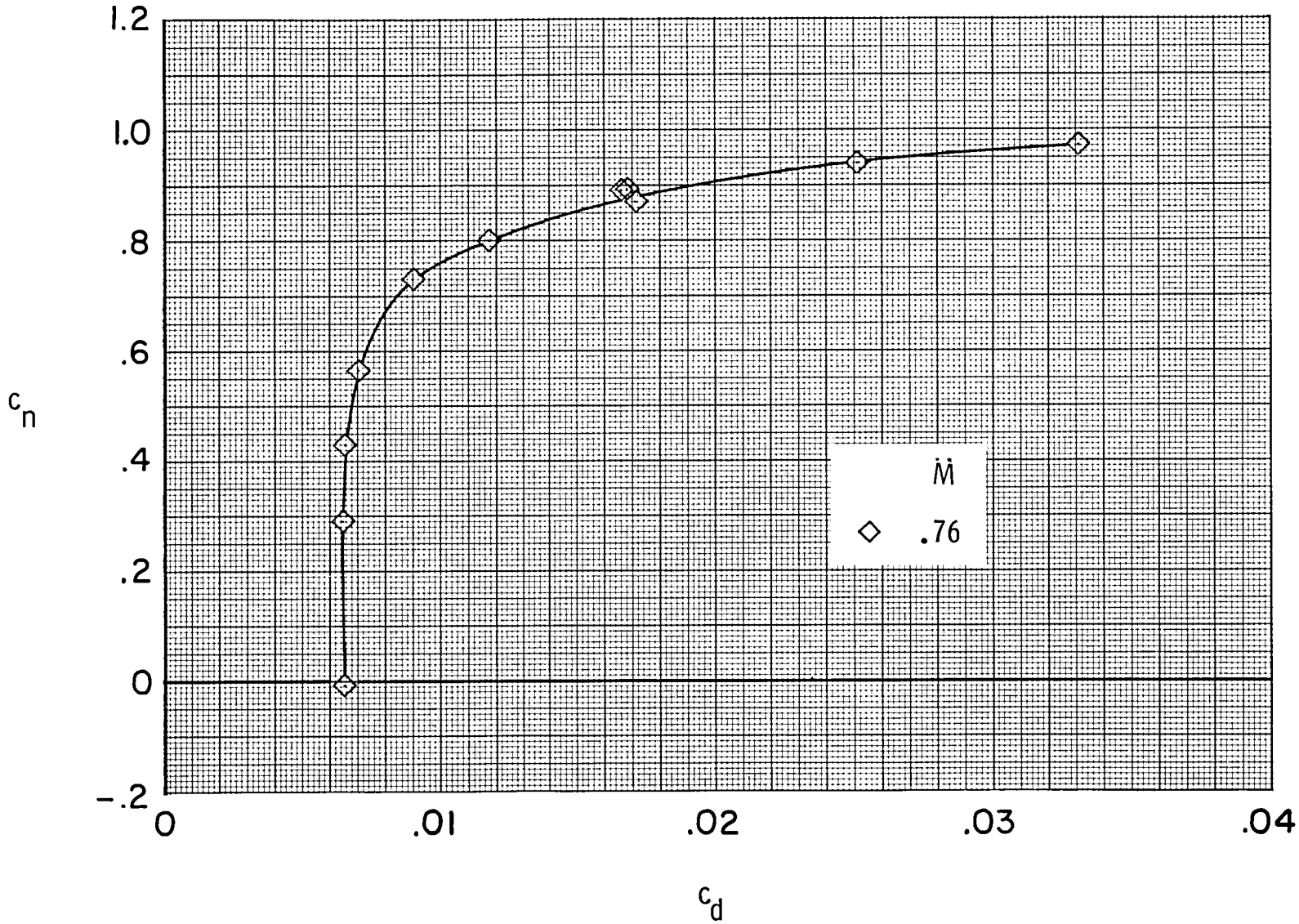

(b) c_n vs c_d.

Figure 34.- Concluded.

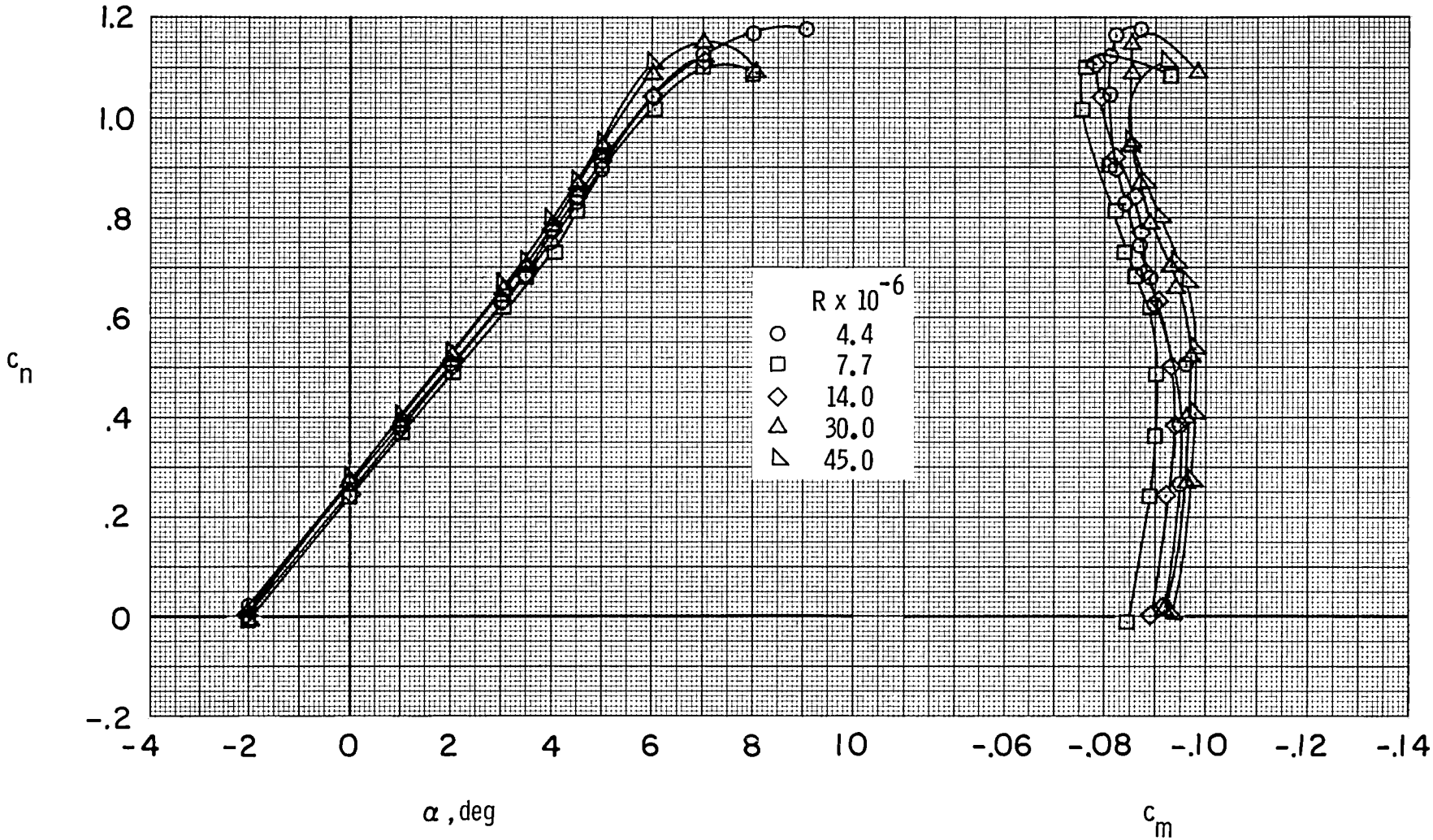

(a) c_n vs α and c_m.

Figure 35.- Effect of Reynolds number on aerodynamic characteristics of airfoil with free transition at $M \approx 0.70$.

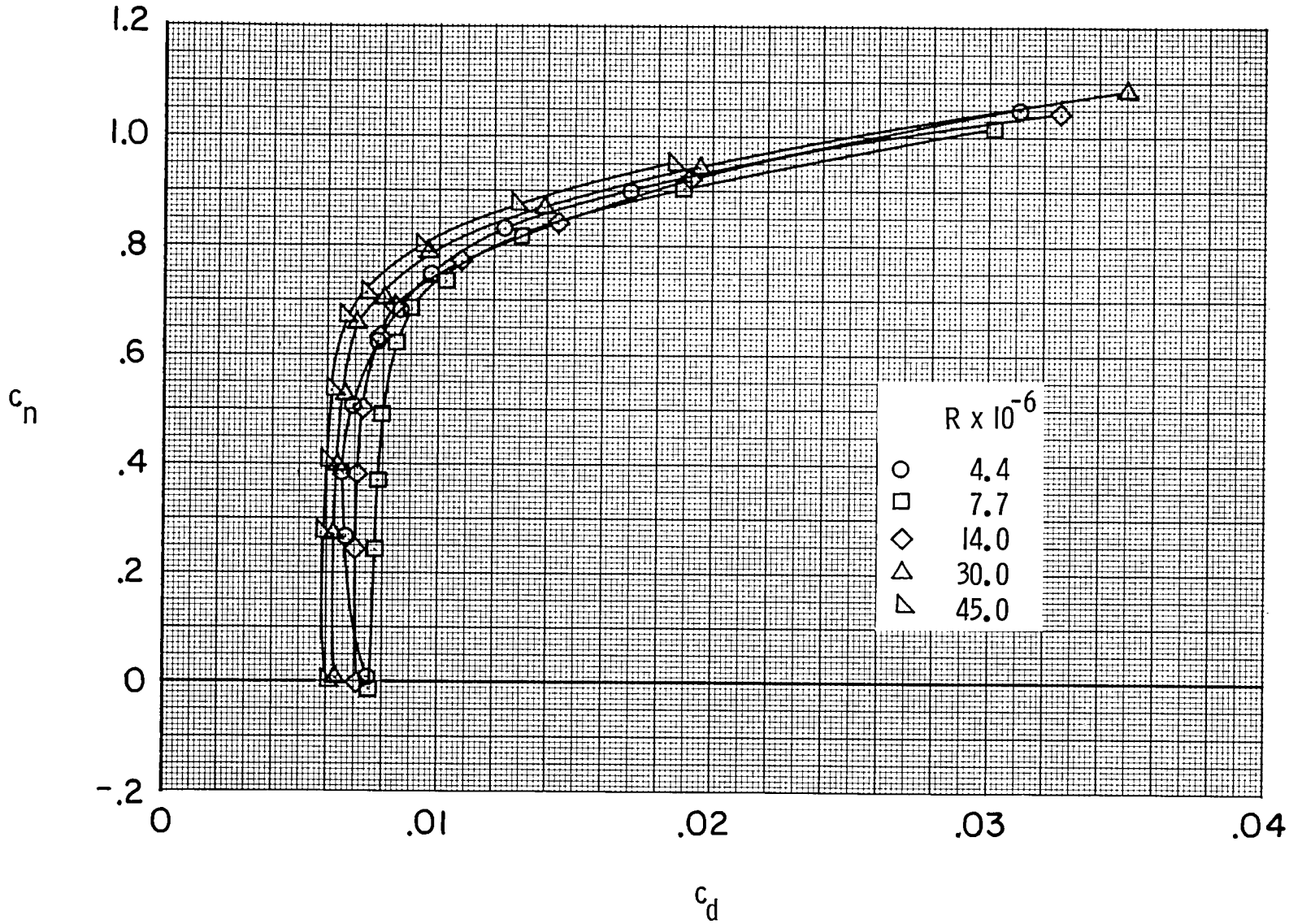

(b) c_n vs c_d.

Figure 35.- Concluded.

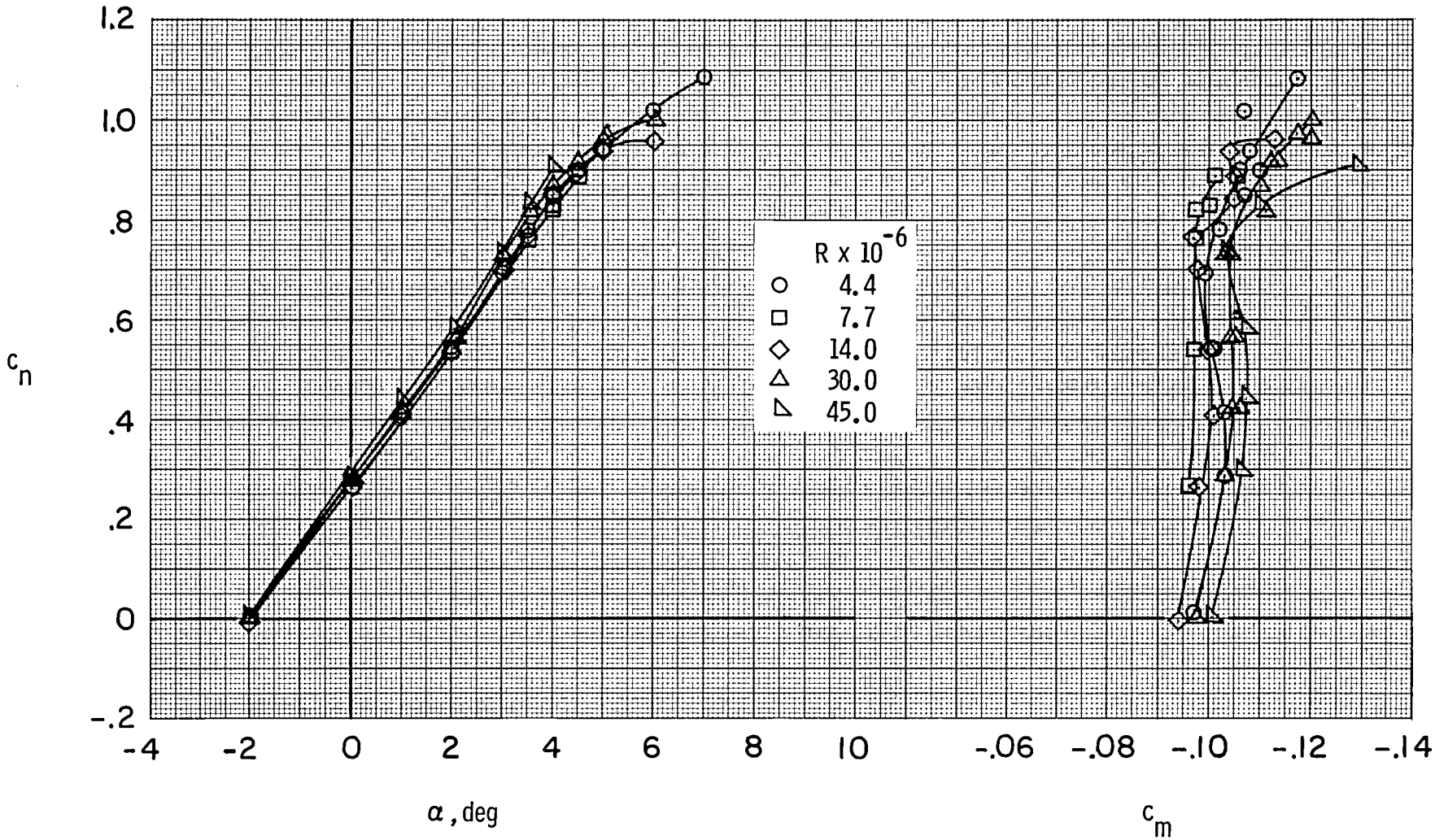

(a) c_n vs α and c_m.

Figure 36.- Effect of Reynolds number on aerodynamic characteristics of airfoil with free transition at $M \approx 0.76$.

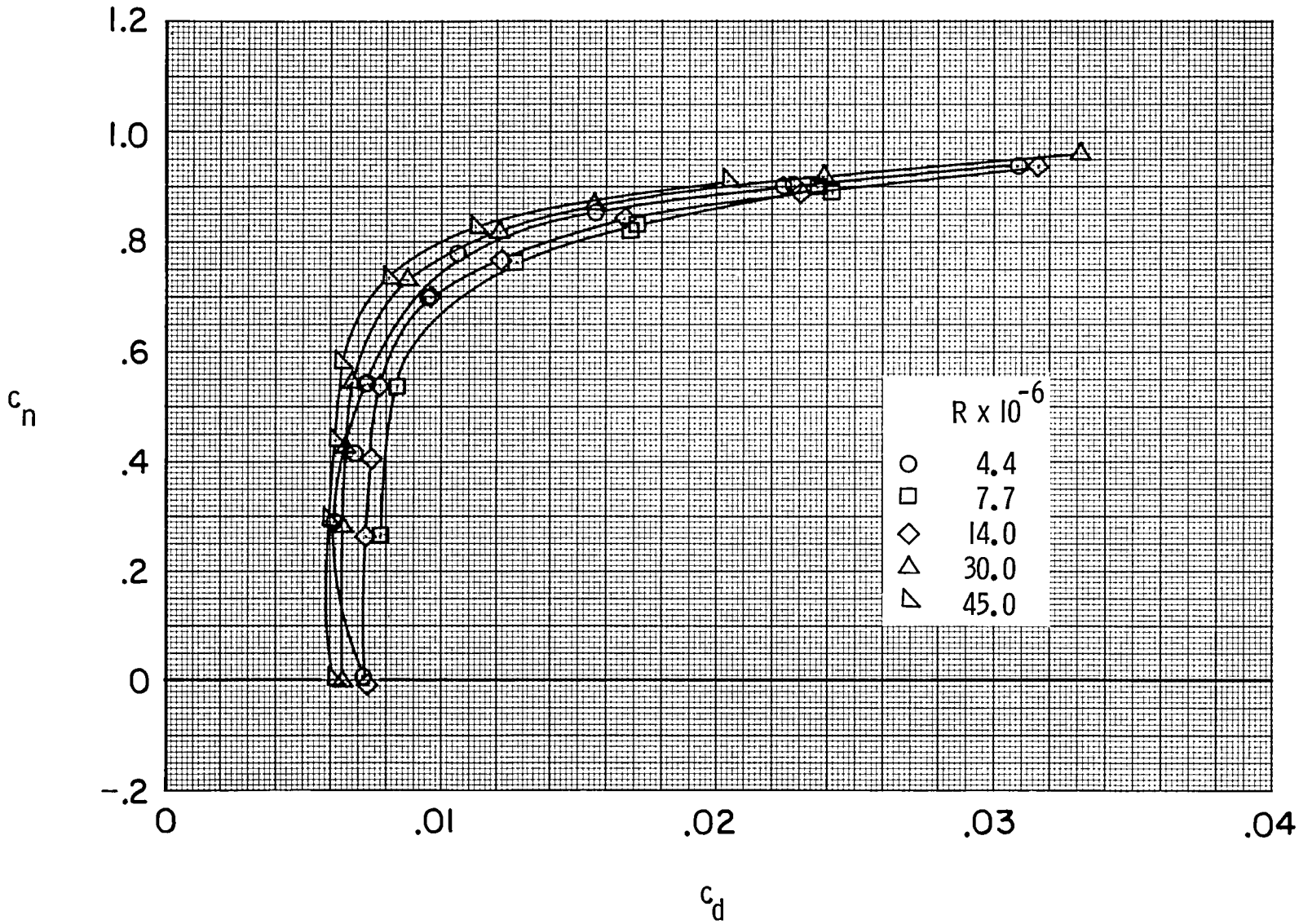

(b) c_n vs c_d.

Figure 36.- Concluded.

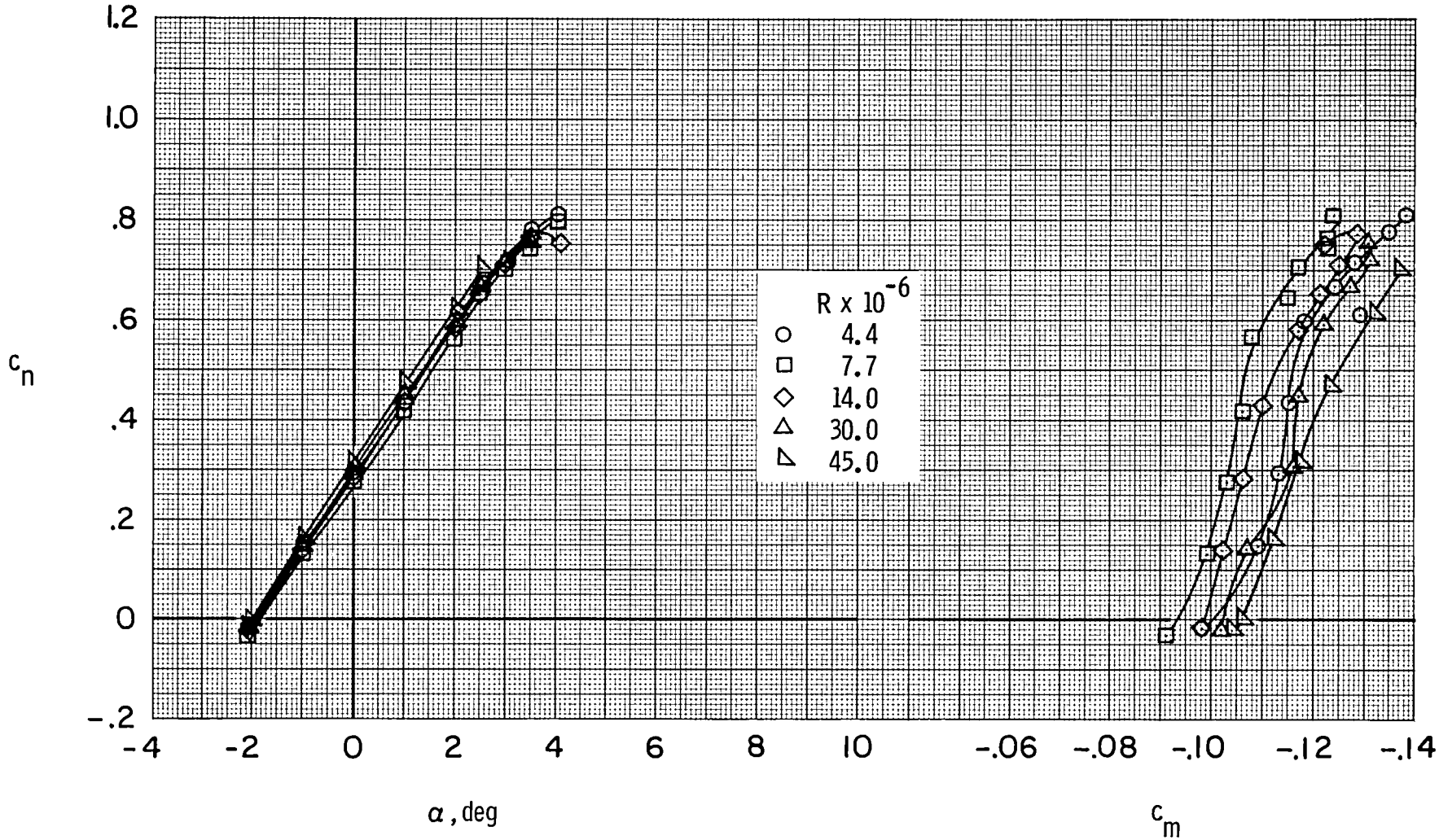

(a) c_n vs α and c_m.

Figure 37.- Effect of Reynolds number on aerodynamic characteristics of airfoil with free transition at $M \approx 0.80$.

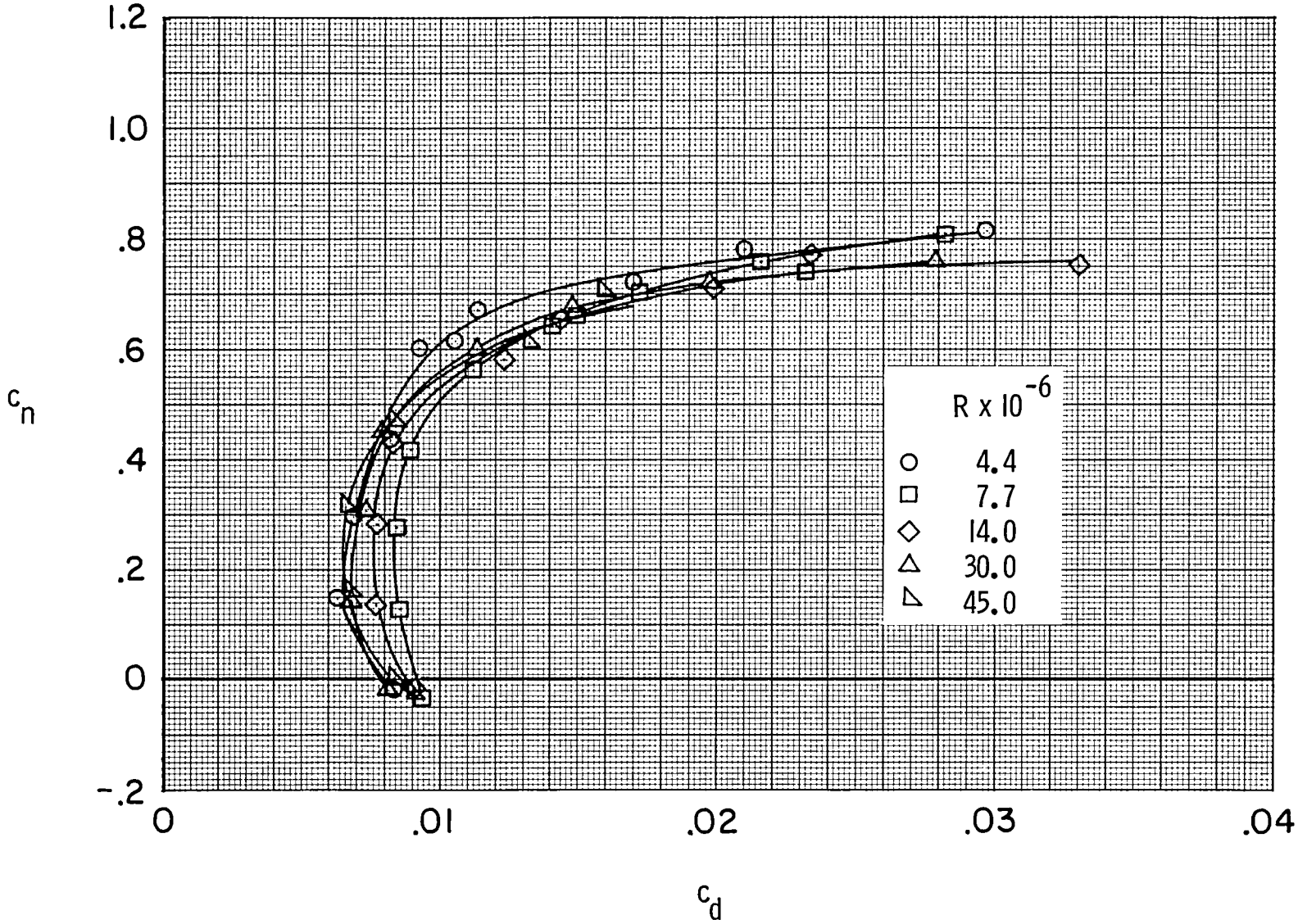

(b) c_n vs c_d.

Figure 37.- Concluded.

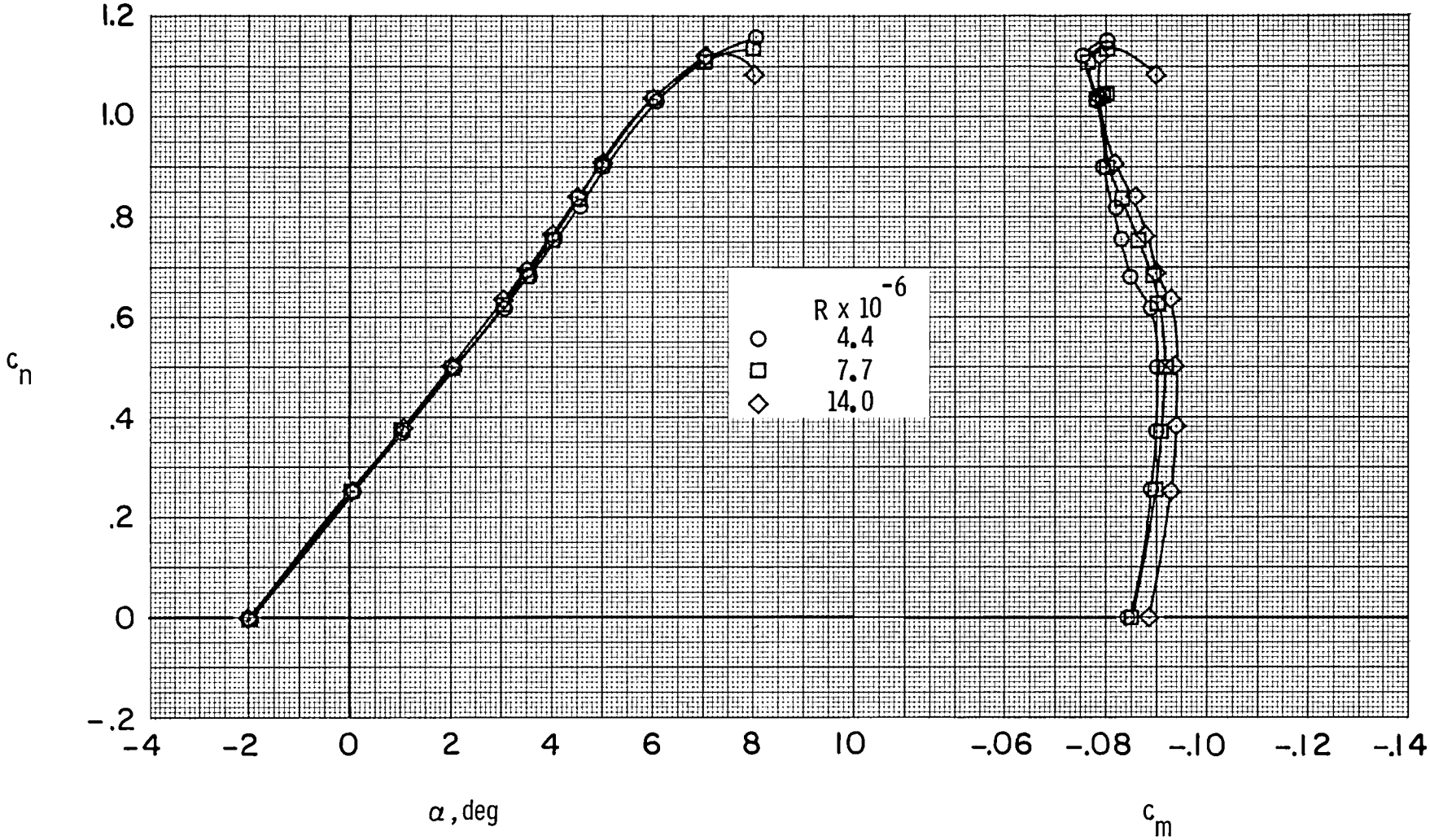

(a) c_n vs α and c_m.

Figure 38.- Effect of Reynolds number on aerodynamic characteristics of airfoil with fixed transition at $M \approx 0.70$.

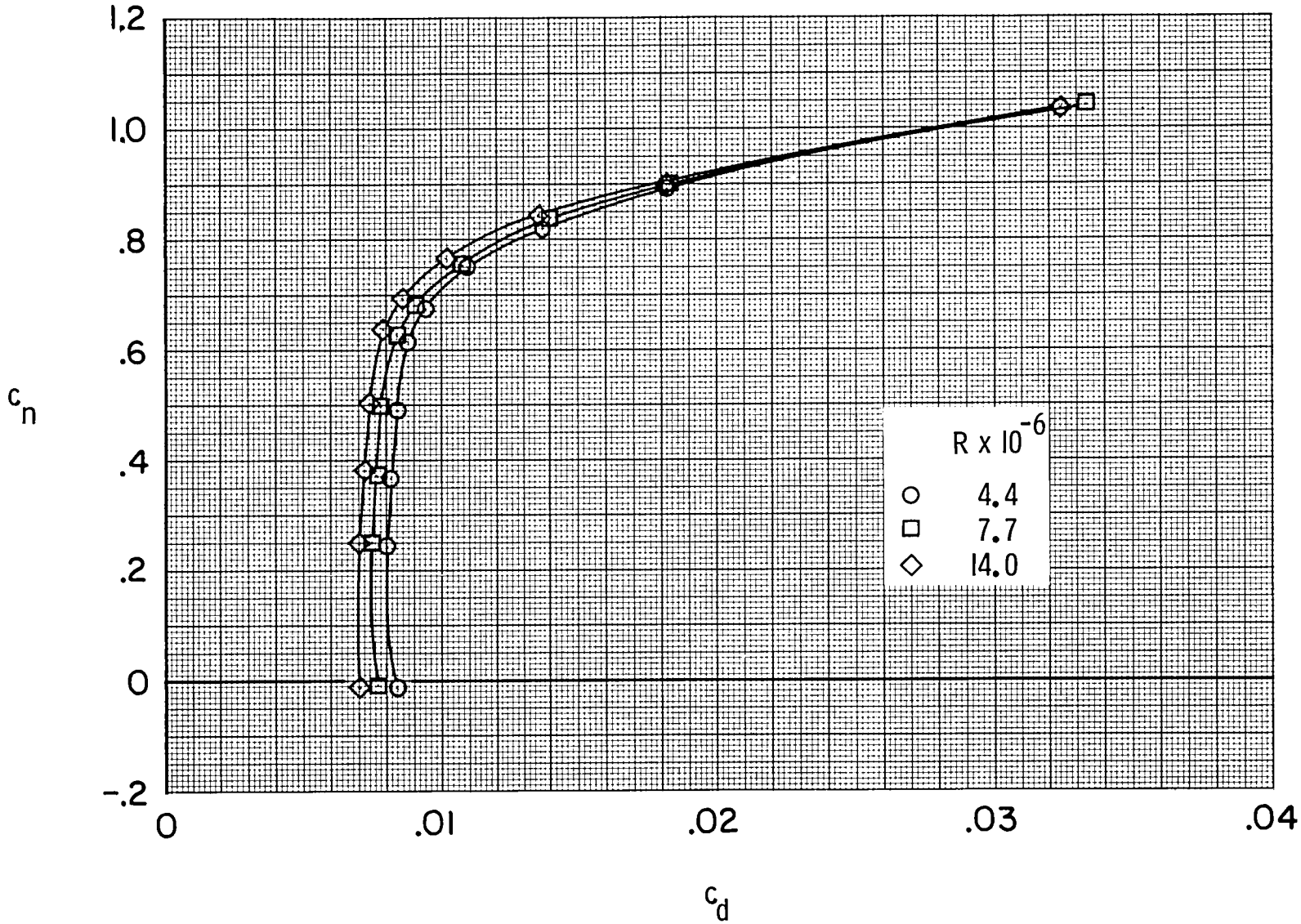

(b) c_n vs c_d.

Figure 38.- Concluded.

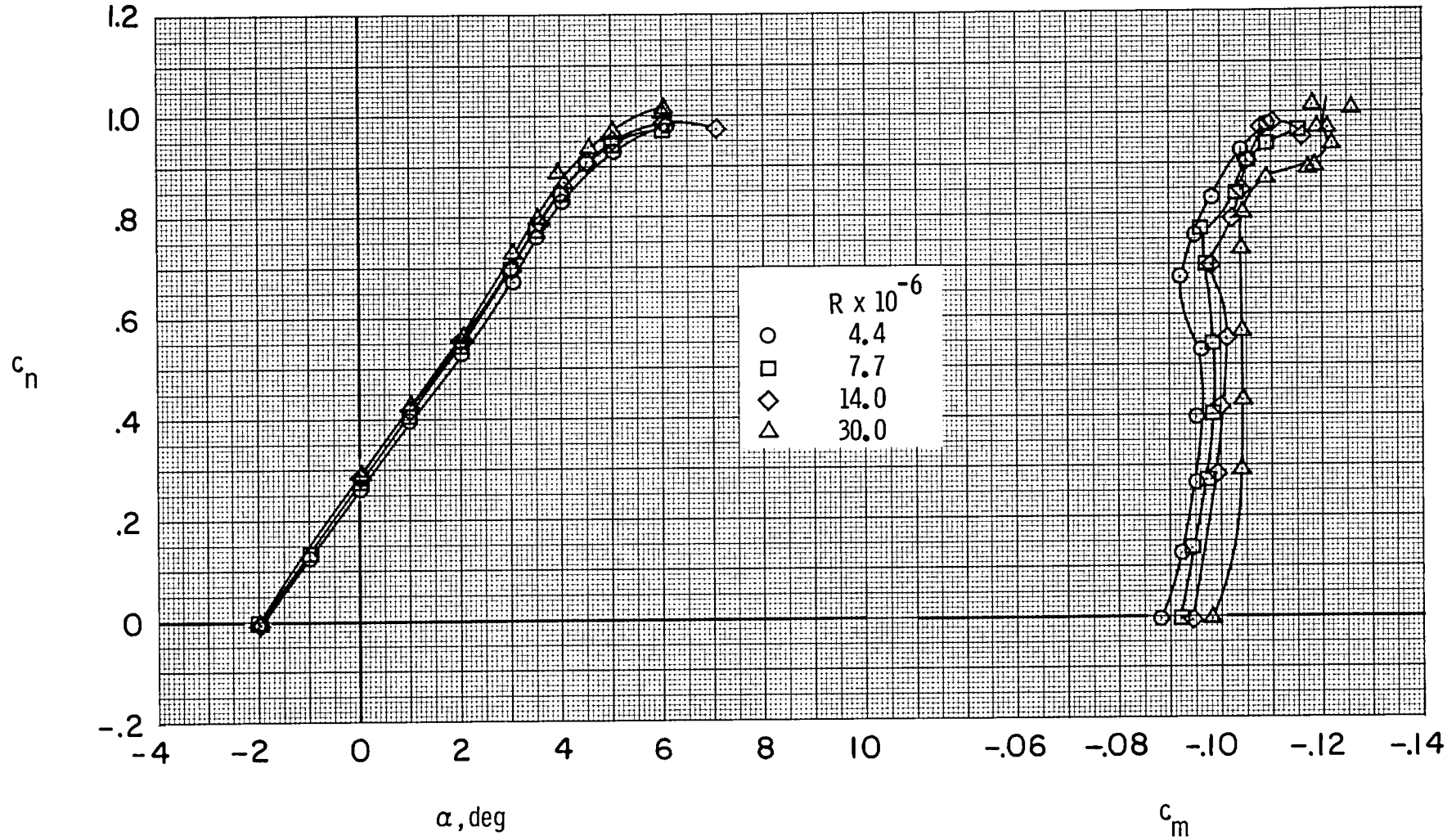

(a) c_n vs α and c_m.

Figure 39.- Effect of Reynolds number on aerodynamic characteristics of airfoil with fixed transition at $M \approx 0.76$.

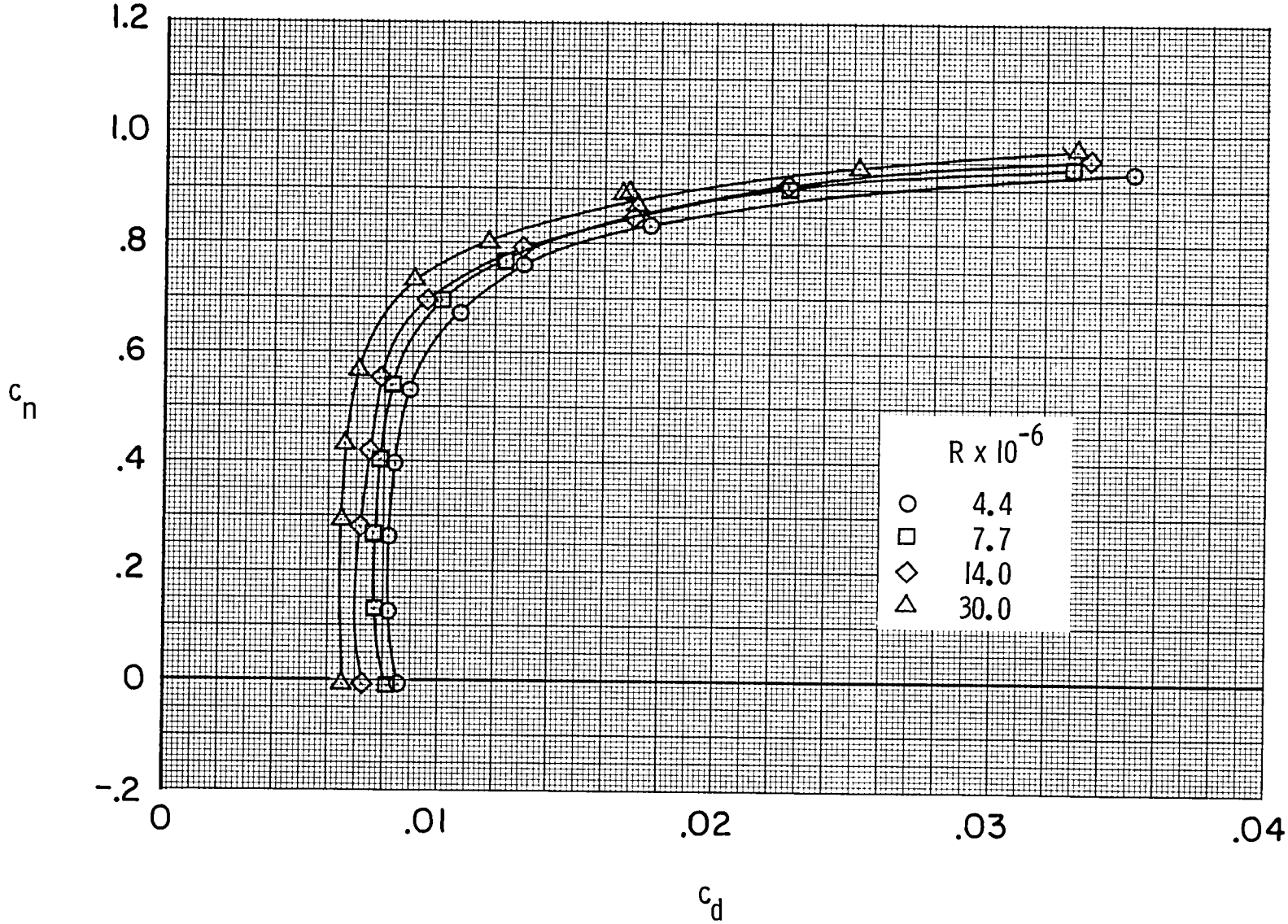

(b) c_n vs c_d.

Figure 39.- Concluded.

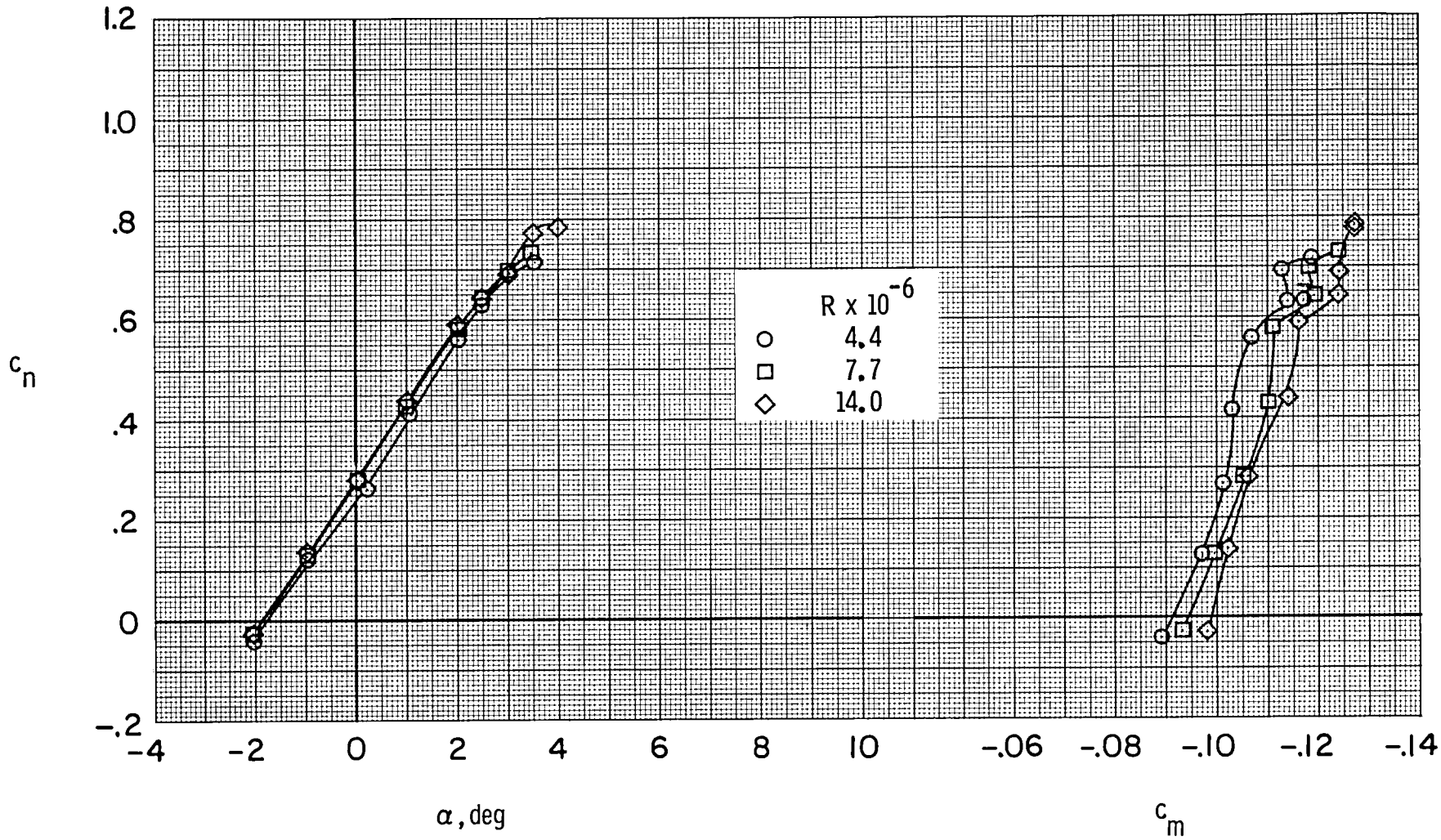

(a) c_n vs α and c_m.

Figure 40.- Effect of Reynolds number on aerodynamic characteristics of airfoil with fixed transition at $M \approx 0.80$.

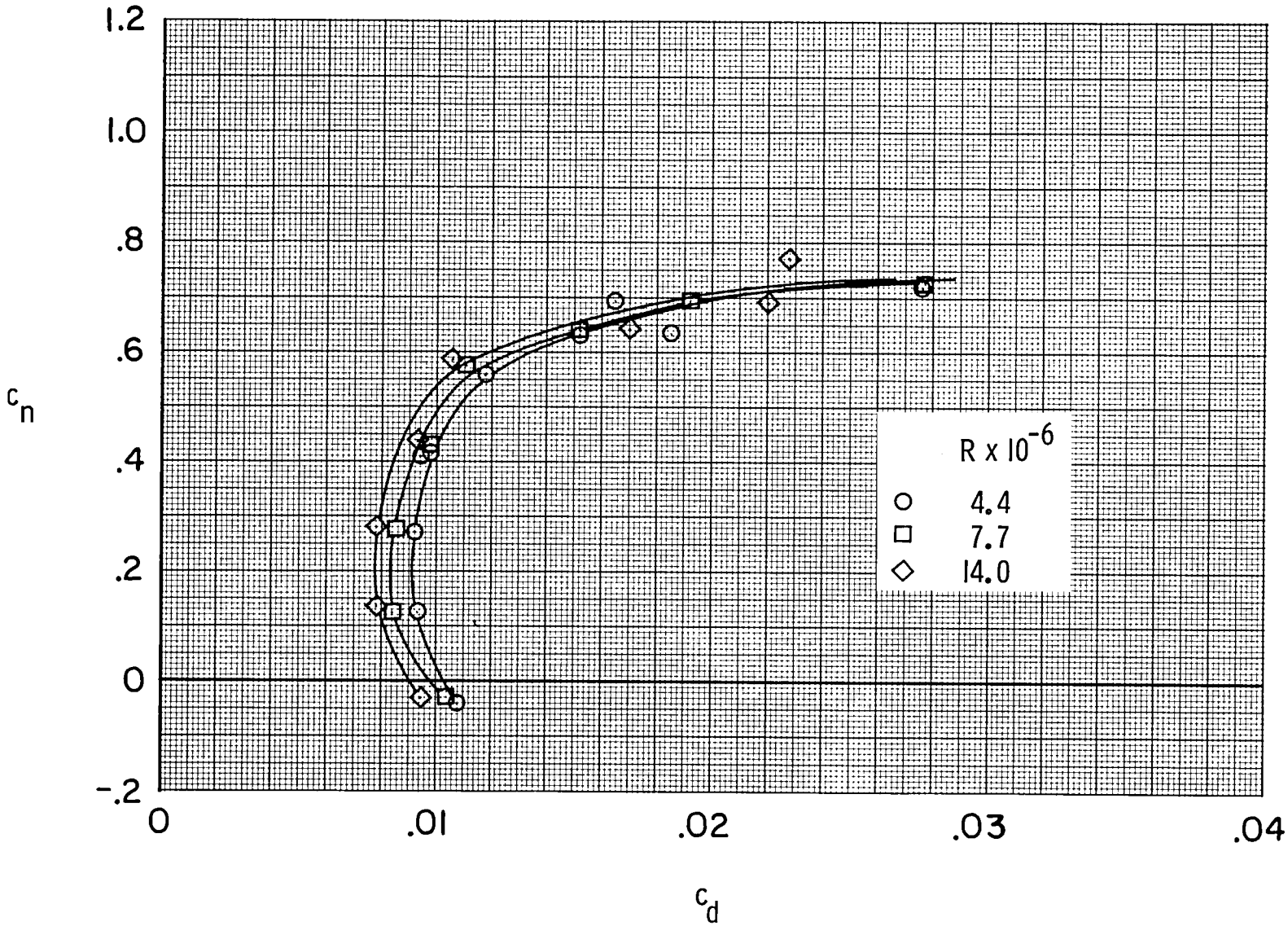

(b) c_n vs c_d.

Figure 40.- Concluded.

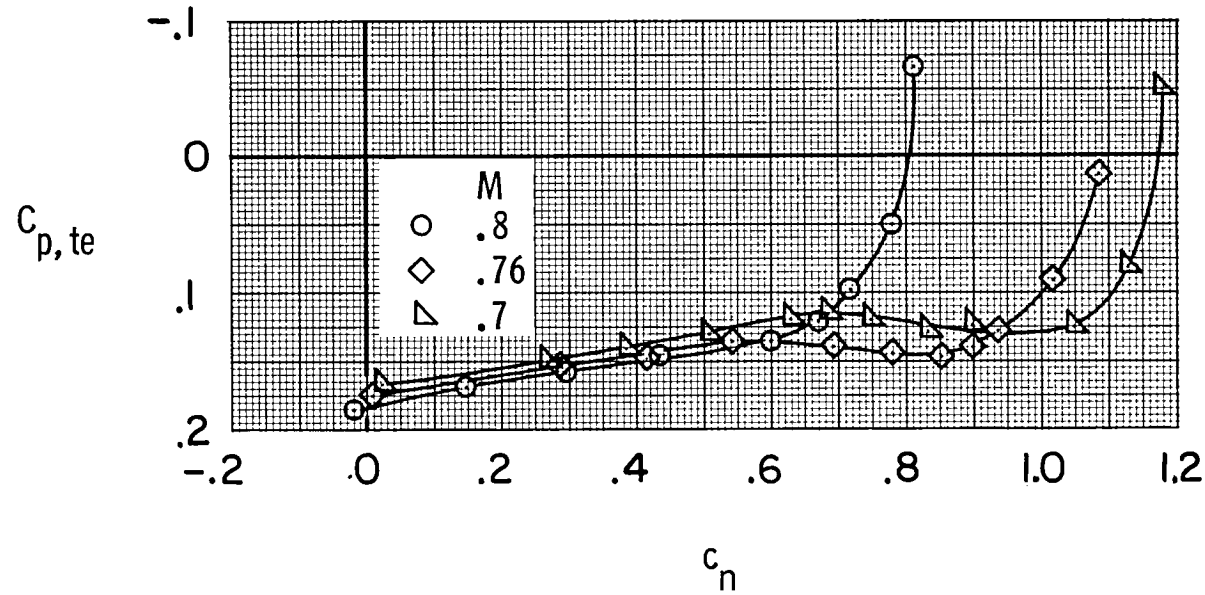

(a) $R \approx 4.4 \times 10^6$.

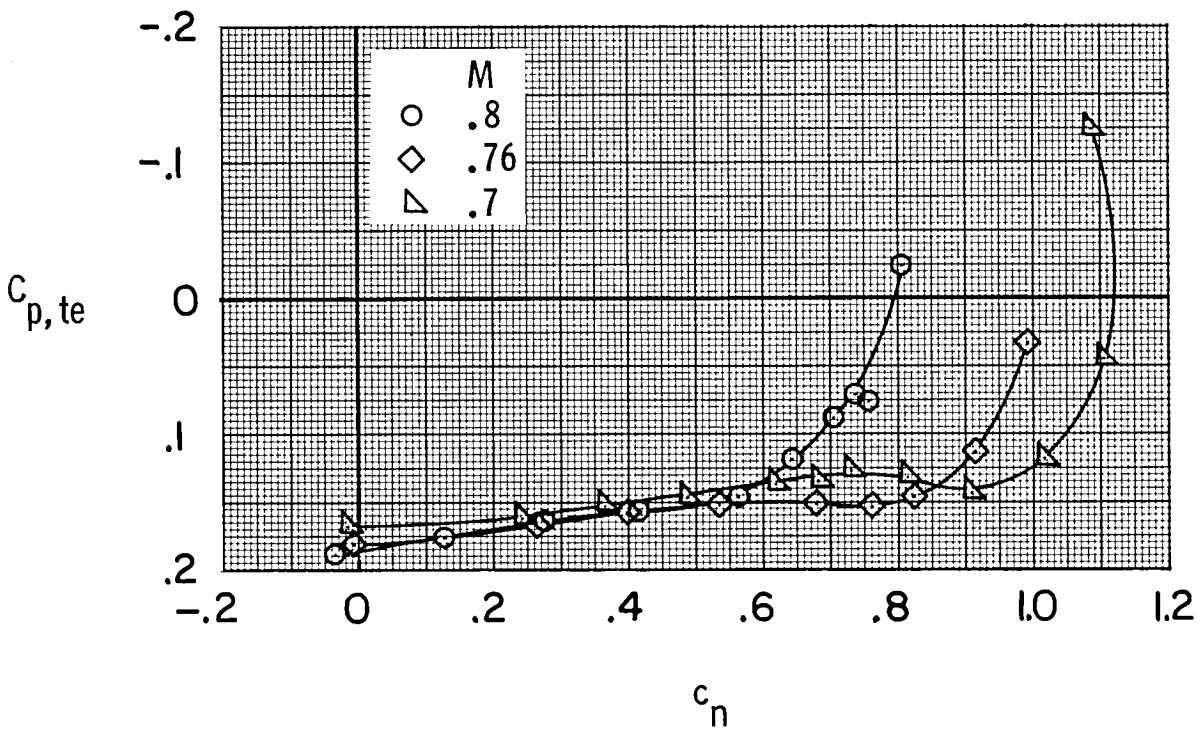

(b) $R \approx 7.7 \times 10^6$.

Figure 41.- Effect of Mach number on variation of trailing-edge pressure coefficient with normal-force coefficient. Free transition.

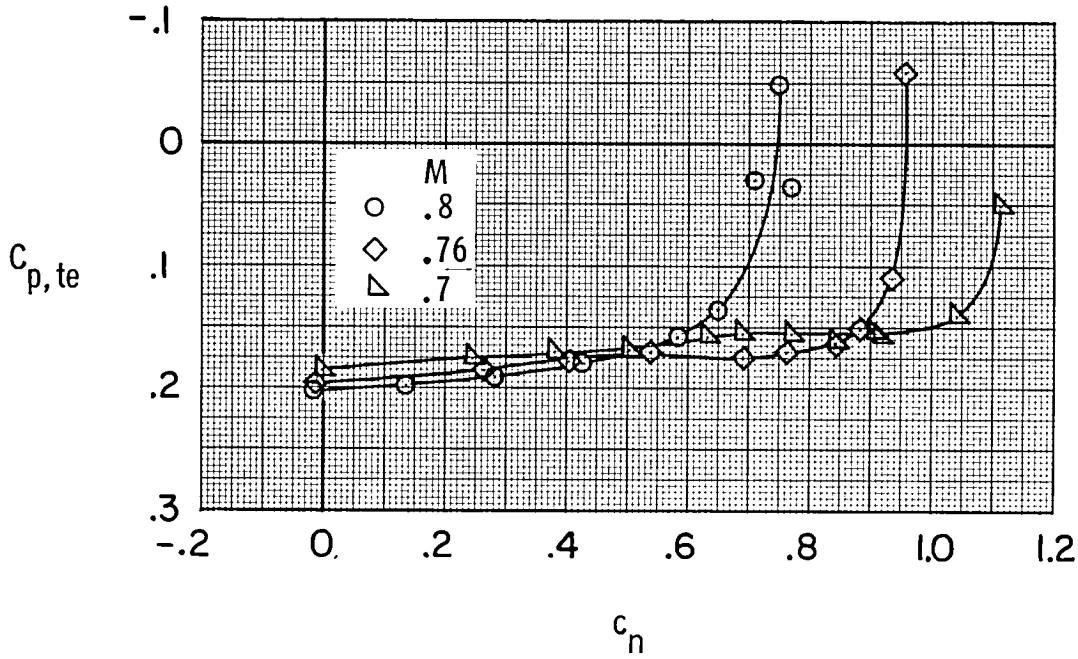

(c) $R \approx 14.0 \times 10^6$.

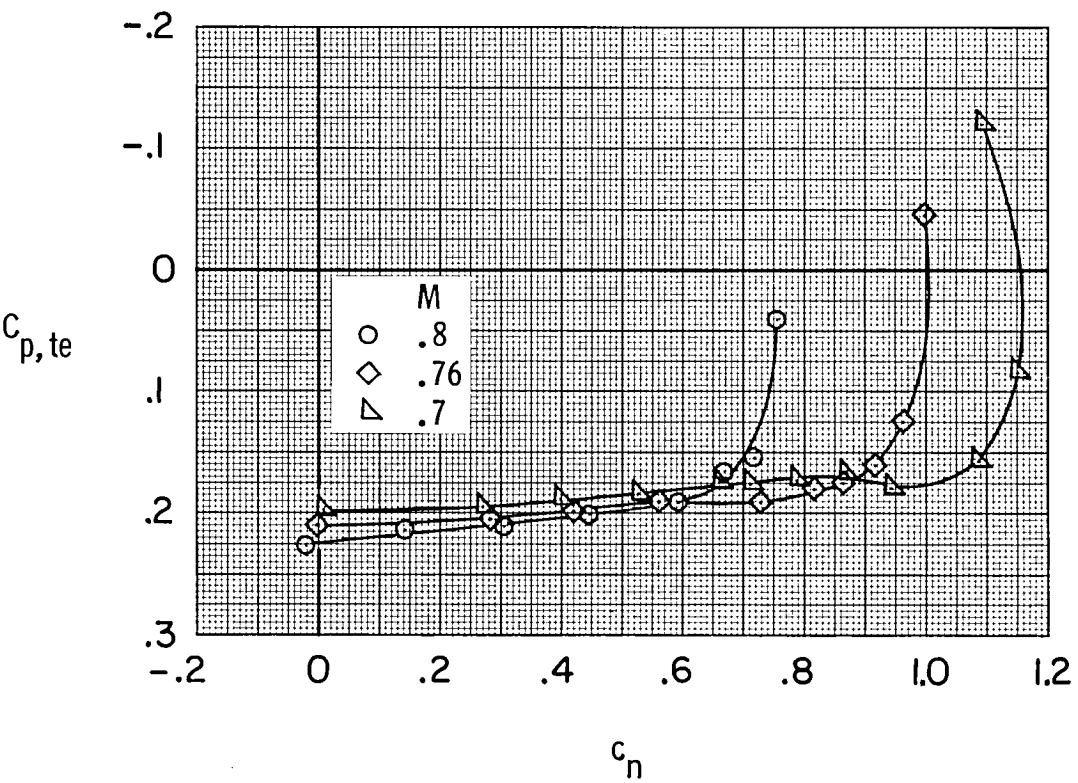

(d) $R \approx 30.0 \times 10^6$.

Figure 41.- Continued.

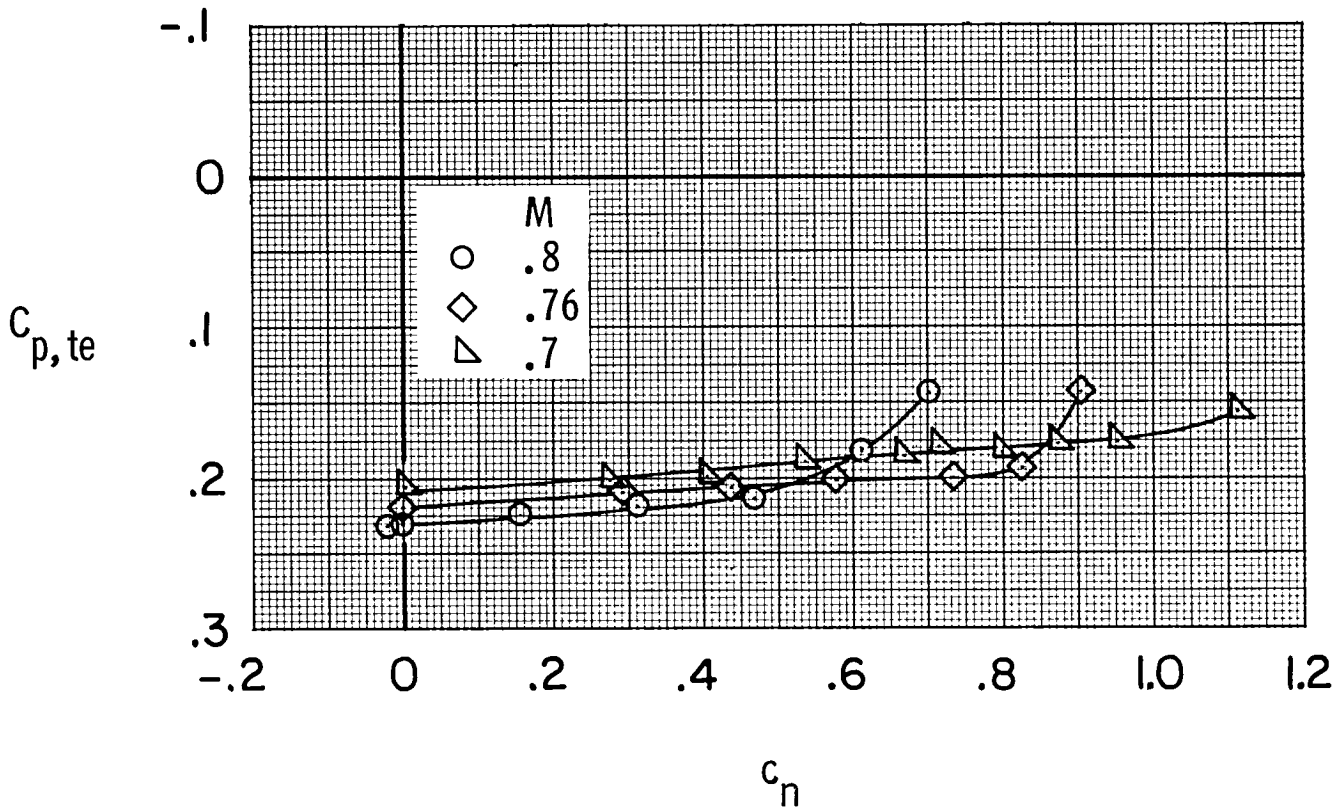

(e) $R \approx 45.0 \times 10^6$.

Figure 41.- Concluded.

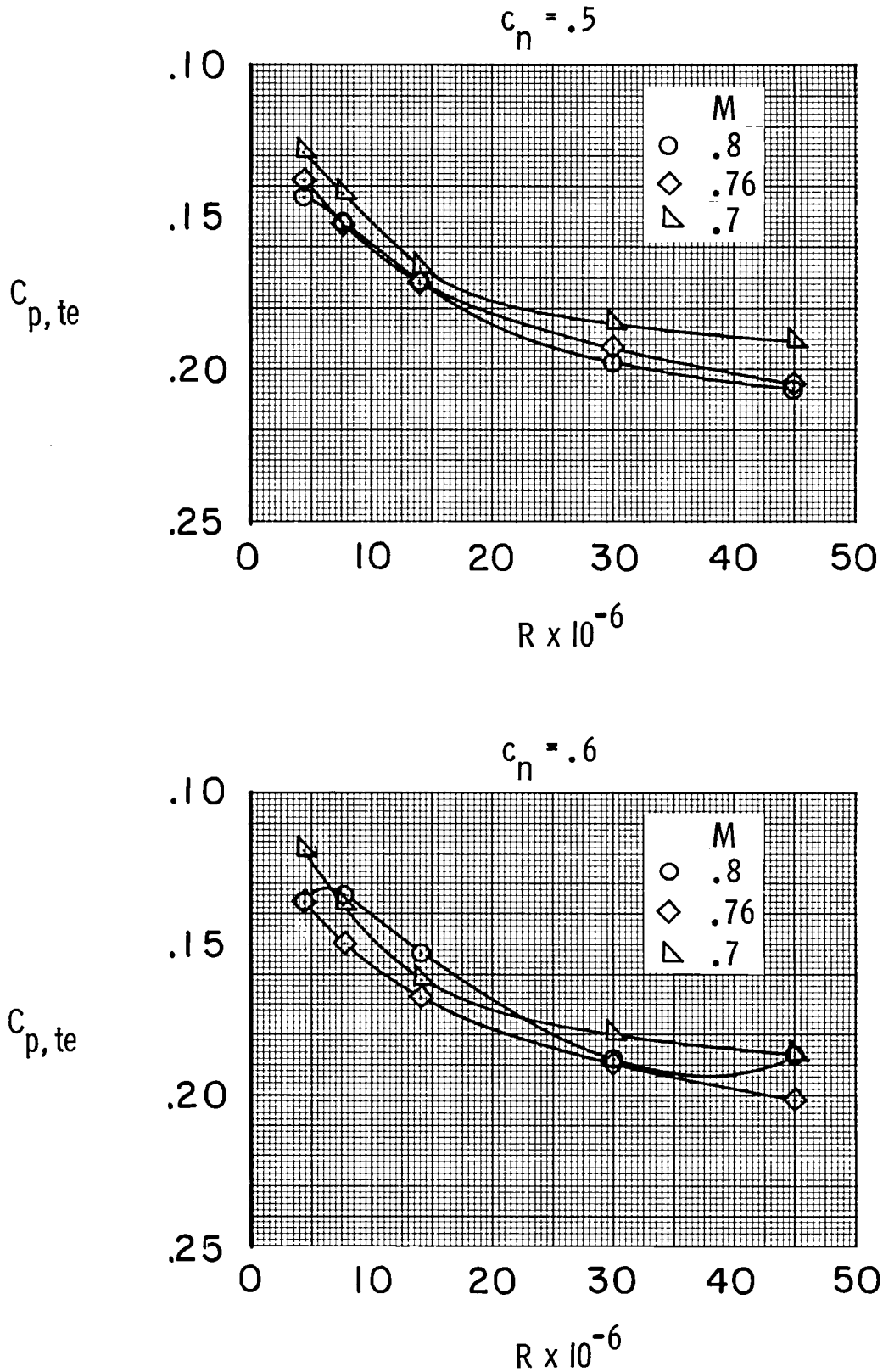

Figure 42.- Effect of Mach number on variation of trailing-edge pressure coefficient with Reynolds number.

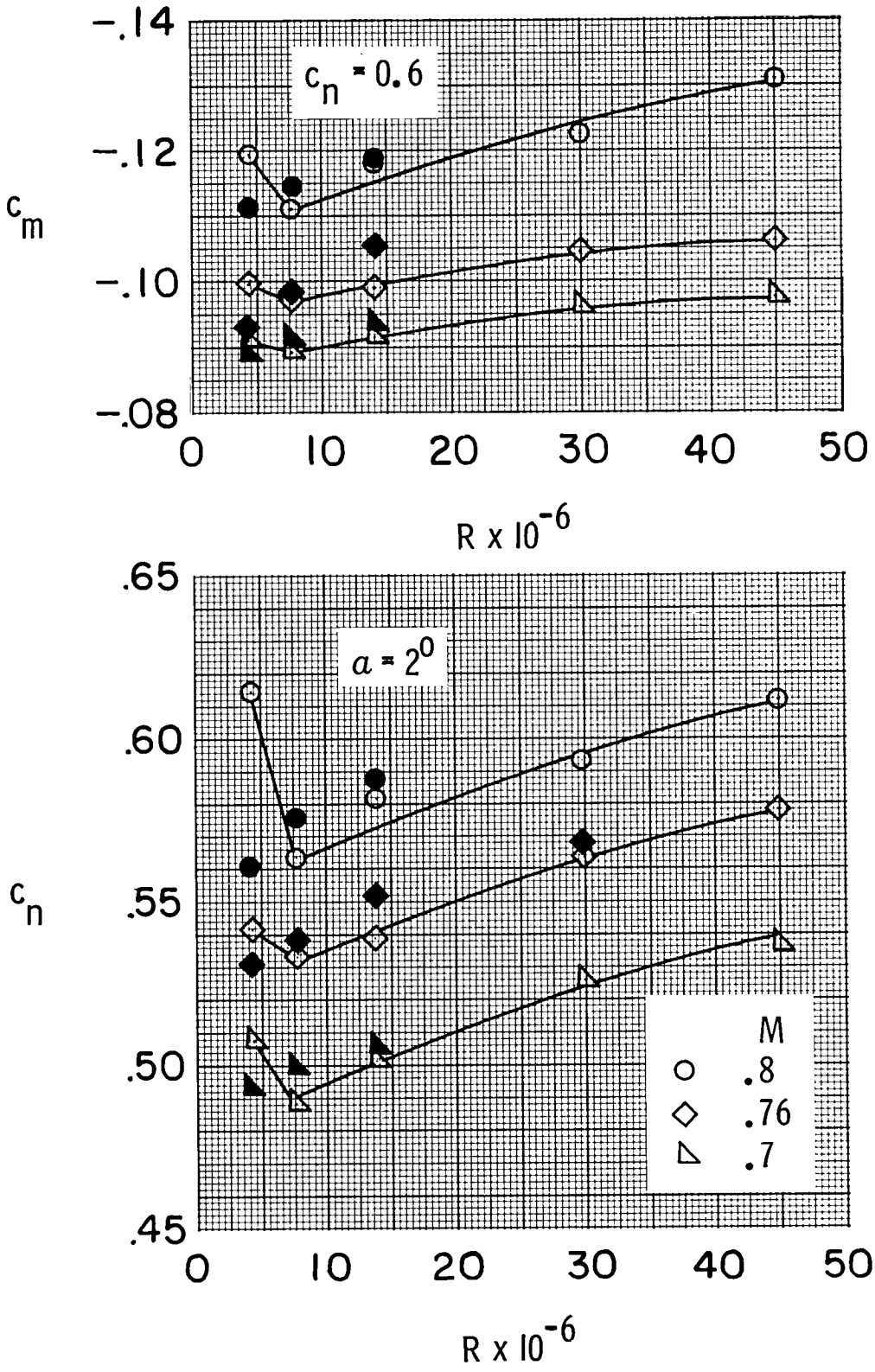

Figure 43.- Effect of Mach number on variation of normal-force and pitching-moment coefficients with Reynolds number. (Solid symbols indicate fixed transition.)

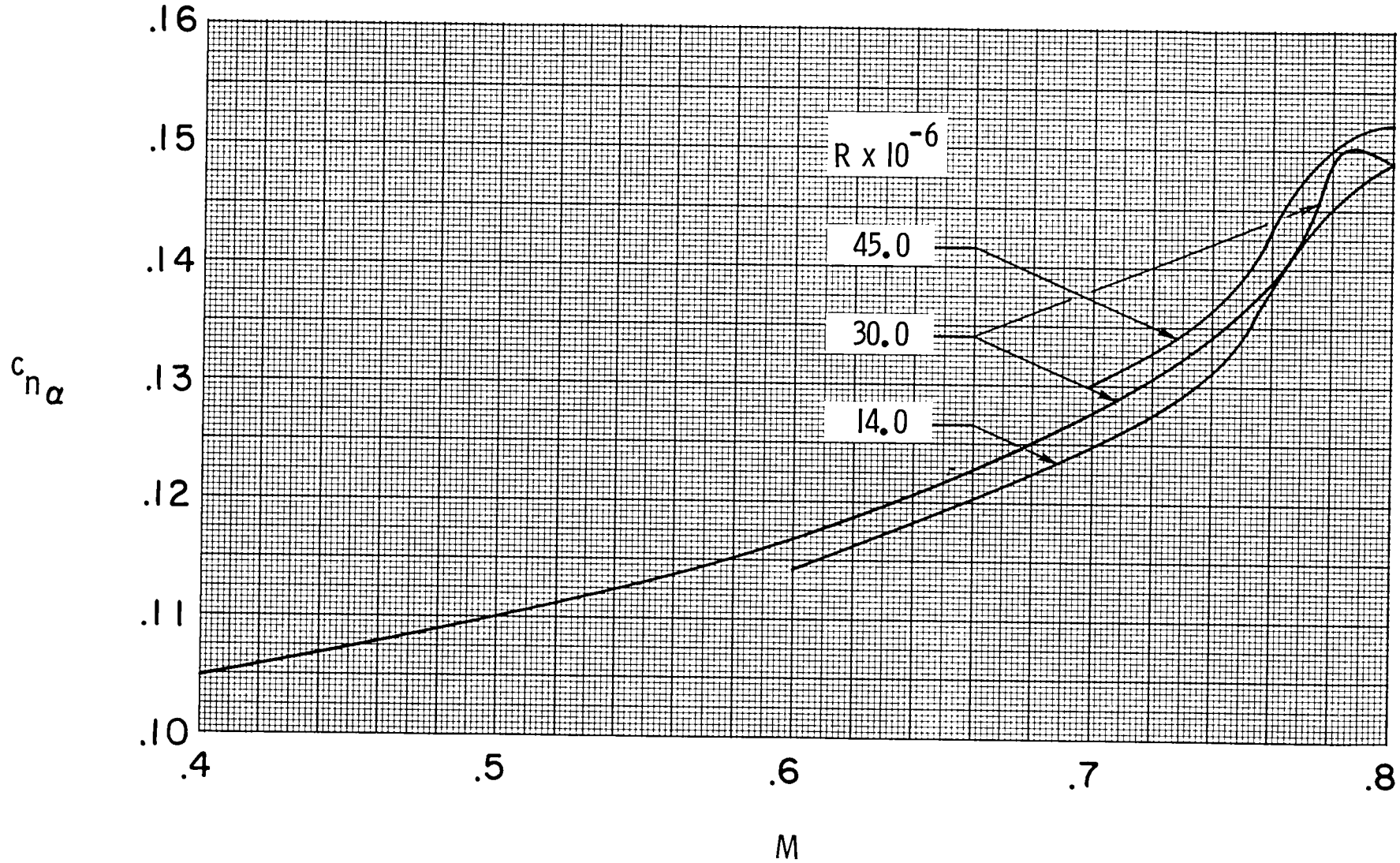

Figure 44.- Effect of Reynolds number on variation of normal-force slope c_{n_α} with Mach number. Free transition; α = -2° to 2°.

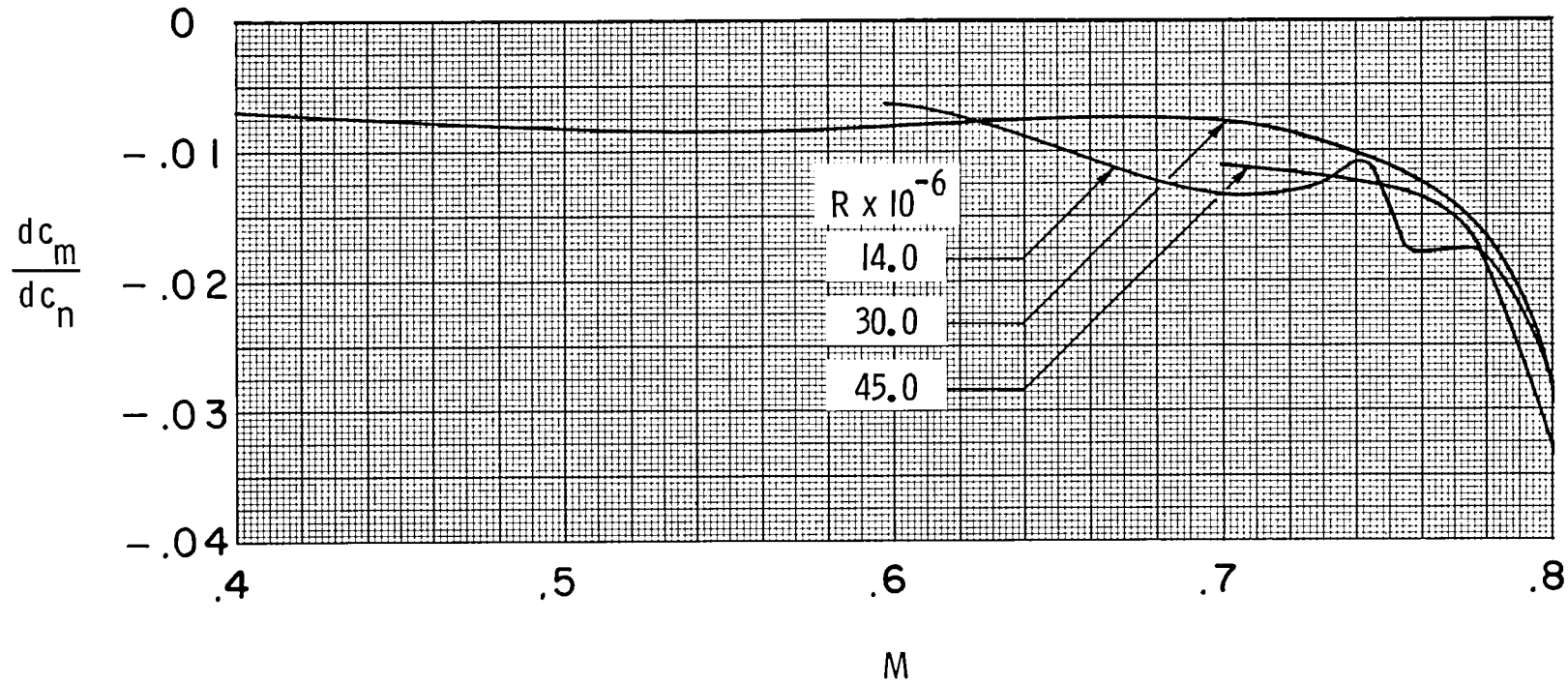

Figure 45.- Effect of Reynolds number on variation of stability parameter dc_m/dc_n with Mach number. Free transition; $\alpha \approx 0°$.

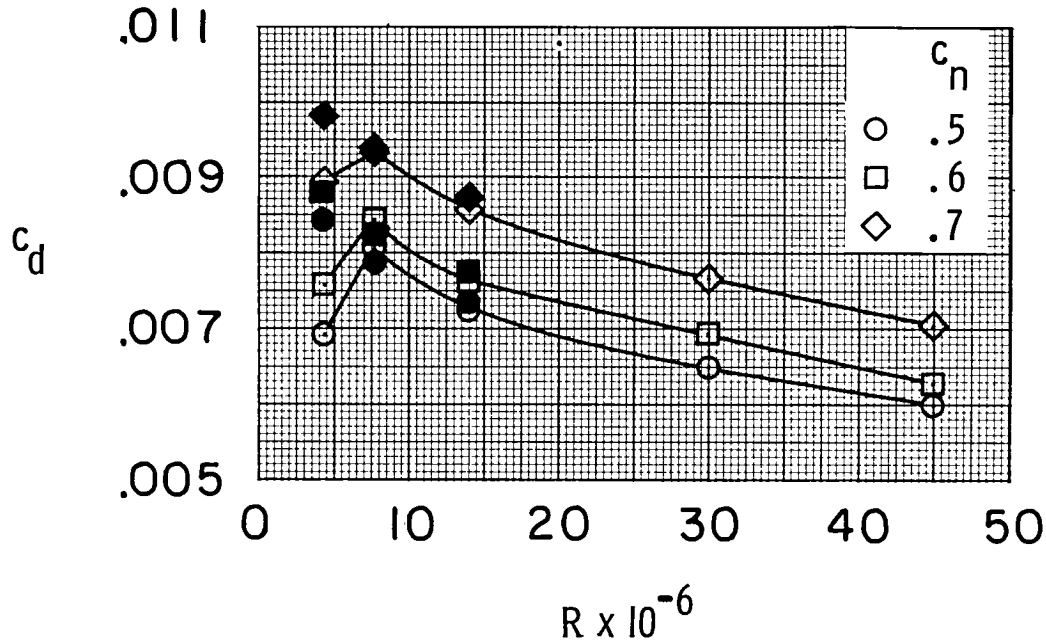

(a) M ≈ 0.70.

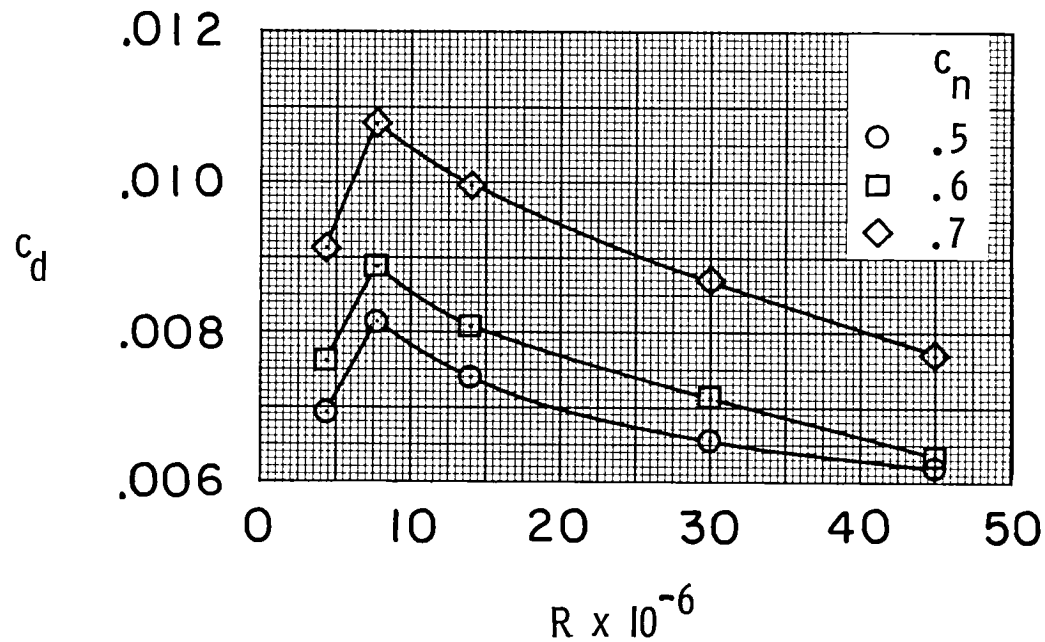

(b) M ≈ 0.74.

Figure 46.- Effect of Mach number on variation of section drag coefficient with Reynolds number. (Solid symbols indicate fixed transition.)

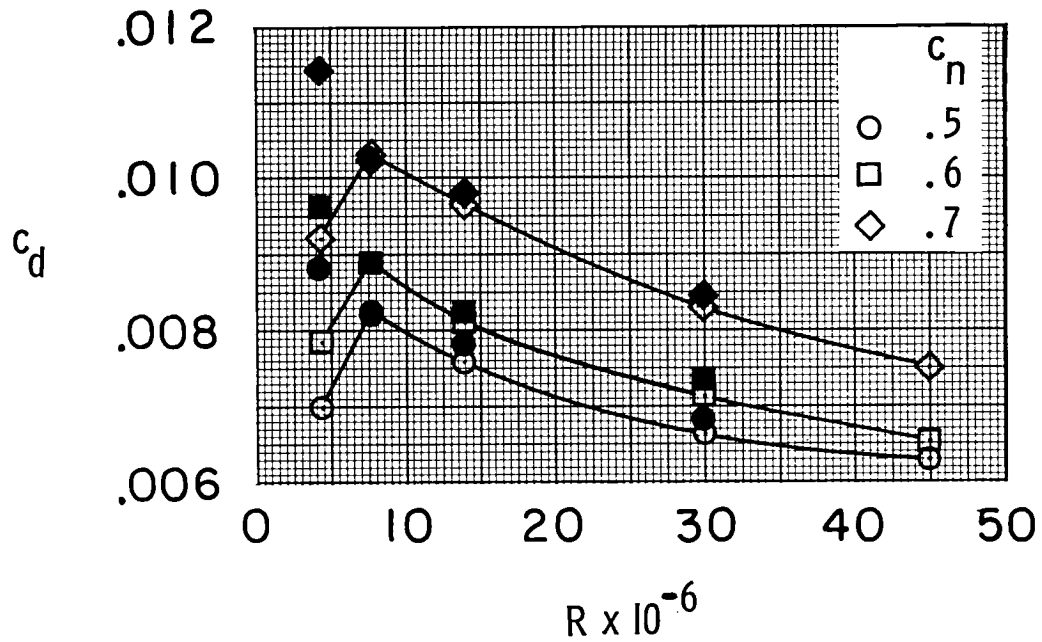

(c) M ≈ 0.76.

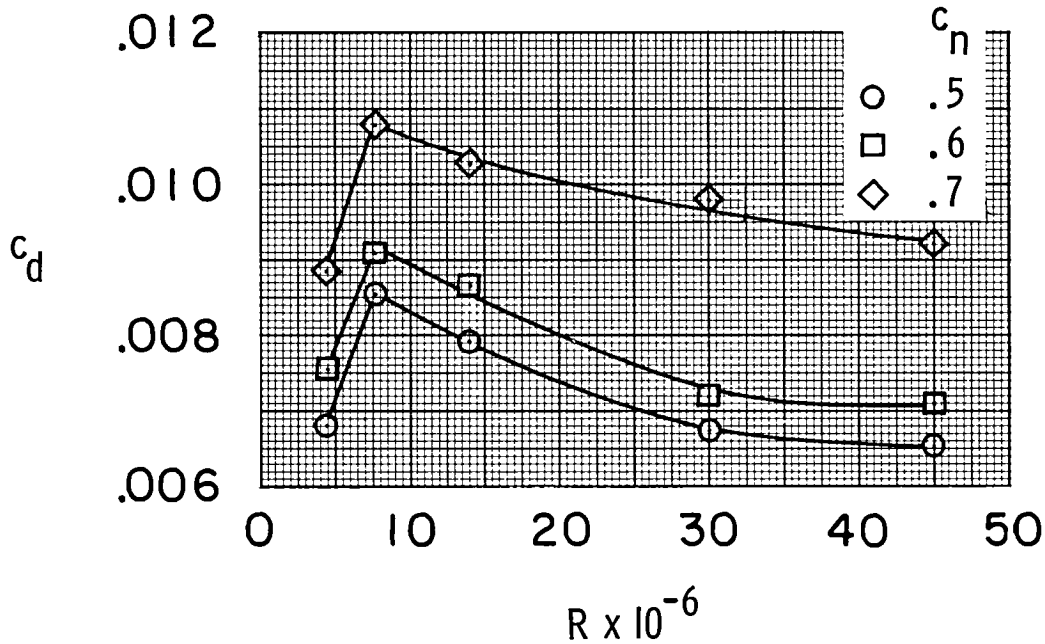

(d) M ≈ 0.78.

Figure 46.- Continued.

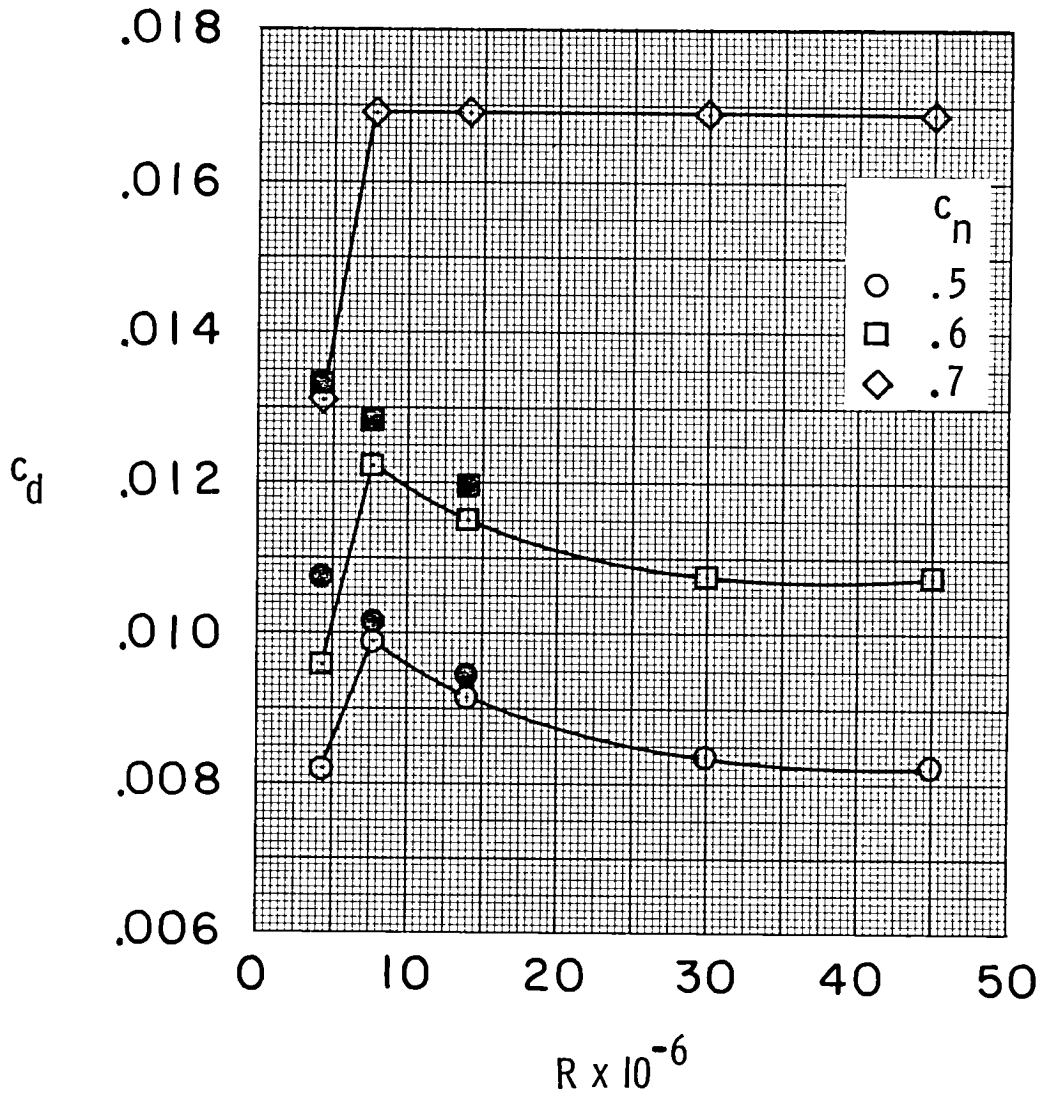

(e) M ≈ 0.80.

Figure 46.- Concluded.

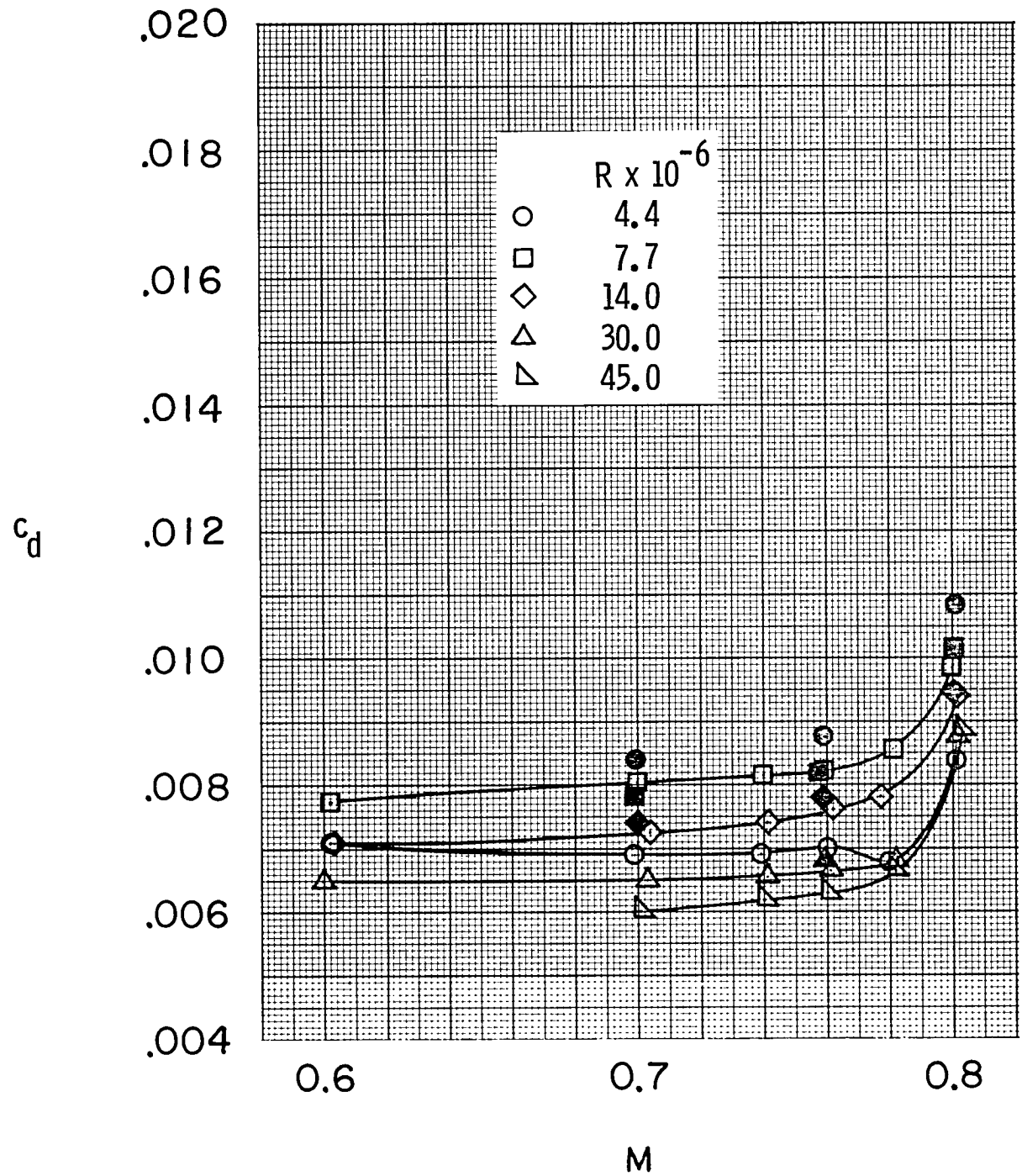

(a) $c_n = 0.5$.

Figure 47.- Effect of Reynolds number on variation of section drag coefficient with Mach number. (Solid symbols indicate fixed transition.)

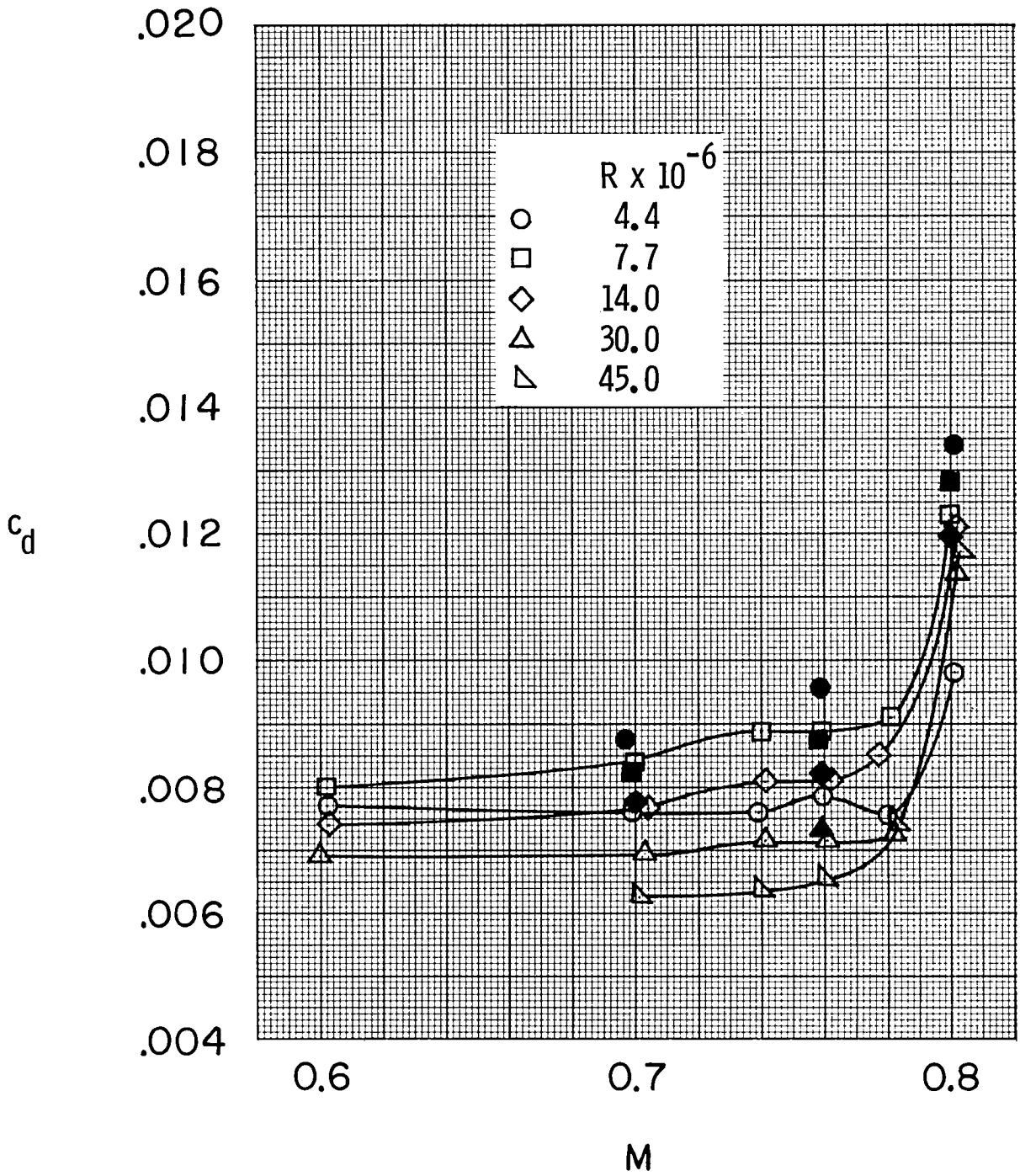

(b) $c_n = 0.6$.

Figure 47.- Continued.

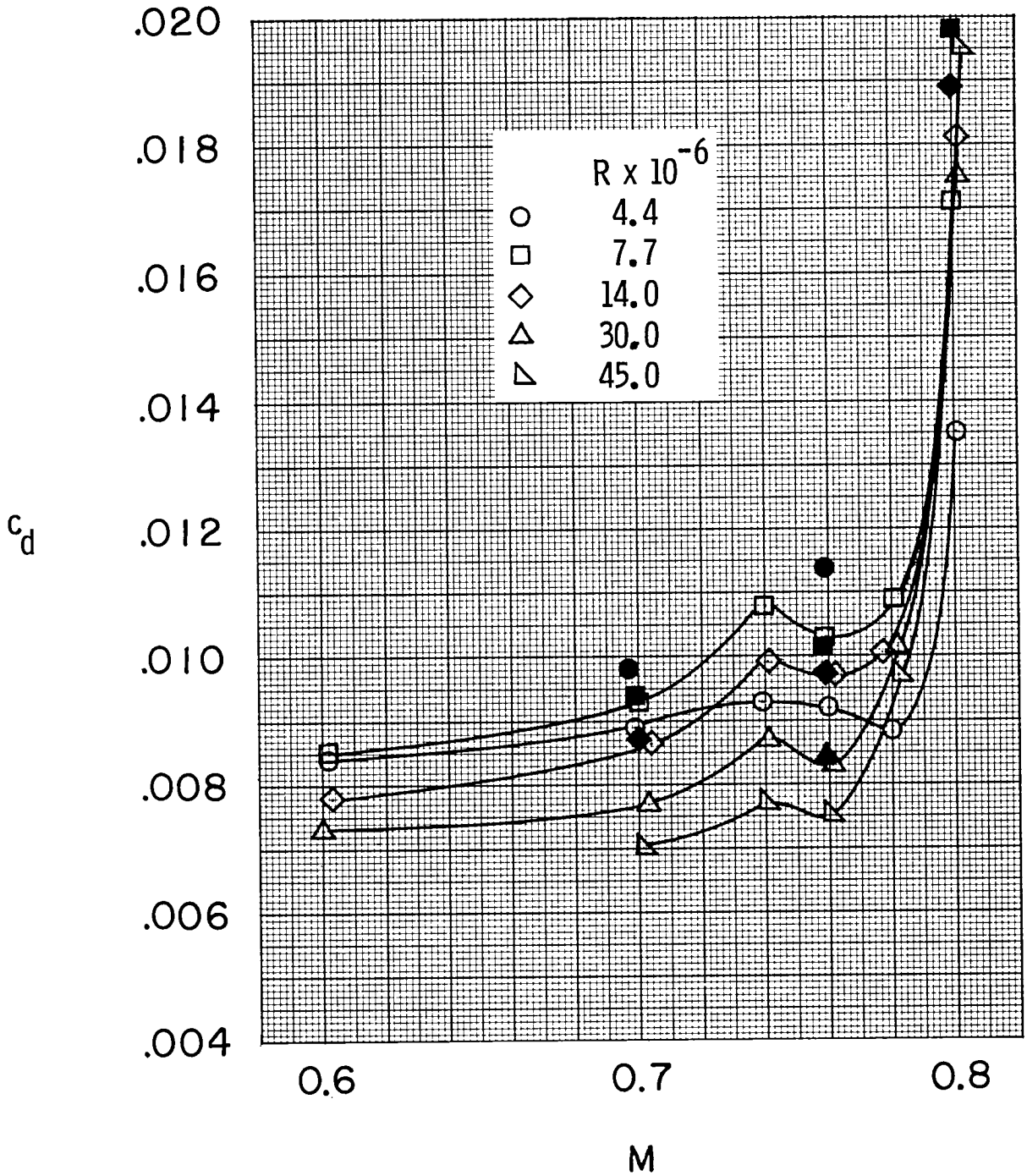

(c) $c_n = 0.7$.

Figure 47.- Concluded.

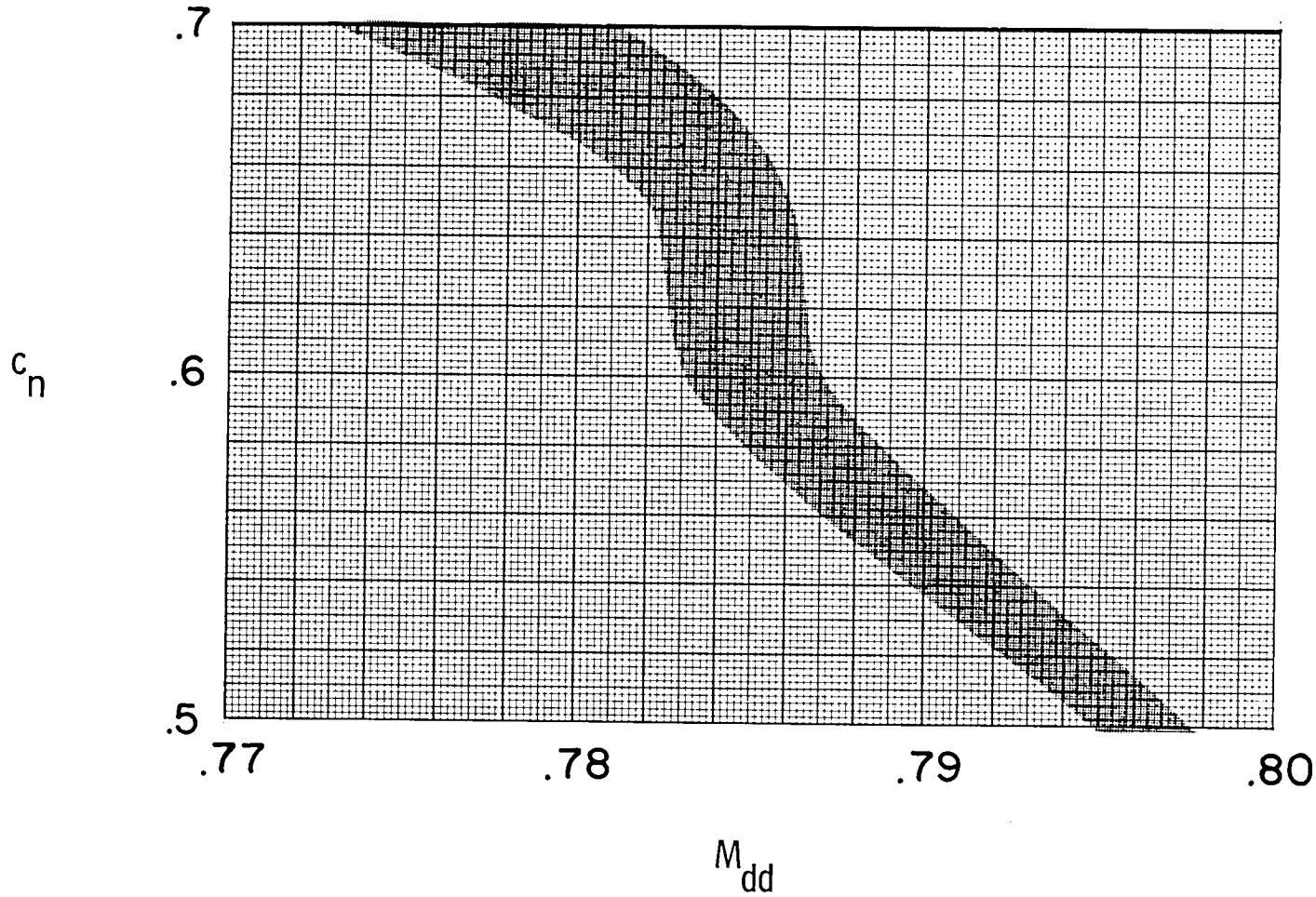

Figure 48.- Characteristic variation of normal-force coefficient with Mach number at drag divergence in Reynolds number range of 14.0×10^6 to 45.0×10^6. Free transition.

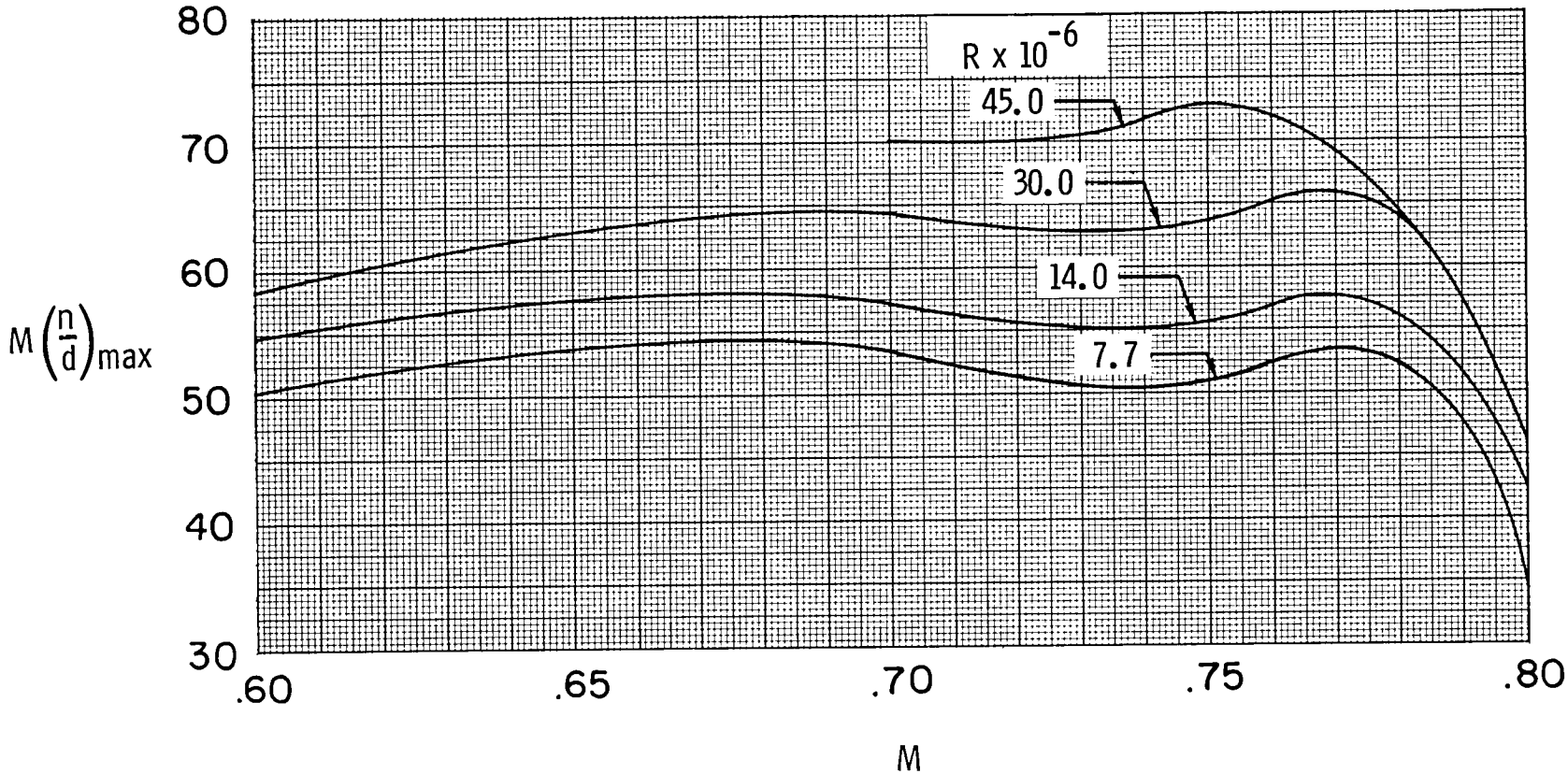

Figure 49.- Effect of Reynolds number on variation of range performance factor $M(n/d)_{max}$ with Mach number. Free transition.

1. Report No.	2. Government Accession No.	3. Recipient's Catalog No.
NASA TM-81922		

4. Title and Subtitle	5. Report Date
HIGH REYNOLDS NUMBER TESTS OF A BOEING BAC I AIRFOIL IN THE LANGLEY 0.3-METER TRANSONIC CRYOGENIC TUNNEL	April 1982
	6. Performing Organization Code: 534-02-13-16
7. Author(s): William G. Johnson, Jr., Acquilla S. Hill, Edward J. Ray, Roger A. Rozendaal, and Thomas W. Butler	8. Performing Organization Report No.: L-15011
	10. Work Unit No.
9. Performing Organization Name and Address: NASA Langley Research Center, Hampton, VA 23665	11. Contract or Grant No.
	13. Type of Report and Period Covered: Technical Memorandum
12. Sponsoring Agency Name and Address: National Aeronautics and Space Administration, Washington, DC 20546	14. Sponsoring Agency Code

15. Supplementary Notes

William G. Johnson, Jr., Acquilla S. Hill, and Edward J. Ray: Langley Research Center, Hampton, Virginia.
Roger A. Rozendaal and Thomas W. Butler: Boeing Commercial Airplane Company, Seattle, Washington.

16. Abstract

A wind-tunnel investigation of an advanced-technology airfoil has been conducted in the Langley 0.3-Meter Transonic Cryogenic Tunnel (TCT). This investigation represents the first in a series of NASA/U.S. industry two-dimensional airfoil studies to be completed in the Advanced Technology Airfoil Test program. Test temperature was varied from ambient to about 100 K at pressures ranging from about 1.2 to 6.0 atm. Mach number was varied from about 0.40 to 0.80. These variables provided a Reynolds number (based on airfoil chord) range from about 4.4×10^6 to 50.0×10^6. This investigation was specifically designed to (1) test a Boeing advanced airfoil from low to flight-equivalent Reynolds numbers; (2) provide the industry participant (Boeing) with experience in cryogenic wind-tunnel model design and testing techniques; and (3) demonstrate the suitability of the 0.3-m TCT as an airfoil test facility. All the objectives of the cooperative test were met. Data are included which demonstrate the effects of fixed transition, Mach number, and Reynolds number on the aerodynamic characteristics of the airfoil. Also included are remarks on the model design, the model structural integrity, and the overall test experience.

17. Key Words (Suggested by Author(s))	18. Distribution Statement
Supercritical airfoil Two-dimensional airfoil Cryogenic wind tunnel High Reynolds number	[redacted] Subject Category 02

19. Security Classif. (of this report)	20. Security Classif. (of this page)	21. No. of Pages	22. Price
Unclassified	Unclassified	129	

Available: NASA's Industrial Applications Centers

NASA-Langley, 1982